

**Di-Thiafulvalene functionalized Phenylene
Acetylene-Polymers for Selective Dispersion of
Single Walled Carbon Nanotubes (SWNTs)**

by

Haseena Shaik

A thesis submitted to the School of Graduate Studies
in partial fulfillment of the requirements for
the degree of Master of Science

Department of Chemistry

Memorial University

St. John's, Newfoundland and Labrador, Canada

May 2015

Abstract

This thesis explores the rational design, synthesis, characterization and applications of conjugated polymers as carbon nanotube (CNT) dispersants. Two Dithiafulvalene (DTF) functionalized Phenylacetylene based polymers were synthesized using Sonogashira cross coupling conditions and Cu-catalyzed homo coupling conditions. DTF unit was introduced by applying “click chemistry” to the side chain of the polymers to form a “centipede-like” macromolecular architecture. The ability of synthesized polymers to disperse SWNTs was tested in various organic solvents using UV-Vis, photoluminescence Raman spectroscopic techniques, and SEM, AFM imaging. Characterization results show, that dispersion is selective for small semiconducting (6,5), (5,6), and (7,6) tubes. Furthermore, Hexane induced SWNTs release experiments were undertaken for the reversible dispersion process to attain “dispersant-free” SWNTs. which could be turned into a very useful technique applicable in material preparation and device fabrication where “additive-free” SWNTs are desired after solution-phase processing (*e.g.*, dispersion) in order to maximize electronic and/or optoelectronic performances.

Acknowledgements

It is a pleasure for me to express my sincere gratitude and respect to my supervisor, Prof. Yuming Zhao, for his genuine guidance and support during my research at Memorial University. Dr. Zhao has been a great mentor and very generous in sharing his rich and valuable knowledge with me. I am truly grateful to him from the bottom of my heart.

I would like to acknowledge my supervisory committee members, Prof. David Thompson and Prof. Christopher Flinn, for their encouragement and helpful suggestions during my research work. I am so grateful to Prof. Alex Adronov, at McMaster University, and his Ph.D student, Mr. Shuai Liang (who obtained his Master's in our group), who have been much appreciated collaborators with our group.

I would also like to thank Dr. Karimulla Mulla and Dr. Guang Chen for their training and invaluable suggestions during my study. I also would like to extend my thanks to all my lab mates, especially to Master's student Ms. Kathleen Woolridge, for her kind help and discussions over the years. Special thanks to all other members of the organic chemistry division for their enthusiasm and team spirit in this program.

I would like to expand my thanks to include all the professors of the organic chemistry department at Memorial, including Prof. Paris Georghiou, Prof. Graham Bodwell, and Prof. Sunil Pansare, for their advice and well-considered suggestions during my study. Finally, I would like to thank my wonderful family and my daughter for their unconditional love and support throughout the course of my program.

Table of Contents

Title	I
Abstract	II
Acknowledgements	III
Tables of Contents	IV
List of Figures	VIII
List of Schemes	XV
List of Tables	XVI
List of Symbols, Abbreviations and Acronyms	XVII

Chapter 1

Introduction	1
1.1. A brief introduction to carbon nanotubes.....	1
1.2. Functionalization of CNTs.....	8
1.2.1. Covalent functionalization.....	8
1.2.2. Non Covalent functionalization.....	17
1.2.2.1. Surfactants as dispersants.....	17
1.2.2.2. Aromatic molecules as dispersants.....	19
1.2.2.3. Biomolecules as dispersants.....	25
1.2.2.4. Polymers as dispersants.....	27
1.3. Outline of the thesis.....	35

1.4. References.....	36
----------------------	----

Chapter 2

Dithiafulvenyl-Functionalized Phenylacetylene Polymers: Synthesis and Characterizations	43
2.1. Objectives of this project.....	43
2.2. Introduction to molecular design.....	44
2.3. Results and discussion.....	49
2.3.1. Synthesis of DTF-phenylacetylene building block 37.....	49
2.3.2. Synthesis of endcapping reagent 53.....	53
2.3.3. Construction of DTF-functionalized homo-coupled polymer 35 and cross-coupled polymer 36.....	54
2.3.4. GPC Analysis.....	56
2.3.5. Electronic and electrochemical properties of polymers 35 and 36.....	57
2.4. Experimental.....	59
2.5. References.....	74

Chapter 3

Dithiafulvenyl-grafted phenylacetylene polymers as selective and reversible dispersants for single-walled carbon nanotubes	76
--	----

3.1. Characterization Techniques.....	77
3.1.1. Absorption Spectroscopy.....	77
3.1.2. Photoluminescence excitation (PLE) mapping studies.....	80
3.1.3. Scanning Electron Microscopy (SEM).....	82
3.1.4. Atomic force microscopy (AFM).....	82
3.1.5. Thermogravimetric analysis (TGA).....	83
3.1.6. Raman Spectroscopy.....	84
3.2. SWNTs –polymer Dispersion Studies.....	87
3.2.1. Characterization of DTF-polymer/SWNTs Complexes.....	89
3.2.1.1. UV-Vis-NIR Results.....	89
3.2.1.2. Photoluminescence excitation mapping studies.....	97
3.2.1.3. AFM Studies.....	99
3.2.1.4. SEM studies.....	100
3.2.1.5. Raman Spectroscopic Studies.....	102
3.2.1.6. TGA Results.....	106
3.3 Releasing of SWNTs from polymer-SWNT Complexes.....	109
3.4 Conclusion.....	112
3.5 Experimental.....	113
3.6 References.....	113

Chapter 4

An attempt to Synthesize TTFV-Cyclic tetramer	117
4.1. Introduction.....	117

4.2. Conclusion.....	123
4.3. References.....	124

Chapter 5

5.1. Conclusions and Future work.....	125
---------------------------------------	-----

List of Figures

Figure 1.1: Three different types of CNT based on the angle of chiral vector	2
Figure 1.2: Various routes to covalently functionalize pristine CNTs	9
Figure 1.3: Chemical structure of boron-chelated tetra aryl-azadipyrromethene functionalized SWNTs.....	10
Figure 1.4: Functionalized SWNTs with <i>N</i> -acetylglucosamine bivalent derivatives through azomethine ylide 1,3-dipolar cyclo addition.....	12
Figure 1.5: Chemical structure of indolizine functionalized SWNTs (top), and a tapping mode AFM image of indolizine functionalized SWNTs (bottom).....	13
Figure 1.6: Process for assembling SWNTs and gold nano-particles using click Chemistry.....	14
Figure 1.7: Synthesis of PCL-functionalized carbon nanotubes.....	15
Figure 1.8: Chemical structures of surfactants and schematic representation showing the adsorbing of surfactants on the nanotube surface	18
Figure 1.9: Sorting of SWNTs using SC and SDBS encapsulation and UV-NIR- spectrum and Raman spectrum of the bands	19
Figure 1.10: Chemical structures of Newkome-dendronizedperylene tetra- carboxydiimides for SWNTs dispersion.....	20
Figure 1.11: Schematic representation showing the noncovalent functionalization of SWNTs.....	21
Figure 1.12: Chemical structures of pyrene (Py)-substituted phthalocyanines.....	23
Figure 1.13: Chemical structure of zinc porphyrin derivative for SWNTs dispersion...	23
Figure 1.14: Chemical structures of pyrene-based amphiphiles equipped with	

Newkometype dendrimers to solubilize nanotubes.....	25
Figure 1.15: Chemical structure of a phospholipid-dextran conjugate.....	26
Figure 1.16: Molecular modeling of the PPE-PPV tetramer (n = 4) in front (a) and side view (b), showing a helical conformation with a proper cavity size (2.0 nm) to host the (12,6) SWNT. For clarity, the tube is shown in orange color (copied from reference 40 with permission).	28
Figure 1.17: Chemical structure of PmPV.....	29
Figure 1.18: Chemical structure of poly(2,5-dioctyloxy-1,4-phenylene- <i>alt</i> -2,5- thienylene) (POPT).....	29
Figure 1.19: Chemical structure of poly(3-alkylthiophenes) for dispersion studies.....	30
Figure 1.20: (a) CoMoCAT solutions sorted by P3DDT, (b) polymer structures of polythiophenes, (c) optical absorption spectra comparing sorted and unsorted CoMoCAT SWNTs	31
Figure 1.21: Chemical structure of poly[2,7-(9,9-dioctyl-fluorene)- <i>alt</i> -2,5-(3- dodecylthiophene)] (PFT).....	32
Figure 1.22: Chemical structure of copolymers of fluorene and dithieno[3,2-b:20,30-d] pyrrole (DTP).....	33
Figure 1.23: Chemical structure of a photo isomerizable conjugated polymer prepared by the Adronov group, showing <i>cis</i> and <i>trans</i> conformations.	34
Figure 2.1: Molecular structures of aryl-grafted poly(phenylene ethylene)s synthesized by click chemistry.....	45
Figure 2.2: Molecular structure of a TTFV-based polymer reported by the Zhao group previously.....	46

Figure 2.3: Molecular structures of DTF-attached oligomers 31-34	47
Figure 2.4: Molecular structures of target DTF-grafted conjugated polymers 35 and 36 in this chapter.....	48
Figure 2.5: GPC chromatogram of polymer 35 . $M_n = 11523$ g/mol, $M_w = 16944$ g/mol, PDI = 1.47. Experimental conditions: columns: T6000M; standard: polystyrene; sample concentration: 1 mg polymer 35 in 3 mL THF.....	56
Figure 2.6: GPC chromatogram of polymer 36 . $R_t = 7.1$, $M_n = 17995$ g/mol, $M_w = 26510$ g/mol, PDI = 1.45. Experimental conditions: columns: T6000M; standard: polystyrene; sample concentration: 1 mg polymer 36 in 3 mL THF.....	57
Figure 2.7: (A) UV-Vis absorption spectra of polymers 35 and 36 and DTF precursor 37 measured in CH_2Cl_2 at room temperature. (B) Cyclic voltammograms of 35 , 36 , and 37 measured in CH_2Cl_2 . Electrolyte: Bu_4NBF_4 (0.1 M); working: glassy carbon; counter: Pt wire; reference: Ag/AgCl; scan rate: 200 mV s^{-1}	59
Figure 3.1: Schematic DOS diagrams for metallic and semiconducting single-walled carbon nanotubes based on a simple band theory model. Allowed optical transitions are illustrated as vertical arrows	79
Figure 3.2: An exemplar electronic absorption spectrum of HiPCO single-walled carbon nanotubes	80
Figure 3.3: PLE map of HiPCO SWNTs dispersed with SDBS in water.....	81
Figure 3.4: a) vibration of carbon atoms in radial direction b) vibrations along the	

nanotube axis, and along the circumference direction	86
Figure 3.5: A representative Raman spectrum of SWNTs	86
Figure 3.6: Schematic illustrations of three design strategies for SWNT dispersion: (A) π -stacking, (B) helical wrapping, and (C) centipede wrapping.....	87
Figure 3.7: Geometry of the trimer of 35 wrapped around a (6, 6) nanotube optimized by the MMFF force field (Note that the $SC_{10}H_{21}$ groups were replaced by hydrogens to save computational cost). (A) Side view, (B) front view. Wrapping angles: $\alpha = 19^\circ$, $\beta = 90^\circ$	89
Figure 3.8: UV-Vis-NIR spectrum of HiPCO and CoMoCAT SWNTs dispersed with polymers 35 (A) and 36 (B) in toluene.....	90
Figure 3.9: UV-Vis-NIR spectrum of HiPCO SWNTs dispersed with polymer 35 in $CHCl_3$	91
Figure 3.10: UV-Vis-NIR spectrum of HiPCO SWNTs dispersed with polymer 35 in chlorobenzene.....	91
Figure 3.11: UV-Vis-NIR spectrum of HiPCO SWNTs dispersed with polymer 35 in CH_2Cl_2	92

Figure 3.12: UV-Vis-NIR spectrum of CoMoCAT SWNTs dispersed with polymer 35 in chlorobenzene, CHCl ₃ , and CH ₂ Cl ₂	93
Figure 3.13: UV-Vis-NIR spectrum of HiPCO SWNTs dispersed with polymer 36 in CHCl ₃	94
Figure 3.14: UV-Vis-NIR spectrum of HiPCO SWNTs dispersed with polymer 36 in chlorobenzene.....	94
Figure 3.15: UV-Vis-NIR spectrum of HiPCO SWNTs dispersed with polymer 36 in CH ₂ Cl ₂	95
Figure 3.16: UV-Vis-NIR spectrum of CoMoCAT SWNTs dispersed with polymer 36 in CHCl ₃	95
Figure 3.17: UV-Vis-NIR spectrum of CoMoCAT SWNTs dispersed with polymer 36 In CH ₂ Cl ₂	96
Figure 3.18: UV-Vis-NIR spectrum of CoMoCAT SWNTs dispersed with polymer 36 in chlorobenzene.....	96
Figure 3.19: PLE maps of HiPCO dispersed in CH ₂ Cl ₂ polymer 36	97

Figure 3.20: PLE maps of CoMoCAT dispersed in CH ₂ Cl ₂ with polymer 35	98
Figure 3.21: AFM image of the suspension of polymer 35 and HiPCO SWNTs drop-cast on a freshly cleaved mica substrate (tapping mode).....	99
Figure 3.22: AFM image of the suspension of polymer 36 and HiPCO SWNTs drop-cast on a freshly cleaved mica substrate (tapping mode).....	100
Figure 3.23: SEM image of the complex of polymer 36 and HiPCO SWNTs after solvent evaporation.....	101
Figure 3.24: SEM image of the complex of polymer 35 and HiPCO SWNTs after solvent evaporation.....	102
Figure 3.25: Raman spectra of polymer 35 complexed with HiPCO-SWNTs (RBM mode) vs Raw HiPCO SWNTs.....	104
Figure 3.26: Raman spectra of polymer 35 complexed with HiPCO-SWNTs (tangential mode) vs Raw HiPCO SWNTs.	104
Figure 3.27: Raman spectra of polymer 35 complexed with CoMoCAT-SWNTs (RBM mode) vs Raw CoMoCAT SWNTs.....	105

Figure 3.28: Raman spectra of polymer 35 complexed with CoMoCAT-SWNTs (tangential mode) vs Raw CoMoCAT SWNTs.....	105
Figure 3.29: TGA profiles of polymer 35 , polymer 35 /CoMoCAT nanotube complexes, raw CoMoCAT nanotubes, and released CoMoCAT nanotubes. Scan rate: 10 °C/min.....	106
Figure 3.30: (A) Photographic image of HiPCO SWNTs dispersed in a CHCl ₃ solution of polymer 35 (1.5 mg/mL). (B) Photographic image showing HiPCO SWNTs precipitated out of the solution of polymer 35 after addition of an equal volume of hexanes. (C) Raman spectra ($\lambda_{\text{ex}} = 785 \text{ nm}$) of raw HiPCO SWNTs, HiPCO SWNTs dispersed with polymer 35 , and HiPCO SWNTs released from polymer 35 after addition of hexanes the solution.....	111
Figure 4.1: Structure of TTFV-phenylacetylene trimer macrocycle 54	118
Figure 4.2: Structure of the target TTFV-phenylacetylene tetramer macrocycle 55	119

List of Schemes

Scheme 2.1: Click approach for DTF-phenylacetylene building block 37	49
Scheme 2.2: Synthesis of <i>S</i> -decyl thione 41	50
Scheme 2.3: Synthesis of aldehyde 43	50
Scheme 2.4: Synthetic route to dithiafulvene acetylene building block 38	51
Scheme 2.5: Synthetic route to diazido-precursor 39	52
Scheme 2.6: Synthetic route to DTF-phenyl acetylene monomer 37	53
Scheme 2.7: Synthesis of iodoarene 53	54
Scheme 2.8: Synthesis of polymer 35 and 36	55
Scheme 4.1: Synthetic route for acetylenic bis-TTFV dimer 59	120
Scheme 4.2: Attempted synthesis of the TTFV-phenylacetylene tetramer macrocycle 55 through homocoupling macrocyclization reaction.....	122

List of Tables

Table 3.1: TGA data of polymer 35 , polymer 35 /SWNT complexes, raw SWNTs, and released SWNTs measured at 137 °C and 400 °C.....	108
---	-----

List of Symbols, Nomenclature or Abbreviations

δ	chemical shift
AFM	atomic force microscopy
aq	aqueous
conc	concentrated
CoMoCAT	cobalt-molybdenum catalyzed
CNTs	carbon nanotubes
calcd	calculated
CV	Cyclic voltammetry
d	deuterium (in NMR solvent, e.g. THF-d8)
d	doublet
E _{pa}	potential of anodic peak
E _{pc}	potential of cathodic peak
equiv	equivalents
Et ₃ N	triethylamine
FET	field effect transistor
FTIR	fourier transform Infrared (spectroscopy)
g	gram(s)
GPa	gigapascal
h	hour(s)
HiPCO	high pressure CO disproportionation
IR	infrared (spectroscopy)

J	(in NMR) coupling constant (Hz)
LED	light emitting diode
LUMO	lowest unoccupied molecular orbital
m	multiplet
m/z	mass to charge ratio
HOMO	highest occupied molecular orbital
MALDI-TOF	matrix assisted laser desorption/ionization–time of flight
Me	methyl
mg	milligram(s)
MHz	megahertz
min	minute(s)
M ⁺	mass peak
Me	methyl, CH ₃
mL	milliliter(s)
MeCN	acetonitrile
mmol	millimole(s)
mol	mole(s)
MWNT	multi-walled nanotube
nm	nanometer
NMR	nuclear magnetic resonance (spectroscopy)
p	para
Ph	phenyl
ppm	parts per million

Q	quartet (in NMR)
rt	room temperature
s	second(s) or singlet
SDS	dodecylsulfonate
SWNT	single-walled nanotube
t	triplet
TFA	trifluoroacetic acid
THF	tetrahydrofuran
TLC	thin layer chromatography
TMS	trimethylsilyl
TMSA	trimethylsilylacetylene
TPa	terapascal
TTFV	tetrathiafulvalene vinylogue
UV-Vis	ultraviolet-visible
UV-Vis-NIR	ultraviolet-visible-near infrared (spectroscopy)
V	volt(s)

Chapter 1

Introduction

1.1 A brief introduction to carbon nanotubes

In 1991 Ijima and co-workers reported a new type of carbon nanostructures, termed carbon nanotubes (CNTs),¹ and this fascinating discovery immediately captured and inspired the imagination of the scientific community, resulting in a great deal of research dedicated to the study of the structural, mechanical, electronic, thermal and optical properties of CNTs, in particular, single-walled carbon nanotubes (SWNTs). The unique properties of SWNTs originate from their distinctive molecular structures. In theory, SWNTs can be thought as a sheet of graphene rolled into a cylindrical tube with a nanometer-size diameter (Figure 1.1). The possible ways of rolling up the graphene sheet can be expressed with the help of two integers, n and m . Each possible integer pair denotes a particular type of SWNT with specific chirality as well as physical and electronic properties. When the two integers are the same ($n=m$), the nanotube is called “*arm chair*”, whereas if one of the integer is zero the corresponding nanotubes is designated as “*zig-zag*”, and if the two integers are not equal ($n \neq m$) then the tube is referred to as “*chiral*”. Electronically, all arm chair ($n=m$) nanotubes are metallic in electronic nature. Zig-zag and chiral nanotubes, however, can be metallic only when the

difference between m and n is a multiple of 3; otherwise, they are semiconducting in nature.

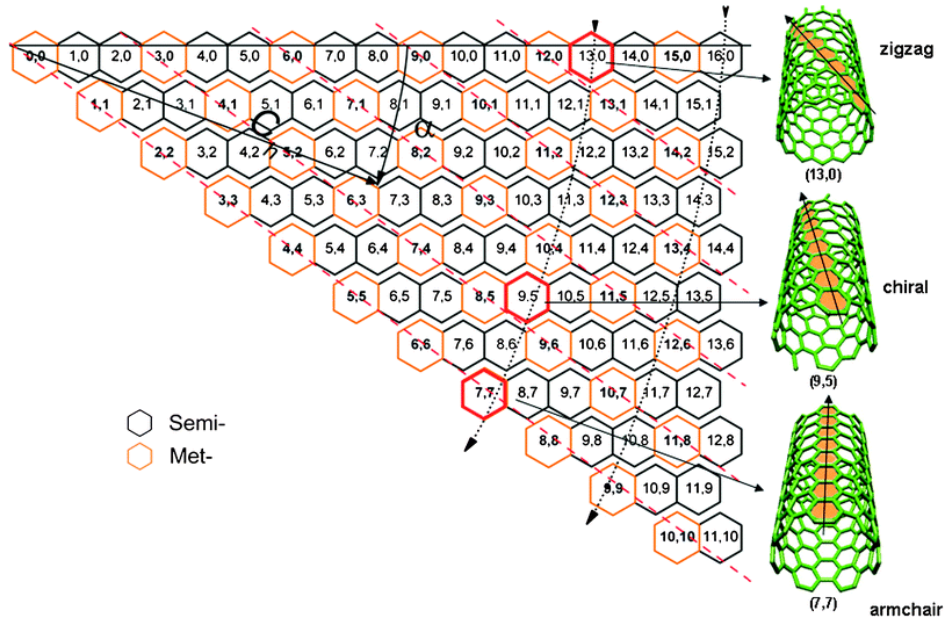


Figure 1.1: Three different types of CNT based on the angle of chiral vector (copied with permission from reference 2a).

Metallic CNTs have a nearly one-dimensional electronic structure and are able to carry high currents because of their very low resistance. Calculated current carrying capacity of individual SWNTs is about 10^9 A cm^{-2} , which is 10 to 1,000 times higher than that of copper. Semiconducting CNTs, on the other hand, exhibit excellent charge-carrier mobility (better than silicon), which make them ideal candidates for the applications of nanoelectronics. Apart from the extraordinary electronic characteristics, CNTs also show superior thermal, superconducting, and mechanical properties. For example, the measured room-temperature thermal conductivity for individual CNTs (3,000W/m K) is

greater than that of natural diamond and in-plane graphite (both 2,000 W/m K) which are generally thought to be the materials with the highest thermal conductivity at moderate temperatures.^{2b} According to a report by Sheng,³ SWNTs with small diameters also possess superconducting behaviour at low temperatures. Experimental calculations show that small-diameter SWNTs have high Young's moduli and tensile strengths. The calculated Young's modulus for an individual nanotube is about 0.64 TPa.² In particular, small-diameter nanotubes have the ability to extend elastically by ca. 5.8% before breaking, as they show strength up to 37 GPa, which is comparable to silicon carbide nanorods.² Moreover, the elastic buckling nature of carbon nanotubes makes them exceedingly tough materials and can tolerate 5 to 10 times more strain energy than silicon carbide rods. The density-normalized modulus and strength of these typical SWNTs are about 19 and 56 times greater than that of the steel wire.²

The extraordinary properties of CNTs have led to very promising applications in various fields. Owing to their high electrochemically accessible surface area, high electronic conductivity, and remarkable mechanical properties, CNTs have been widely applied as supercapacitors in devices that use electrochemical double-layer charge injection. Usually, the capacitance of an electrochemical device depends on the charge separation between the electrode and electrolyte. In ordinary dielectric capacitors, the separation occurs be at the micrometer level. For CNT-capacitors, however, the separation can be reduced to a range of only a few nanometers. The high nanotube surface area accessible to the electrolyte leads to very large capacitances (15-200 F/g)

making them ideal candidates for supercapacitors. The capacitances of CNTs result in large amounts of charge injection when only a few volts are applied.⁴ Moreover, the supercapacitors can be operated at very high temperatures given the high thermal stability of CNTs.^{4,5} CNT-based supercapacitors can be used in applications where much higher power capabilities than batteries and much higher storage capacities than ordinary capacitors are required; for instance, hybrid electric vehicles that can provide rapid acceleration.

As a result of their small diameters and long aspect ratios, CNTs can generate high local fields under applied potentials. These local fields cause emission of electrons from the tips of nanotubes, making them effective field emission electron sources.⁶ Considering this phenomenal characteristic of nanotubes, in recent years, industrial and academic research on electronic devices has extensively employed CNTs as field emission electron sources for flat panel displays, lamps, gas discharge tubes providing surge protection, and X-ray and microwave generators. The manufacturing of nanotube field-emitting surfaces is relatively easy and the resulting devices show excellent performances, including stable emission, long lifetimes, and low emission threshold potentials.⁶ Unlike tungsten and molybdenum tip arrays, they do not deteriorate in moderate vacuum (10^{-8} torr). The current density obtained is about 4 A cm^{-2} , which is higher than the 10 mA cm^{-2} needed for flat panel field emission displays and 0.5 A cm^{-2} required for microwave power amplifier tubes.⁷ The extraordinary electronic properties of CNTs have led to very promising applications in the design and fabrication of

nanometer-sized electronic devices such as nanotube field-effect transistors (FETs), single-electron tunneling transistors, rectifiers and three-terminal and four-terminal electronic devices.⁸

In addition to the fascinating applications in electronics, non-metallic nanotubes have been often used in various chemical and bio-sensors, wherein the extremely small sizes of CNTs are taken advantage of as the key sensing element to produce ultrasensitive and fast responses. Recently, Balasubramanian *et al.* have demonstrated a highly sensitive label-free biosensor for the detection of nucleic acids, which was based on the use of CNT field-effect devices. The sensor was reported to be capable of detecting as low as 2,000 copies of deoxyribonucleic acid (DNA) molecules in a 30 microliter sample droplet.⁹ Another major commercial application of CNTs is to function as the conducting components in polymer composites. Depending on the polymer matrix, conductivities of 0.01 to 0.1 S/cm can be obtained upon 5% loading of CNTs. Incorporation of CNTs into plastics can potentially provide structural materials with dramatically increased modulus and strength.¹⁰ Most recently, the applications of CNTs have been greatly expanded in the fields of materials science and chemical engineering. Popular research areas emerged recently include solar cells, fuel cells, memories, separation membranes and filters, purification systems, sensors, clothes, hydrogen storage, just to name few.¹¹ The future technology is expected to be mostly built on advances made in nanomaterials. CNTs as one of the most important nanoscale building blocks should continuously drawn considerable attention from academic and industrial communities.

CNTs can be produced in large quantities using various methods. In the early age of CNT production history, high temperature preparation techniques such as arc discharge and laser ablation/evaporation of carbon were successfully used.¹¹ These methods involve the condensation of hot gaseous carbon atoms generated from the evaporation of solid carbon. The costly equipment and high energy consumption for these methods, however, make them only applicable on the laboratorial scale. Recently, these methods have been gradually replaced by the low-temperature chemical vapour deposition (CVD) technique, which can be easily scaled up to industrial production levels. In the past few years, some non-standard approaches have also been successfully established such as liquid pyrolysis and bottom-up organic synthesis for the production of high-quality CNTs. Despite the advancements made, many researchers so far still believe that the laser ablation method is superior to many others in terms of growing SWNTs with high quality and high purity. The laser ablation method was first developed by Smalley's group at Rice University.¹² Further improvements were made by the Thess and Rao groups, who used a double-beam laser as the energy source for CNT production.¹¹ Recently, the Resasco group developed a method to produce the so-called CoMoCAT nanotubes, which involves CO disproportionation (decomposition into C and CO₂) at 700 to 950 °C to grow SWNTs with a narrow distribution of tube diameters.¹¹

So far, no matter what CNT preparation method is to be used, the CNTs obtained invariably contain a number of impurities whose types and amounts depend on the technique applied. Most of the above mentioned techniques produce powders comprised

of only a small fraction of CNTs together with a significant amount of carbonaceous particles such as nanoscale crystalline graphite, amorphous carbon, fullerenes, and different metals (typically Fe, Co, Mo or Ni) that were introduced as catalysts during the synthesis. Many analytical techniques have been developed to characterize the structure, purity and chirality of CNTs, such as UV-Vis-NIR, photoluminescence, Raman spectroscopy, and thermogravimetric analysis (TGA). Collectively, these methods provide a comprehensive characterization on the purity and structural integrity of SWNTs. As discussed above, the properties of SWNTs vary with the individual tube length, diameter and chirality. Unfortunately, all known methods produce SWNTs as mixtures of tubes with various chiral indices rather than a single chirality. Certain applications of SWNTs are therefore impeded by the unavailability of a certain type of SWNTs from commercial sources. In addition, as-produced SWNTs have a strong tendency towards bundling and aggregation due to van der Waals intertube attractions, rendering pristine SWNTs insoluble in most organic and aqueous solvents. The poor solubility and processability thus impose a tremendous hurdle to the purification of SWNTs after the initial production phase. Therefore, one of the most fundamental challenges in the current SWNT research is how to develop an effective method(s) to improve the solubility of nanotubes and to efficiently separate or enrich particular types of SWNTs with homogeneous structures (*e.g.*, diameter, length), electronic types (*i.e.*, semiconducting, metallic), or chiral parameters.

1.2 Functionalization of CNTs

1.2.1 Covalent functionalization

One of the most promising routes to improve the solubility and processability of CNTs relies on chemical functionalization of CNTs. The functionalization methods are generally divided into two categories, covalent and non-covalent approaches. Covalent functionalization can be done by attachment of functional groups to the defect sites or termini of nanotubes, or direct linkage of functional groups onto the sidewalls of nanotubes. Figure 1.2 shows the schematic of various popular covalent functionalization routes, including carboxylation, fluorination, ozonolysis, osmylation, derivatization with azomethine ylides, radical addition, and halogenation. These reactions chemically modify the molecular structures of pristine SWNTs, bringing about not only improved solution-phase processability but also novel chemical and supramolecular properties to the CNTs.¹³

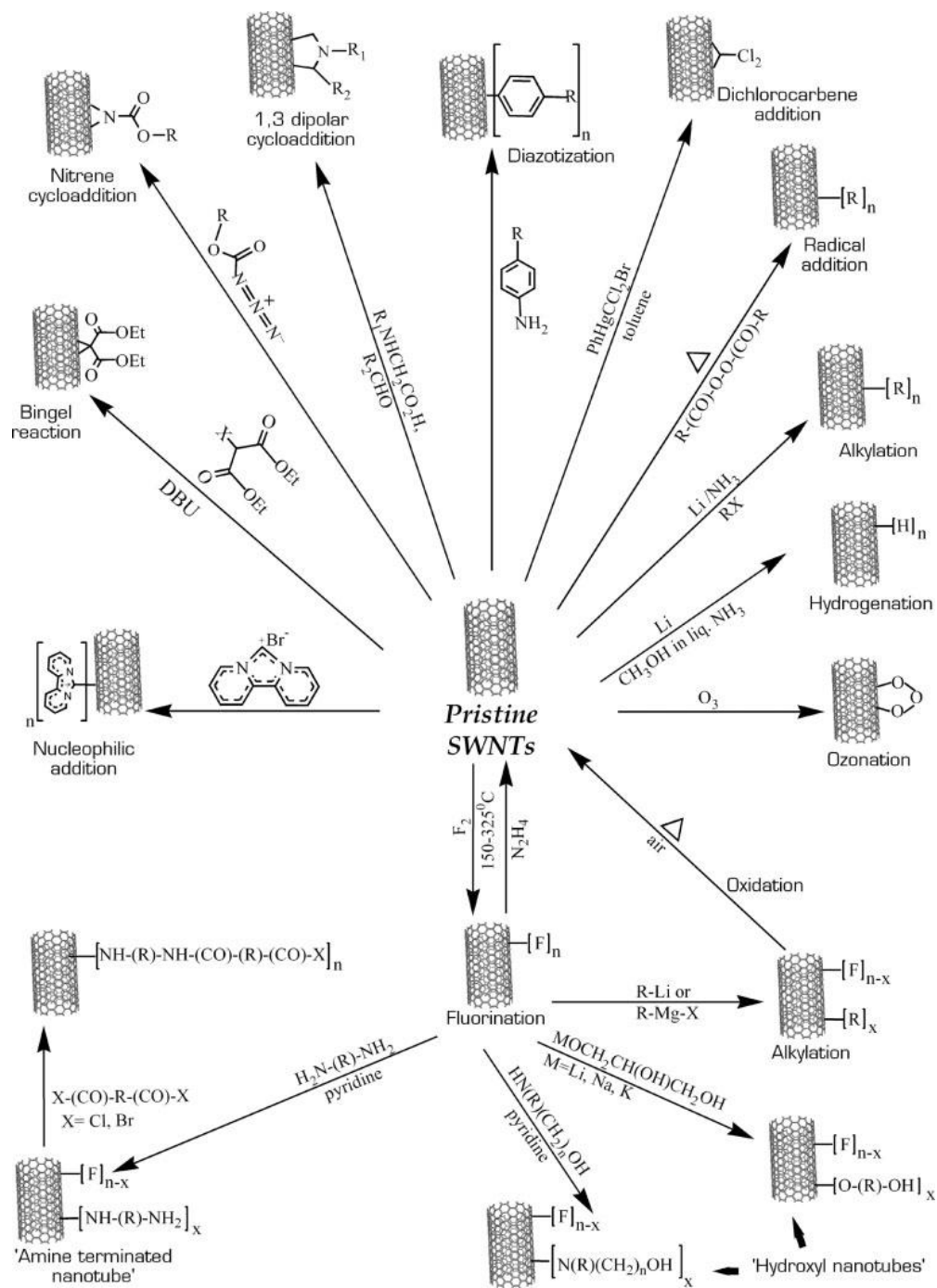


Figure 1.2: Various routes to covalently functionalize pristine CNTs (copied with permission from reference 13).

The properties of covalently functionalized SWNTs **1** were characterized by a number of spectroscopic/ microscopic techniques. The electronic interactions between the boron azadipyrromethene groups (electron donors) and SWNTs (electron acceptors) were investigated by steady-state absorption and fluorescence spectroscopy, as well as transient absorption spectroscopy. The experimental results verified that efficient electron transfer took place from the photo-excited boron azadipyrromethene to SWNTs, and the resulting radical ion pair state has a relatively long lifetime (1.2 ns). This finding suggests that SWNT-based donor-acceptor systems could be used as active building components in organic photovoltaic devices.

Besides the carboxylation of CNTs, 1,3-dipolar cycloaddition of azomethine ylides on the side wall of SWNTs has also been a popular strategy to covalently functionalize SWNTs. For example, in a recent work reported by Hong *et al.*, an *N*-acetylglucosamine bivalent derivative was covalently attached to SWNTs through azomethine ylide 1,3-dipolar cycloaddition in a high efficiency. The resulting glycosylated SWNTs **2** (Figure 1.4)¹⁵ could form bio-compatible dispersion in solution, which were successfully used in an *in vivo* imaging application.

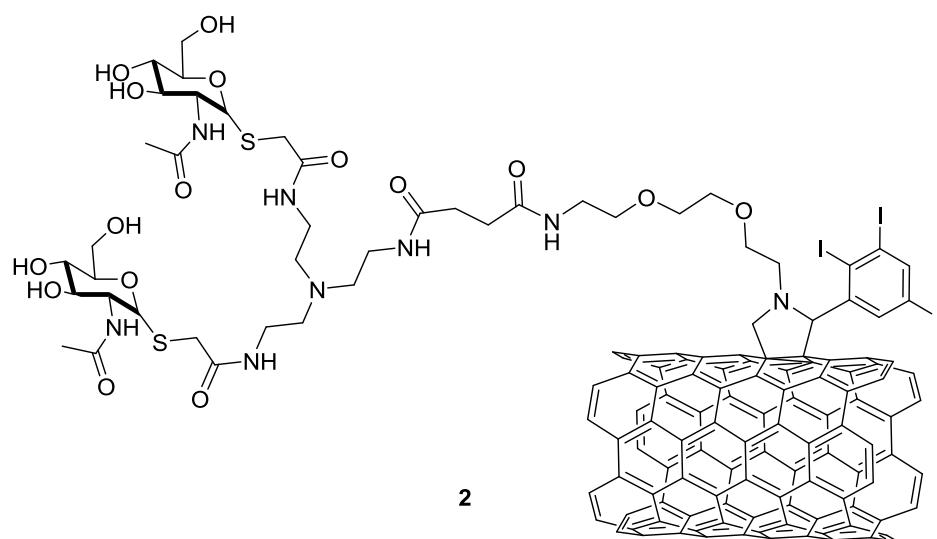


Figure 1.4: Functionalized SWNTs with *N*-acetylglucosamine bivalent derivatives through azomethine ylide 1,3-dipolar cycloaddition.

The Coleman group recently came up with another approach to conduct 1,3-dipolar cycloaddition on SWNTs. The method used pyridinium ylides to react with the SWNT surface, resulting in the formation of an indolizine, an important class of compounds with interesting pharmacological and luminescent properties. Subsequently, the ester groups on the indolizine-functionalized SWNTs were transformed to amides by treatment with *N,N*-dimethylethylenediamine, which were then quaternized by reaction with iodomethane.¹⁶ AFM experiments were performed to investigate the electrostatic interactions of positively charged indolizine functionalized SWNTs with citrate stabilized gold nanoparticles on a mica surface (Figure 1.5), and the results showed that the functional groups were present over the entire length of the carbon nanotube.

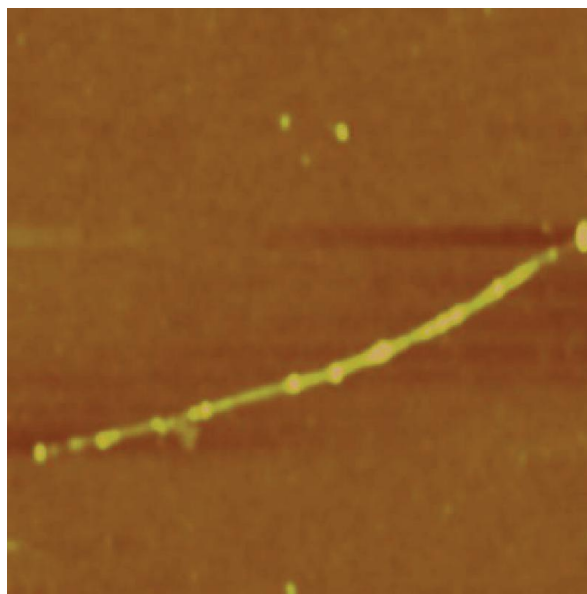
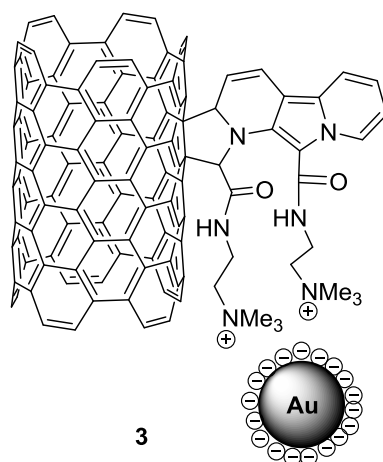


Figure 1.5: Chemical structure of indolizine-functionalized SWNTs **3** (top), and a tapping mode AFM image of indolizine-functionalized SWNTs with gold nanoparticles (bottom). (Copied with permission from the reference 16).

Cho's group devised a "click chemistry"-based strategy to functionalize SWNTs with gold nanoparticles. This method has profound implications for constructing diverse

nanohybrids based on carbon nanotubes and metal nanoparticles. In Cho's experiments, SWNTs were reacted with *p*-aminophenyl propargyl ether through a solvent-free diazotization reaction to produce alkyne-grafted SWNTs.¹⁷ As shown in Figure 1.6, the resulting alkynylated SWNTs were coupled with azido-functionalized gold nanoparticles through the Cu(I)-catalysed azide-alkyne [3+2] cycloaddition (CuAAC) to achieve covalent attachment of gold nanoparticles to SWNTs.

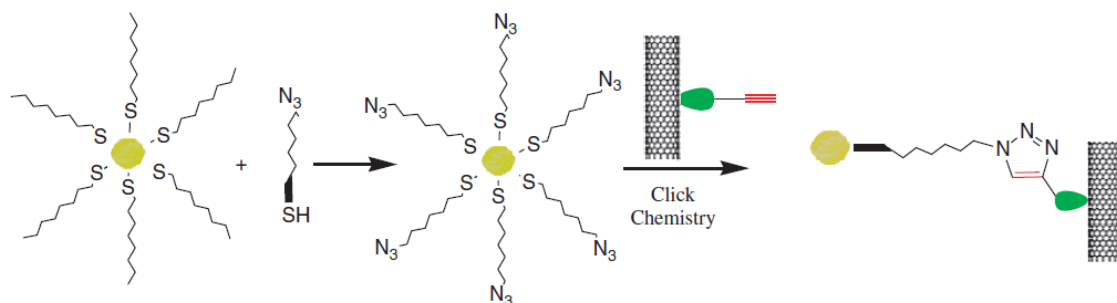


Figure 1.6: Synthesis of gold nanoparticle-functionalized SWNTs via a click strategy developed by Cho (copied with permission from the reference 17).

A similar click strategy has been demonstrated by the same group for the functionalization of multi-wall carbon nanotubes (MWNTs) with various biomolecules such as peptides and polysaccharides. In this work, poly(ϵ -caprolactone) (PCL), a biodegradable and biocompatible polymer, was connected to MWNTs. It was observed that the molecular weight of click-generated PCL was a crucial factor influencing the efficacy of the dispersion and thermal stability of the biologically active SWNT nanocomposites (Figure 1.7).¹⁸

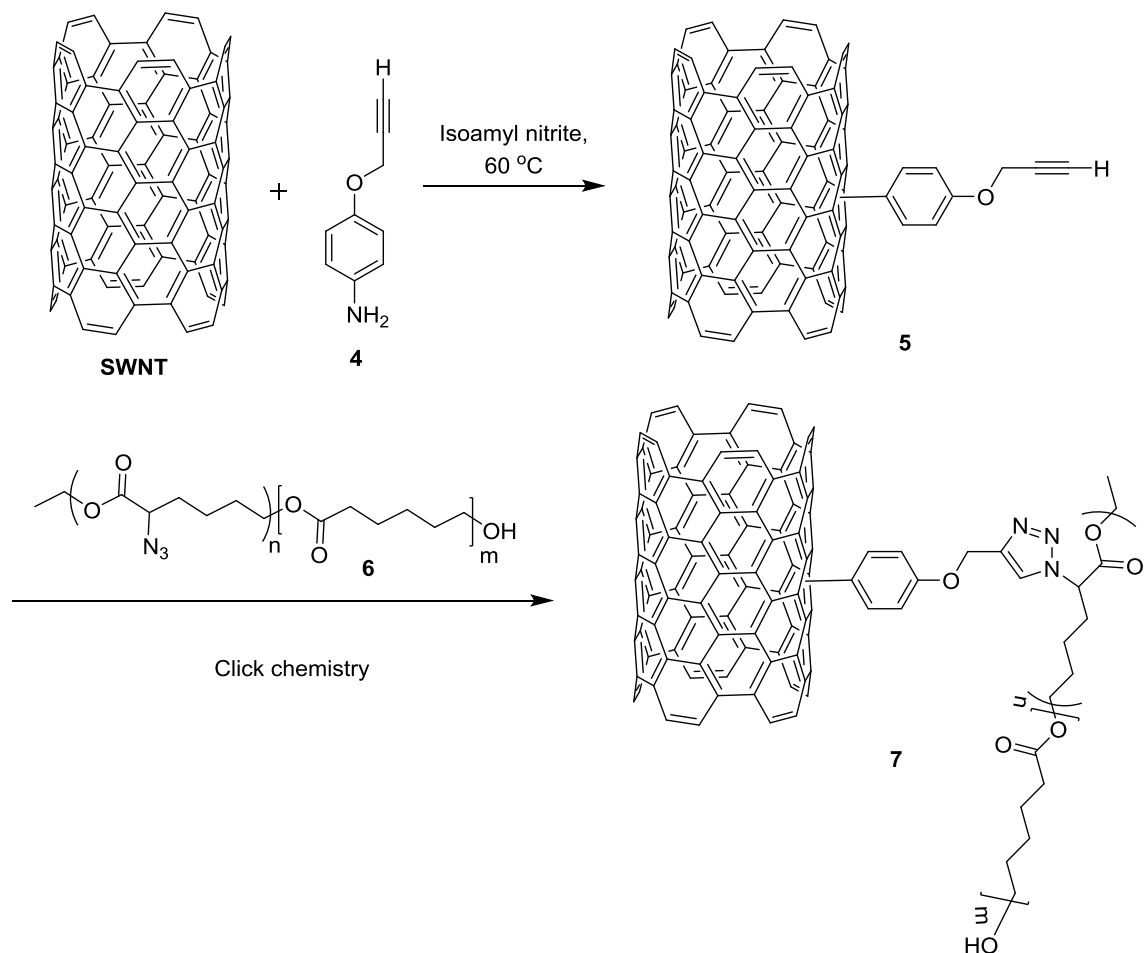


Figure 1.7: Synthesis of PCL-functionalized SWNTs **7** developed by Cho.

Guldi *et al.* recently reported a study of controlled functionalization of CNTs with photo- and electroactive building blocks. A series of electron donor–acceptor systems based on SWNTs and porphyrins was prepared by covalent functionalization of SWNTs with zinc porphyrins (ZnPs) using click chemistry.¹⁹ Due to the strong electronic coupling between the photo- and electroactive constituents, a rapid excited-state deactivation of ZnP through charge transfer to the nanotubes was observed. This feature indicated that

the SWNT–ZnPs hybrids could be applicable in fabrication of solar energy/electronic devices.

As demonstrated in the above examples, covalent functionalization methods can flexibly introduce a large variety of chemical moieties onto the surface of SWNTs, which in turn greatly facilitate tailoring the properties of the nanotube surface. On the other hand, the covalent approach inevitably results in certain drawbacks with respect to retaining intrinsic electronic, optical, and mechanical properties of SWNTs, since certain carbon atoms on the sidewalls of SWNTs are changed from sp^2 to sp^3 hybridization in forming new covalent bonds. Such a problem can be circumvented by using the noncovalent functionalization approach, in which various chemical species are bound to the surface of SWNTs through noncovalent forces, such as π - π stacking and/or van der Waals interactions. In comparison with the covalent methods, preservation of the desired properties of pristine nanotubes is a substantial advantage for the noncovalent approach. The enormous π -surface of SWNTs can engender significant noncovalent affinity for surfactants, small π -conjugated molecules, polymers, and bio-macromolecules. In the following section, the discussion is focused on SWNT composites or hybrid materials derived from noncovalent functionalization; in particular, the properties of noncovalently functionalized SWNTs are highlighted in terms of improved solubility in various solvents and their applications in the fields of molecular electronics and nanoscience.

1.2.2 Noncovalent functionalization of SWNTs

1.2.2.1 Surfactants as dispersants

The adsorption of ionic and nonionic surfactants is one of the most promising approaches to attain good SWNT solubilization in combination with the preservation of intrinsic electronic and mechanical properties. In order to provide an efficient solubilizing effect, the surfactant should: (i) form a very stable micellar structure around the SWNTs to competes with the strong aggregation of the nanotubes; (ii) posses a polar tail, preferably long and disordered in structure, to provide a large solvation shell to keep the long and rigid nanotubes suspended in the solvent. If the polar tail is charged, the aggregation of SWNTs can be further prevented by columbic repulsions between the surfactant-coated SWNTs.²⁰ As outlined in Figure 1.8, the most commonly used surfactants for SWNT dispersion are sodium dodecyl sulphate (SDS), sodium dodecyl benzenesulphonate (SSBD), and sodium pyrenebutyrate (SPB).

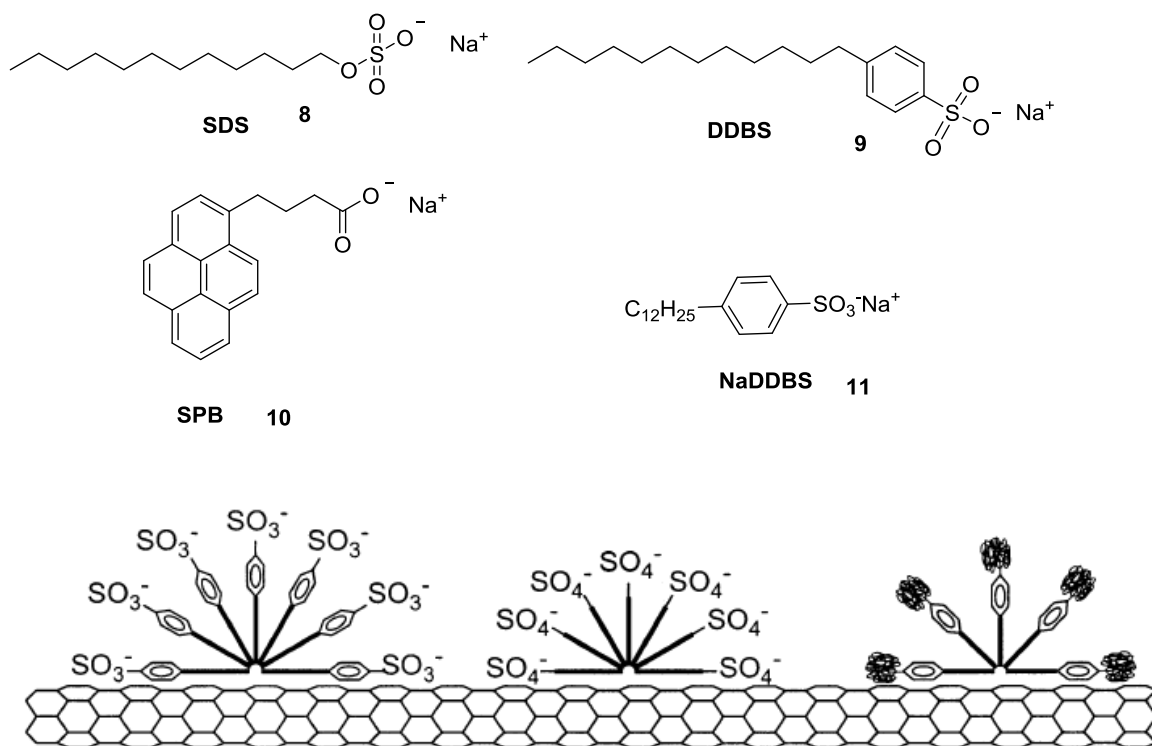


Figure 1.8: Chemical structures of surfactants and schematic representation showing the adsorption of surfactants on the nanotube surface (copied with permission from reference 21).²¹

Arnold *et al.* reported their work on the sorting of carbon nanotubes according to diameter, bandgap, and electronic type with the aid of structure-discriminating surfactants. By this method, they acquired purified SWNTs in which >97% are within a narrow diameter distribution using a scalable technique of density-gradient ultracentrifugation. Furthermore, by using mixtures of two surfactants (SDS and DDBS) which competitively adhere to the SWNT surface, they have achieved optimal separation of metallic and semiconducting SWNTs (Figure 1.9). It was suggested that these

materials could be used in fabrication of thin-film electrical devices containing networked SWNTs.²²

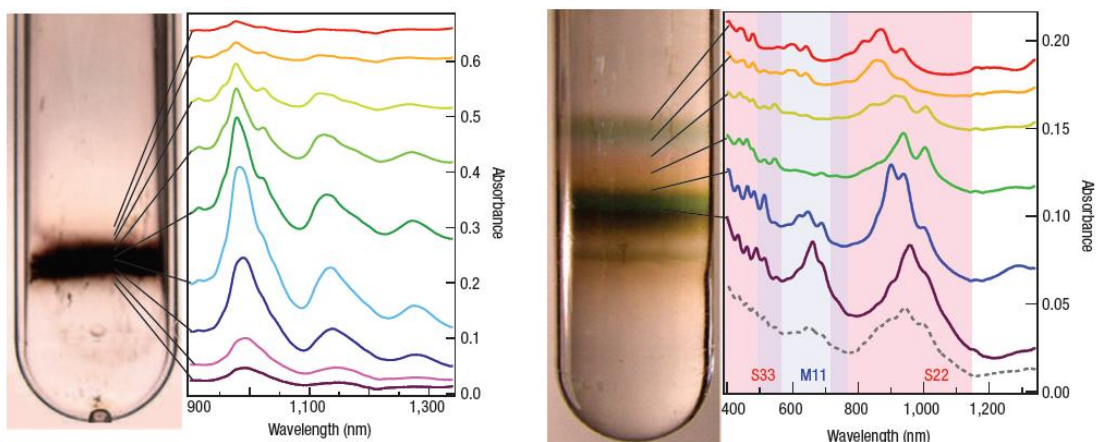


Figure 1.9: Sorting of SWNTs using SC and SDBS encapsulation and UV-NIR-spectrum and Raman spectrum of the bands (copied with permission from reference 22).

1.2.2.2 Aromatic molecules as dispersants

Aromatic polycyclic molecules, such as pyrene, pyrene, and their derivatives^{23,24} are excellent candidates for dispersion/dissolution of SWNTs. A strong and specific interaction between polyaromatics and SWNTs can occur through π -stacking to form supramolecular assemblies.

According to the report by Hirsh *et al.*, a molecule containing a hydrophilic dendritic structure and a nonpolar polyaromatic subunit can strongly interact with the SWNTs, hence acting as an ideal SWNT dispersant. Based on this hypothesis, they

synthesized a series of water-soluble Newkome-type dendritic perylenetetracarboxydiimides²⁵ as aromatic amphiphiles for dispersion of SWNTs in aqueous media. SWNT bundles were successfully broken down by these dendrimers, affording stable suspensions of individualized nanotubes.²⁴ As shown in Figure 1.10, the polycyclic aromatic core of the dendrimers can interact strongly with the nanotube surface via π -stacking, while the solvophilic appendants (R) aid the dissolution of SWNTs in dipolar solvents such as water.

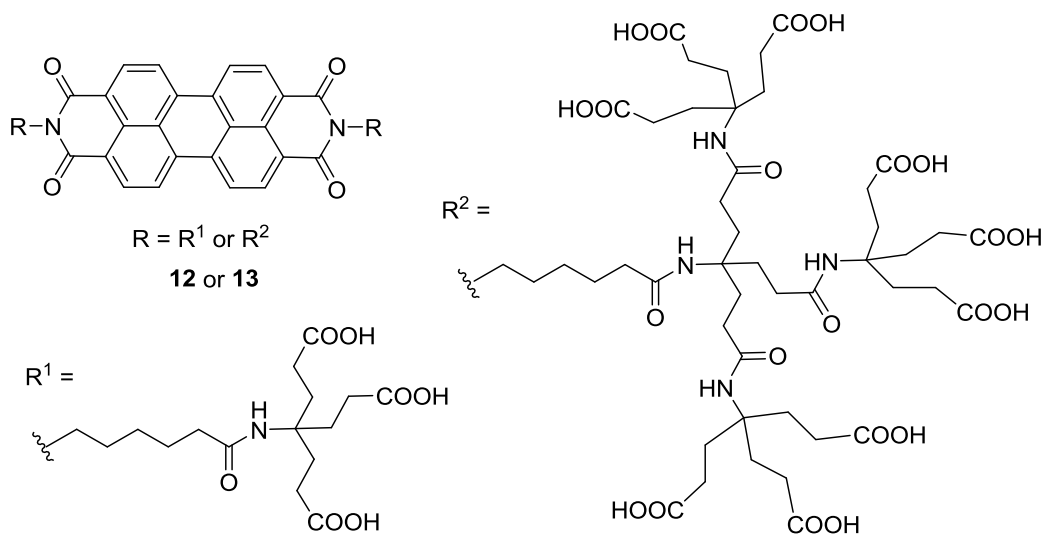


Figure 1.10: Structures of Newkome-dendronized perylenetetracarboxydiimides **12** and **13** as SWNTs dispersants.

In another relevant report, Guldi and Prato prepared a novel nanohybrids by noncovalent functionalization of SWNTs with polycyclic aromatic moieties and their derivatives^{26,27,28} to gain improved solubilities as well as to develop new photovoltaic

materials. The resulting electron donor-acceptor nanocomposites, upon photoexcitation, underwent fast electron transfer followed by the generation of charge-separated species with microsecond lifetimes. The researchers then disclosed the consequences of SWNTs interacting with a pyrene derivative and water-soluble porphyrins based on photophysical and electrochemical analyses.²⁹

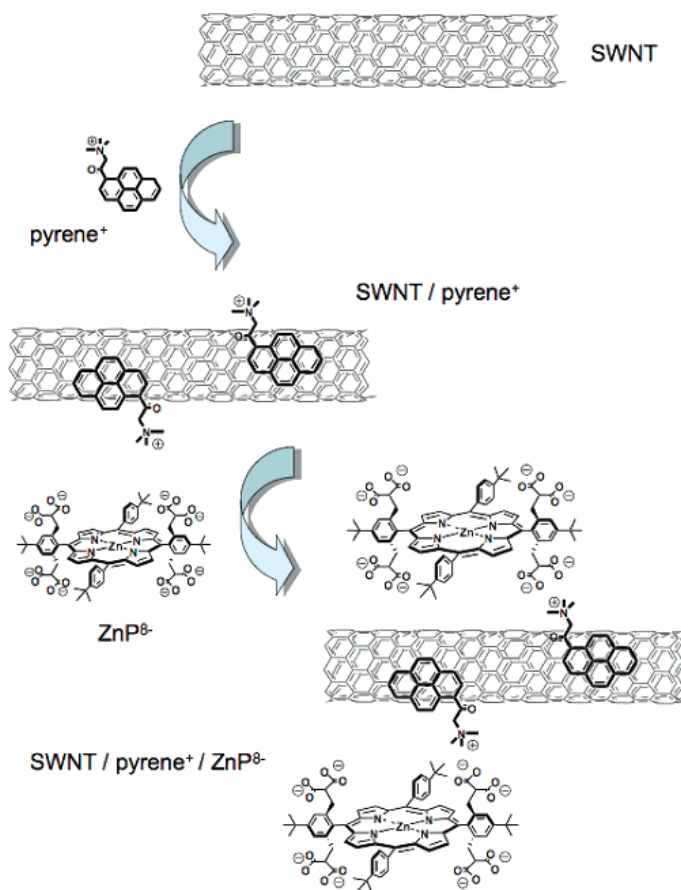


Figure 1.11: Schematic representation showing the noncovalent functionalization of SWNTs with polyaromatic compounds by Guldi and Prato (copied with permission from reference 29).

In the abovementioned research, a charged pyrene derivative, 1-(trimethylammonium acetyl)pyrene, (pyrene^+), was employed to interact with SWNTs, generating a remarkably stable SWNT/ pyrene^+ hybrid through the formation of π - π interactions in aqueous solution (Figure 1.11). This process allowed SWNTs to be suspended in aqueous solution with solubilities as high as 0.20 mg/mL. The SWNT/ pyrene^+ hybrids were covered with positive charges. As a result, they could attract and be associated with negatively charged porphyrin derivatives through electrostatic interactions to form 1:1 electron donor-acceptor nanohybrids. The binding constants were determined to be on the magnitude of 10^4 M^{-1} . Fluorescence and transient absorption investigations in aqueous solution showed that long-lived radical ion pairs (microseconds lifetime) were formed upon electronic excitation of the porphyrin moieties in SWNT/ pyrene^+ /Zn-porphyrin complex.²⁹

In a recent work undertaken by Guldi *et al.*, a new family of pyrene (Py)-substituted phthalocyanines (Pcs), i.e., ZnPc-Py and H₂Pc-Py, were used as assembling units to form stable electron donor/acceptor nanohybrid with SWNTs.³⁰ The pyrene group, owing to its strong ability to adhere to SWNT sidewalls by means of π - π interactions, served as the anchoring group to immobilize metal-free (H₂Pc) as well as zinc (ZnPc) phthalocyanines on the surface of SWNTs (Figure 1.12). Transient absorption experiments of the resulting SWNT suspensions reveal a photoinduced electron transfer from the singlet excited state of ZnPc or H₂Pc to SWNTs. Integration of these nanohybrids into photoactive electrodes could result in stable and reproducible

photocurrents, with efficiency as high as 15 and 23% with and without an applied bias of +0.1 V. These results bode well for the application of the noncovalent functionalized electron donor-acceptor SWNT hybrids in solar energy conversion.

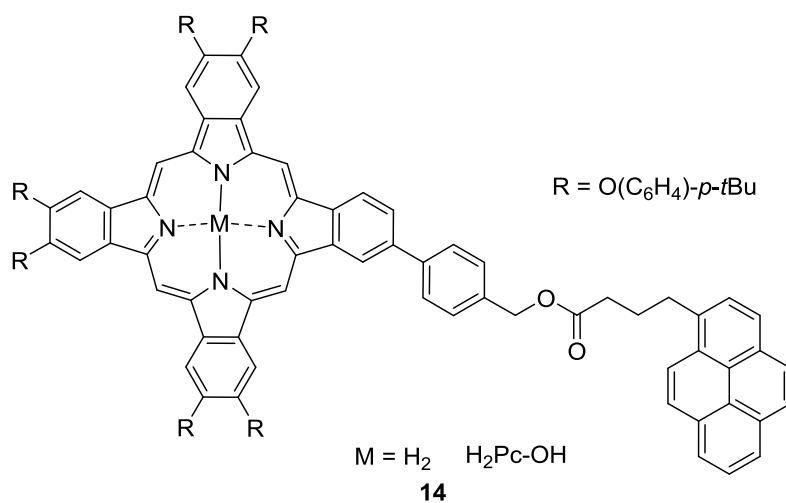


Figure 1.12: Chemical structures of pyrene (Py)-substituted phthalocyanines **14**.

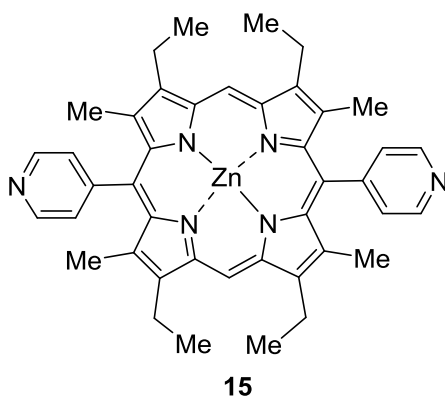


Figure 1.13: Chemical structure of zinc porphyrin derivative **15**.

The Stoddart group fabricated SWNT/FET devices using functionalized SWNTs prepared by noncovalent attachment of a zinc porphyrin derivative to SWNTs (Figure 1.13). They investigated the electron/charge transfer within the donor-acceptor SWNT hybrids.³¹ Usually the porphyrins are considered to be electron donors.²⁶ In this particular case, however, they reported SWNTs as electron donors, and the porphyrin molecules as electron acceptors. The photo-responsiveness of the zinc porphyrin-coated SWNT/FET was investigated by illumination with a light-emitting diode (LED), with the observed shifts of the threshold voltages moving towards positive voltages. This direction of threshold voltage shift indicated that electrons were transferred from SWNTs to the zinc porphyrin. One explanation for this electron-transfer process is that, upon photo-excitation of the zinc porphyrin, some of the electrons that have been transferred to the SWNT in the ground state are transferred back to the zinc porphyrin molecule in the excited state. The magnitude of the photo-induced electron transfer was found to be dependent on both the wavelength and the intensity of applied light, with a maximum value of 0.37 electrons per zinc porphyrin for light at 420 nm and 100 W m^{-2} .

Hirsch *et al.* recently demonstrated that pyrene-based amphiphiles (Figure 1.14) equipped with Newkome-type dendrimers could act as dispersants to yield soluble nanotubes.³² It was observed that the dispersion efficiency was the highest for the first-generation Newkome-dendronized pyrene in basic media (pH 10). Most interestingly, the detailed investigation pointed towards the preferential solubilization of large diameter

nanotubes, indicating fine tuning of substituents can lead to selective dispersion of SWNTs by diameter.

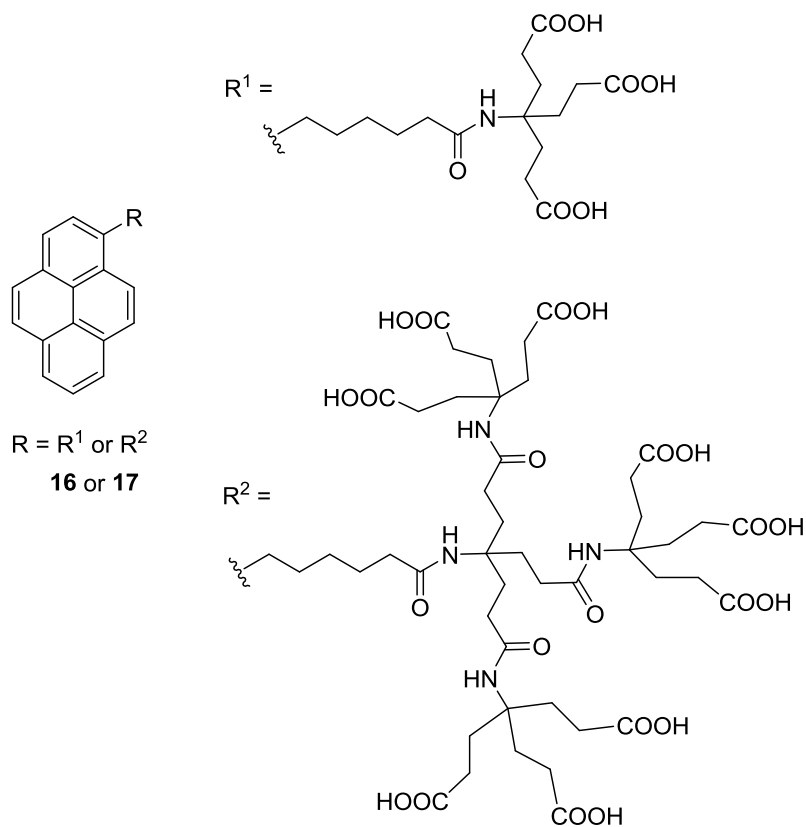


Figure 1.14: Chemical structures of pyrene-based amphiphiles **16** and **17** equipped with Newkometype dendrimers as SWNT dispersants.

1.2.2.3 Biomacromolecules as dispersants

A considerable amount of research has been dedicated to noncovalent functionalization of SWNTs with biomacromolecules in both aqueous and organic solutions. The biomacromolecules employed in the noncovalent functionalization of SWNTs range from

simple monosaccharides, to complex polysaccharides, proteins, enzymes, DNA, and others.³³⁻³⁵

Recently, Dai *et al.* reported the synthesis of a phospholipid-dextran conjugate, in which the phospholipid, 1,2-distearoyl-*sn*-glycero-3-phosphoethanolamine (DSPE), is bound to the reducing end of the dextran at a single point (Figure 1.15).³⁶ The resulting material is able to form self-assemblies easily in water. It also forms stable coatings on the surface of CNTs. These dextran-based nanocoatings showed stability under a wide range of pH levels, salt conditions, and introduction of serum.

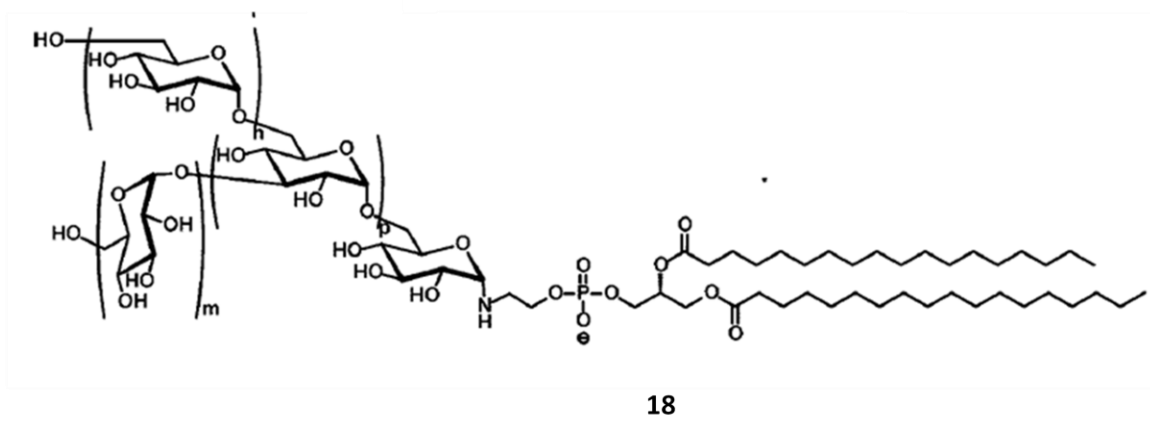


Figure 1.15: Chemical structure of a phospholipid-dextran conjugate **18** (copied from the reference 36 with permission).

The dextran-coated materials also show improved photophysical properties when compared with similar suspensions in PEG functionalized-phospholipids that commonly used thiol-terminated PEG (PEG-SH). Specifically, SWNTs coated with phospholipid-

dextran exhibit a several-fold enhancement in photoluminescence, which could make these dextran-DSPE suspensions useful for *in vivo* imaging and therapeutic applications.³⁶

1.2.2.4 Polymers as dispersants

Polymers, especially π -conjugated polymers,³⁷⁻⁴⁷ have been used as excellent wrapping agents to achieve noncovalent functionalization of SWNTs. The driving forces for the SWNT-polymer interactions include π - π stacking and van der Waals attraction between the conjugated polymers and the surface of SWNTs. Over the past decade, there has been a great deal of research work dedicated to the preparation of polymer-functionalized SWNTs for improved solubility in various solvents and for sorting out specific types of tubes based on homogenous physical and electronic properties.

A very interesting approach was recently reported by Pong *et al.*, which led to the production of SWNTs with narrow diameter distribution using a copolymer, poly(phenylene ethynylene)-*co*-poly(phenylene vinylene), as a diameter-selective dispersant.⁴⁸ The Pong group incorporated a sequential treatment of the HiPCO nanotubes with nitric acid. Spectroscopic techniques as well as microscopic studies have proven that nitric acid could selectively remove the SWNTs with small diameters. The copolymer not only effectively dispersed the carbon nanotubes but also gave rise to good selectivity towards SWNTs with specific diameters and properties. The experimental work was also combined with a molecular modeling study (Figure 1.16), where the PPV-PPE tetramer was predicted to give a proper cavity size for hosting the appropriate

SWNTs. The same group has studied the wrapping of poly[(*m*-phenylene vinylene)-*alt*-(*p*-phenylene vinylene)] (PmPV) **19** (Figure 1.17) around SWNTs, and it was found that the helical conformation of the polymer played a significant role in discriminating the SWNTs.⁴⁰ More specifically, the copolymer could selectively interact with SWNTs of certain diameters, whereas the remaining nanotubes were either weakly covered by the copolymer or not covered at all, leading to their precipitation during the centrifugation procedure. This behavior has been attributed to the size of the cavity created by the helical conformation of the PmPV and also to the copolymer selectivity towards enhanced wrapping around metallic nanotubes in comparison with semiconducting nanotubes.

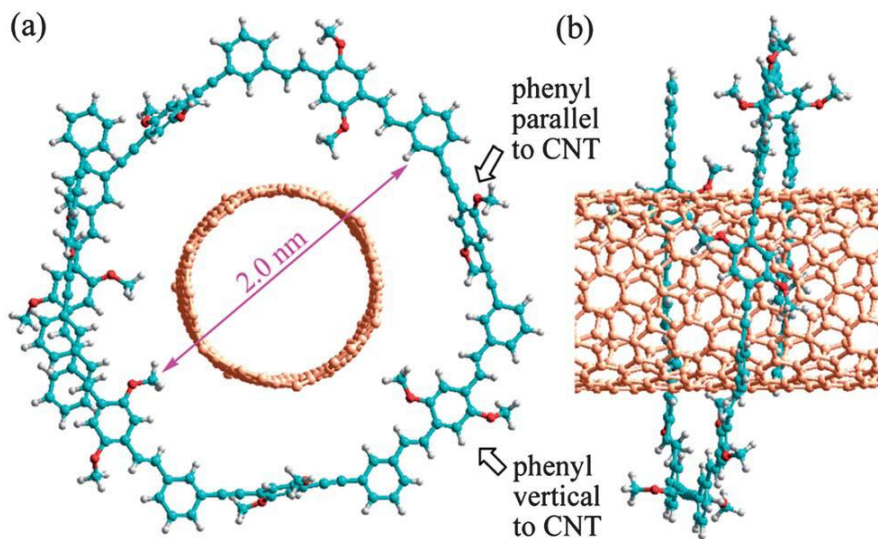


Figure 1.16: Molecular modeling of the PPE-PPV tetramer ($n = 4$) in front (a) and side view (b), showing a helical conformation with a proper cavity size (2.0 nm) to host the

(12,6) SWNT. For clarity, the tube is shown in orange color (copied from reference 40 with permission).

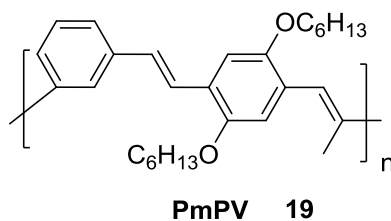


Figure 1.17: Chemical structure of PmPV **19**.

Prato and Guldi reported the synthesis of an electron donor/acceptor nano-composite comprised of suitably functionalized polythiophenes **18** (Figure 1.18) associated with SWNTs through van der Waals and electrostatic interactions on photoactive ITO electrodes.⁴⁹ The chromophore-functionalized polymer played the role of electron donors, while SWNTs acted as electron acceptors. The resulting composite layers provided promising photoconversion efficiencies and the finding is considered innovative for the facile preparation of materials exhibiting enhanced current performance.

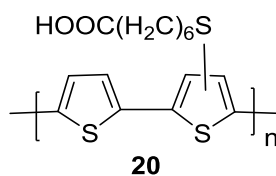


Figure 1.18: Chemical structure of poly(2,5-dioctyloxy-1,4-phenylene-*alt*-2,5-thienylene) (POPT) **20**.

Another flexible conjugated polymer, poly-(2,5-dioctyloxy-1,4-phenylene-*alt*-2,5-thienylene) (POPT) (**21**, Figure 1.19) was reported by Guldi *et al.* to suspend SWNTs in solution.⁵⁰ This POPT/SWNTs system exhibited excellent stability in solution and at the air–water interface. Coating of those stable dispersions on solid substrates was done through the Langmuir–Blodgett (LB) technique to successfully yield composite thin films.

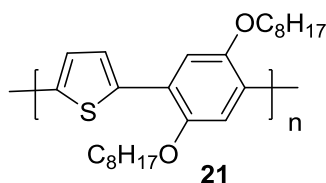


Figure 1.19: Chemical structure of poly(3-alkylthiophenes) **21**.

Another interesting category of conjugated polymers for SWNTs dispersions is the poly(3-alkylthiophene)s due to their solubility and conductive properties under specific conditions. For example, very recently Wang *et al.* reported⁵¹ a high-yielding method to selectively disperse semiconducting CoMoCAT (CO disproportionation on Co-Mo catalysts) single-walled carbon nanotubes (SWNTs) with regioregular poly(3-alkylthiophenes) polymers (Figure 1.20b). The dispersion yield was directly correlated to the length of the alkyl side chains in the polymer. Molecular dynamics simulations in explicit toluene (real toluene molecules) indicated that polythiophenes with longer alkyl side chains bind strongly to SWNTs, due to the increased overall surface contact area with the nanotube. Furthermore, the sorting process selectively enriched smaller diameter

CoMoCAT SWNTs with larger bandgaps, which is ideal for solar cell applications. Additionally, the sorted CoMoCAT SWNTs were employed in the fabrication of thin-film transistors with excellent uniformity and device performance.

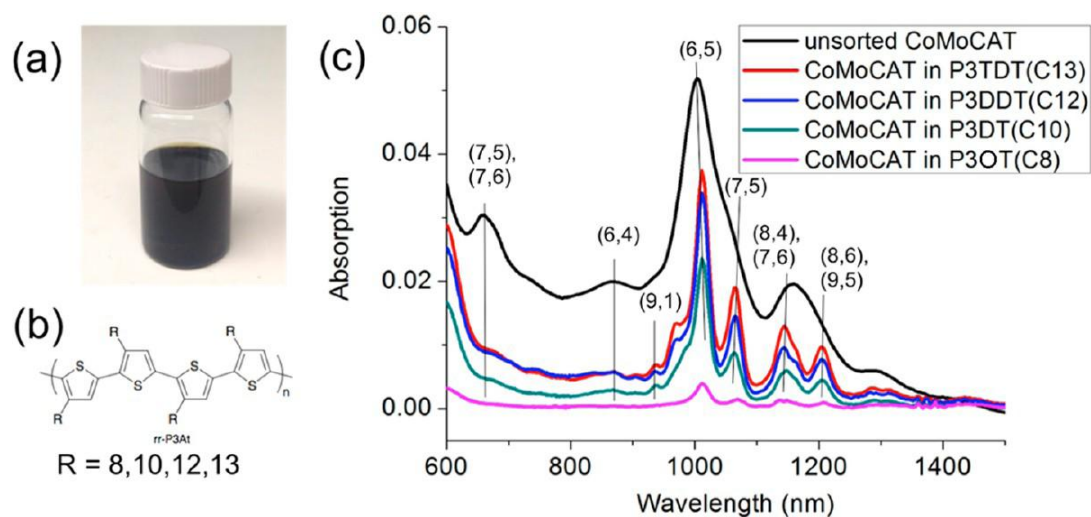


Figure 1.20: (a) CoMoCAT solutions sorted by P3DDT, (b) polymer structures of polythiophenes, (c) optical absorption spectra comparing sorted and unsorted CoMoCAT SWNTs (copied with permission from reference 51).

Adronov's research group has made a significant contribution to the preparation of nanocomposites with SWNTs and various types of conjugated polymers through noncovalent bonding.⁵²⁻⁵⁵ The materials exhibited unique properties such as increased solubility in various organic solvents and optoelectronic applications, depending on the conjugated polymer incorporated in each case.

The Adronov group has conducted the synthesis and characterization of poly[2,7-(9,9-dioctyl-fluorene)-*alt*-2,5-(3-dodecylthiophene)] (PFT) **22** (Figure 1.21) in order to evaluate the dependence of the molecular weight of polymer on the solubility of the finally prepared polymer–SWNT complexes. By this approach PFT was synthesized and then fractionated into eight different parts with a range of molecular weights from 5 to 85 kg mol⁻¹ through recycling reparative gel permeation chromatography (GPC). They further investigated the interactions of each of these fractions with HiPCO SWNTs. The best results concerning solubility in THF were found when the molecular weight of polymer was in the range of 10–35 kg mol⁻¹, whereas polymers with higher and lower molecular weights than this range would give much lower solubility.⁵³

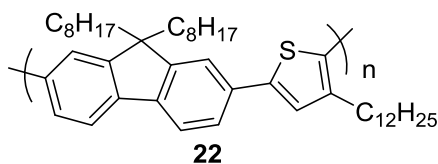


Figure 1.21: Structure of poly[2,7-(9,9-dioctyl-fluorene)-*alt*-2,5-(3-dodecylthiophene)] (PFT) **22**.

A new class of highly soluble alternating copolymers of fluorene and dithieno[3,2-b:20,30-d] pyrrole (DTP) has been prepared by applying the Suzuki polycondensation approach (Figure 1.22). The resulting poly(fluorene) and poly(pyrrole) complex architectures are highly soluble and show novel optoelectronic properties. Supramolecular complexes of these polymers with SWNTs exhibited excellent thermal

stability under inert atmosphere (*e.g.*, Ar) as evidenced by thermogravimetric analysis (TGA). Both transmission electron microscopy (TEM) and photoluminescence experiments revealed that the polymers could efficiently and selectively disperse SWNTs, despite the complexity of the conjugated copolymers involved.⁵²

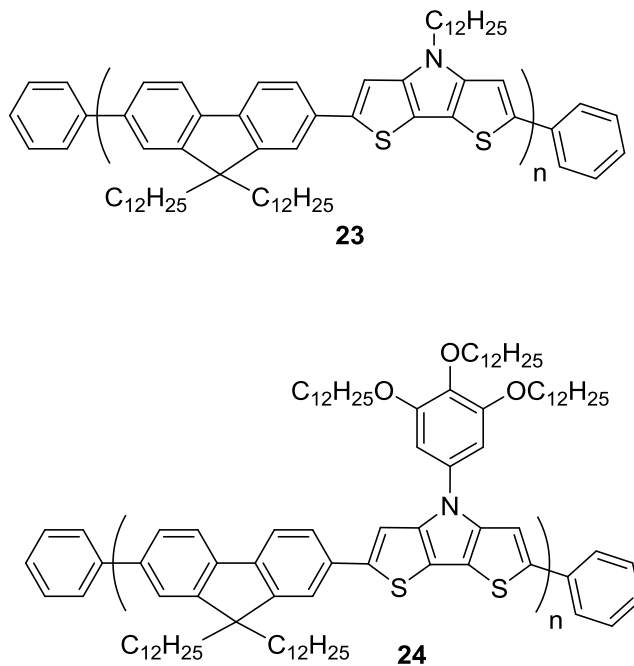


Figure 1.22: Chemical structure of copolymers of fluorene and dithieno[3,2-b:20,30-d]pyrrole (DTP) **23** and **24**.

Furthermore, by incorporating azo units into the fluorene based conjugated polymers using Suzuki polycondensation, the Andronov group has successfully synthesized a photo-isomerizable conjugated polymer (Figure 1.23). The polymer exhibited good solubility in a number of organic solvents, including THF, toluene, and

chloroform. Upon interaction with SWNTs, the supramolecular complexes showed excellent thermal stability in Ar. Photoluminescence mapping studies confirmed that these polymers were more selective towards small diameter nanotubes.⁵⁶

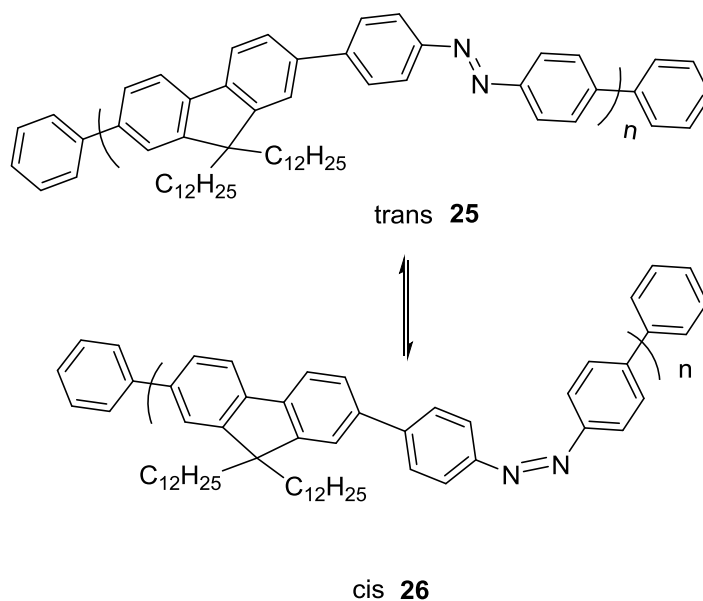


Figure 1.23: Chemical structure of a photo-isomerizable conjugated polymer prepared by the Adronov group, showing *cis* and *trans* isomerization.

Another type of commonly used polymers for noncovalent functionalization of CNTs via π - π interactions are styrene-based polymers.⁵⁷ A few articles have been published on the use of homopolymers with aromatic groups such as poly(4-vinylpyridine)⁵⁸ and poly(*para*-hydroxystyrene),⁵⁹ in order to wrap around the CNT surface.

1.3 Outline of this thesis

As reviewed in the previous sections, polymers have been found to serve as excellent wrapping agents for noncovalent functionalization of CNTs as a result of π - π stacking and van der Waals interactions between the polymer chains containing aromatic rings and the CNT surface. Through this approach, the noncovalently functionalized CNTs can attain improved solubility quite remarkably in various solvents, with the electronic and optical properties of pristine CNT preserved.

The main objective of this MSc dissertation was aimed at making a further contribution to new noncovalent functionalization methods for SWNTs using polymers as effective and selective dispersants. This was expected to be achieved by rational design of DTF (dithiafulvalene) grafted poly(phenylacetylene)s. The conjugate polymers studied in this thesis have been proven as strong dispersants to SWNTs, and found to display selectivity for particular types of SWNTs. The polymers also enabled easy release of SWNTs at controlled solvent conditions which will eventually lead to an efficient non-destructive and recyclable method for SWNT purification. The detailed content of this work can be divided into two parts: (1) the synthesis and characterization of DTF-phenylacetylene polymers, and (2) selective dispersion and releasing studies of SWNTs with DTF- polymers.

Chapter 2 describes the rational design and synthetic procedure to achieve DTF-phenylacetylene polymers, their purification and detailed characterizations. In Chapter

3, the properties of DTF-polymers and their supramolecular complexes with SWNTs were studied by UV-Vis-NIR, Raman spectroscopy, atomic force microscopy (AFM), scanning electron microscopy (SEM), cyclic voltammetry, and fluorescence mapping studies. Experimental results showed that the dispersion of SWNTs with the DTF-polymers gave high selectivity for small semiconducting (6,5), (5,6), and (7,6) tubes, and “dispersant-free” SWNTs could be readily released from the SWNT/polymer suspensions under easy solvent control. In Chapter 4, an unsuccessful attempt to synthesize tetrathiafulvalene vinylogue (TTFV)-based macrocycle was discussed. Finally, the summary and conclusions on the entire thesis work carried out during my master’s program are provided in Chapter 5.

1.4 References

- (1) Iijima, S. *Nature* **1991**, *354*, 56-58.
- (2) a) Liu, C. H.; Liu, Y.Y.; Zhang, Y.H.; Wei, R. R.; Zhang, H. L. *Phys. Chem. Chem. Phys.* **2009**, *11*, 7257-7267. b) Baughman, R. H.; Zakhidov, A. A.; de Heer, W. A. *Science* **2002**, *297*, 787-792.
- (3) Tang, Z. K.; Zhang, L.; Wang, N.; Zhang, X. X.; Wen, G. H.; Li, G. D.; Wang, J. N.; Chan, C. T.; Sheng, P. *Science* **2001**, *292*, 2462-2465.
- (4) An, K. H.; Kim, W. S.; Park, Y. S.; Moon, J. M.; Bae, D. J.; Lim, S. C.; Lee, Y. S.; Lee, Y. H. *Adv. Funct. Mater.* **2001**, *11*, 387-392.

- (5) Baughman, R. H. *Science* **1999**, 284, 1340-1344.
- (6) de Heer, W. A.; Châtelain, A.; Ugarte, D. *Science* **1995**, 270, 1179-1180.
- (7) Zhu, W.; Bower, C.; Zhou, O.; Kochanski, G.; Jin, S. *Appl. Phys. Lett.* **1999**, 75, 873-875.
- (8) Fuhrer, M. S.; Nygård, J.; Shih, L.; Forero, M.; Yoon, Y.-G.; Mazzoni, M. S. C.; Choi, H. J.; Ihm, J.; Louie, S. G.; Zettl, A.; McEuen, P. L. *Science* **2000**, 288, 494-497.
- (9) Kurkina, T.; Vlandas, A.; Ahmad, A.; Kern, K.; Balasubramanian, K. *Angew. Chem. Int. Ed.* **2011**, 50, 3710-3714.
- (10) Biercuk, M. J.; Llaguno, M. C.; Radosavljevic, M.; Hyun, J. K.; Johnson, A. T.; Fischer, J. E. *Appl. Phys. Lett.* **2002**, 80, 2767-2769.
- (11) Prasek, J.; Drbohlavova, J.; Chomoucka, J.; Hubalek, J.; Jasek, O.; Adam, V.; Kizek, R. *J. Mater. Chem.* **2011**, 21, 15872-15884.
- (12) Nikolaev, P.; Bronikowski, M. J.; Bradley, R. K.; Rohmund, F.; Colbert, D. T.; Smith, K. A.; Smalley, R. E. *Chem. Phys. Lett.* **1999**, 313, 91-97.
- (13) Banerjee, S.; Hemraj-Benny, T.; Wong, S. S. *Adv. Mater.* **2005**, 17, 17-29.

- (14) Flavin, K.; Lawrence, K.; Bartelmess, J.; Tasior, M.; Navio, C.; Bittencourt, C.; O'Shea, D. F.; Guldi, D. M.; Giordani, S. *ACS Nano* **2011**, *5*, 1198-1206.
- (15) Sung, Y. H.; Gerard, T.; Khuloud, T.; Belén, B.; Hanene, A. B.; Sergio, L. P.; Peter, D. N.; Robert, B. S.; Ciara, F.; Stephen, J. M.; Malcolm, L. H. G.; Kostas, K.; D., B. *Nature Mater.* **2010**, *9*, 485–490. .
- (16) Bayazit, M. K.; Coleman, K. S. *J. Am. Chem. Soc.* **2009**, *131*, 10670-10676.
- (17) Sravendra, R.; Indresh, k.; Hye, J. Y.; C., J. W. *J. Nanosci. Nanotechnol.* **2009**, *9*.
- (18) Rana, S.; Yoo, H. J.; Cho, J. W.; Chun, B. C.; Park, J. S. *J. Appl. Polym. Sci.* **2011**, *119*, 31-37.
- (19) Palacin, T.; Khanh, H. L.; Jousseme, B.; Jegou, P.; Filoramo, A.; Ehli, C.; Guldi, D. M.; Campidelli, S. *J. Am. Chem. Soc.* **2009**, *131*, 15394-15402.
- (20) Wenseleers, W.; Vlasov, I. I.; Goovaerts, E.; Obraztsova, E. D.; Lobach, A. S.; Bouwen, A. *Adv. Funct. Mater.* **2004**, *14*, 1105-1112.
- (21) Islam, M. F.; Rojas, E.; Bergey, D. M.; Johnson, A. T.; Yodh, A. G. *Nano Lett.* **2003**, *3*, 269-273.
- (22) Michael S. A; Alexander A. G; James F. H; Samuel I. S; H., M. C. *Nature Nanotechnology* **2006**, *1*, 60-65.

- (23) Sgobba, V.; Troeger, A.; Cagnoli, R.; Mateo-Alonso, A.; Prato, M.; Parenti, F.; Mucci, A.; Schenetti, L.; Guldi, D. M. *J. Mater. Chem.* **2009**, *19*, 4319-4324.
- (24) Backes, C.; Schmidt, C. D.; Hauke, F.; Böttcher, C.; Hirsch, A. *J. Am. Chem. Soc.* **2009**, *131*, 2172-2184.
- (25) Schmidt, C. D.; Böttcher, C.; Hirsch, A. *Eur. J. Org. Chem.* **2007**, *2007*, 5497-5505.
- (26) Guldi, D. M.; Rahman, G. M. A.; Jux, N.; Tagmatarchis, N.; Prato, M. *Angew. Chem. Int. Ed.* **2004**, *43*, 5526-5530.
- (27) Sgobba, V.; Rahman, G. M. A.; Guldi, D. M.; Jux, N.; Campidelli, S.; Prato, M. *Adv. Mater.* **2006**, *18*, 2264-2269.
- (28) Mateo-Alonso, A.; Ehli, C.; Chen, K. H.; Guldi, D. M.; Prato, M. *J. Phy. Chem. A* **2007**, *111*, 12669-12673.
- (29) Ehli, C.; Rahman, G. M. A.; Jux, N.; Balbinot, D.; Guldi, D. M.; Paolucci, F.; Marcaccio, M.; Paolucci, D.; Melle-Franco, M.; Zerbetto, F.; Campidelli, S.; Prato, M. *J. Am. Chem. Soc.* **2006**, *128*, 11222-11231.
- (30) Bartelmess, J.; Ballesteros, B.; de la Torre, G.; Kiessling, D.; Campidelli, S.; Prato, M.; Torres, T.; Guldi, D. M. *J. Am. Chem. Soc.* **2010**, *132*, 16202-16211.

- (31) Hecht, D. S.; Ramirez, R. J. A.; Briman, M.; Artukovic, E.; Chichak, K. S.; Stoddart, J. F.; Grüner, G. *Nano Lett.* **2006**, *6*, 2031-2036.
- (32) Backes, C.; Mundloch, U.; Ebel, A.; Hauke, F.; Hirsch, A. *Chem. Eur. J.* **2010**, *16*, 3314-3317.
- (33) Barone, P. W.; Strano, M. S. *Angew. Chem. Int. Ed.* **2006**, *45*, 8138-8141.
- (34) Star, A.; Steuerman, D. W.; Heath, J. R.; Stoddart, J. F. *Angew. Chem. Int. Ed.* **2002**, *41*, 2508-2512.
- (35) Ishibashi, A.; Nakashima, N. *Chem. Eur. J.* **2006**, *12*, 7595-7602.
- (36) Goodwin, A. P.; Tabakman, S. M.; Welsher, K.; Sherlock, S. P.; Prencipe, G.; Dai, H. *J. Am. Chem. Soc.* **2008**, *131*, 289-296.
- (37) Star, A.; Stoddart, J. F.; Steuerman, D.; Diehl, M.; Boukai, A.; Wong, E. W.; Yang, X.; Chung, S.-W.; Choi, H.; Heath, J. R. *Angew. Chem. Int. Ed.* **2001**, *40*, 1721-1725.
- (38) Steuerman, D. W.; Star, A.; Narizzano, R.; Choi, H.; Ries, R. S.; Nicolini, C.; Stoddart, J. F.; Heath, J. R. *J. Phy. Chem. B* **2002**, *106*, 3124-3130.
- (39) Keogh, S. M.; Hedderman, T. G.; Lynch, P.; Farrell, G. F.; Byrne, H. J. *J. Phy. Chem. B* **2006**, *110*, 19369-19374.

- (40) Yi, W.; Malkovskiy, A.; Chu, Q.; Sokolov, A. P.; Colon, M. L.; Meador, M.; Pang, Y. *J. Phys. Chem. B* **2008**, *112*, 12263-12269.
- (41) Star, A.; Stoddart, J. F. *Macromolecules* **2002**, *35*, 7516-7520.
- (42) Star, A.; Liu, Y.; Grant, K.; Ridvan, L.; Stoddart, J. F.; Steuerman, D. W.; Diehl, M. R.; Boukai, A.; Heath, J. R. *Macromolecules* **2003**, *36*, 553-560.
- (43) Cheng, F.; Imin, P.; Lazar, S.; Botton, G. A.; de Silveira, G.; Marinov, O.; Deen, J.; Adronov, A. *Macromolecules* **2008**, *41*, 9869-9874.
- (44) Liu, X.; Ly, J.; Han, S.; Zhang, D.; Requicha, A.; Thompson, M. E.; Zhou, C. *Adv. Mater.* **2005**, *17*, 2727-2732.
- (45) Cheng, F.; Adronov, A. *Chem. Eur. J.* **2006**, *12*, 5053-5059.
- (46) Nakayama-Ratchford, N.; Bangsaruntip, S.; Sun, X.; Welsher, K.; Dai, H. *J. Am. Chem. Soc.* **2007**, *129*, 2448-2449.
- (47) Naito, M.; Nobusawa, K.; Onouchi, H.; Nakamura, M.; Yasui, K.-i.; Ikeda, A.; Fujiki, M. *J. Am. Chem. Soc.* **2008**, *130*, 16697-16703.
- (48) Chen, Y.; Malkovskiy, A.; Wang, X.-Q.; Lebron-Colon, M.; Sokolov, A. P.; Perry, K.; More, K.; Pang, Y. *ACS Macro Lett.* **2011**, *1*, 246-251.

- (49) Rahman, G. M. A.; Guldi, D. M.; Cagnoli, R.; Mucci, A.; Schenetti, L.; Vaccari, L.; Prato, M. *J. Am. Chem. Soc.* **2005**, *127*, 10051-10057.
- (50) Giancane, G.; Ruland, A.; Sgobba, V.; Manno, D.; Serra, A.; Farinola, G. M.; Omar, O. H.; Guldi, D. M.; Valli, L. *Adv. Funct. Mater.* **2010**, *20*, 2481-2488.
- (51) Wang, H.; Koleilat, G. I.; Liu, P.; Jiménez-Osés, G.; Lai, Y.-C.; Vosgueritchian, M.; Fang, Y.; Park, S.; Houk, K. N.; Bao, Z. *ACS Nano* **2014**, *8*, 2609-2617.
- (52) Imin, P.; Imit, M.; Adronov, A. *Macromolecules* **2011**, *44*, 9138-9145.
- (53) Imin, P.; Cheng, F.; Adronov, A. *Polym. Chem.* **2011**, *2*, 1404-1408.
- (54) Imin, P.; Cheng, F.; Adronov, A. *Polym. Chem.* **2011**, *2*, 411-416.
- (55) Pang, X.; Imin, P.; Zhitomirsky, I.; Adronov, A. *Macromolecules* **2010**, *43*, 10376-10381.
- (56) Imin, P.; Imit, M.; Adronov, A. *Macromolecules* **2012**, *45*, 5045-5050.
- (57) Carrillo, A.; Swartz, J. A.; Gamba, J. M.; Kane, R. S.; Chakrapani, N.; Wei, B.; Ajayan, P. M. *Nano Lett.* **2003**, *3*, 1437-1440.
- (58) Rouse, J. H. *Langmuir* **2004**, *21*, 1055-1061.
- (59) Ma, C.; Zhang, W.; Zhu, Y.; Ji, L.; Zhang, R.; Koratkar, N.; Liang, J. *Carbon* **2008**, *46*, 706-710.

Chapter 2

Dithiafulvenyl-Functionalized Phenylacetylene

Polymers: Synthesis and Characterizations

2.1 Objectives of this project

Single-walled carbon nanotubes (SWNTs) have attracted great interest due to their wide range of applications in numerous fields. The intertube attractive forces between individual SWNTs lead to strong bundling and aggregation effects on as-produced SWNTs. As a result, SWNTs exhibit very low solubility in various solvents, which in turn brings limitations in their practical application and processing. To overcome this problem, as described in Chapter 1, various functionalization methods such as covalent and noncovalent approaches have been developed, in which the noncovalent functionalization is considered to be superior to others as it can improve the solubility and processability of SWNTs with their intrinsic properties essentially unperturbed. In the meantime, rationally designed noncovalent functionalization of SWNTs can enable specific types of SWNTs to be selectively removed from heterogeneous mixtures by controlled supramolecular interactions.¹ Furthermore, the properties of noncovalently functionalized SWNTs can be tuned to facilitate applications in molecular electronics and nanomaterial science.²⁻⁴

In order to produce effective dispersion of SWNTs in the solution phase, significant noncovalent attractions such as π - π and/or van der Waals interactions are required to occur between dispersants and SWNTs. Wrapping polymers around nanotubes is one of the popular methods for enhanced dispersion of the CNTs into various solvents. In this chapter, dithiafulvalene (DTF)-functionalized phenyleneacetylene-based conjugated polymers have been designed and synthesized for nanotube dispersion. The polymers can induce selective dispersion of small semiconducting (5, 6) (6, 5) and (6, 7) nanotubes in organic media. In addition, simple solvent-controlled release of nanotubes from polymer/SWNTs composites has been shown to occur.

2.2 Introduction to molecular design

Previously, the Zhao group has reported the use of linear conjugated polymers such as poly(*p*-phenylene ethynylene)s (PPEs), and poly(*p*-phenylene vinylene)s (PPVs) to disperse SWNTs in different organic solvents.⁵ The effectiveness of these conjugated polymers at dispersing CNTs was found to be correlated with the structure and electronic nature of the polymers.

To deepen our understanding of the polymer effect, highly π -extended aromatic groups such as anthracene and pyrene were incorporated into the backbone of the conjugated polymers (Figure 2.1) by using click chemistry and Sonogashira coupling

Very recently, as shown in Figure 2.2, a TTFV-based polymer was designed and synthesized by our group to achieve reversible dispersion and release of SWNTs in organic solution under the control of clean and scalable inputs such as pH or redox stimuli.⁷

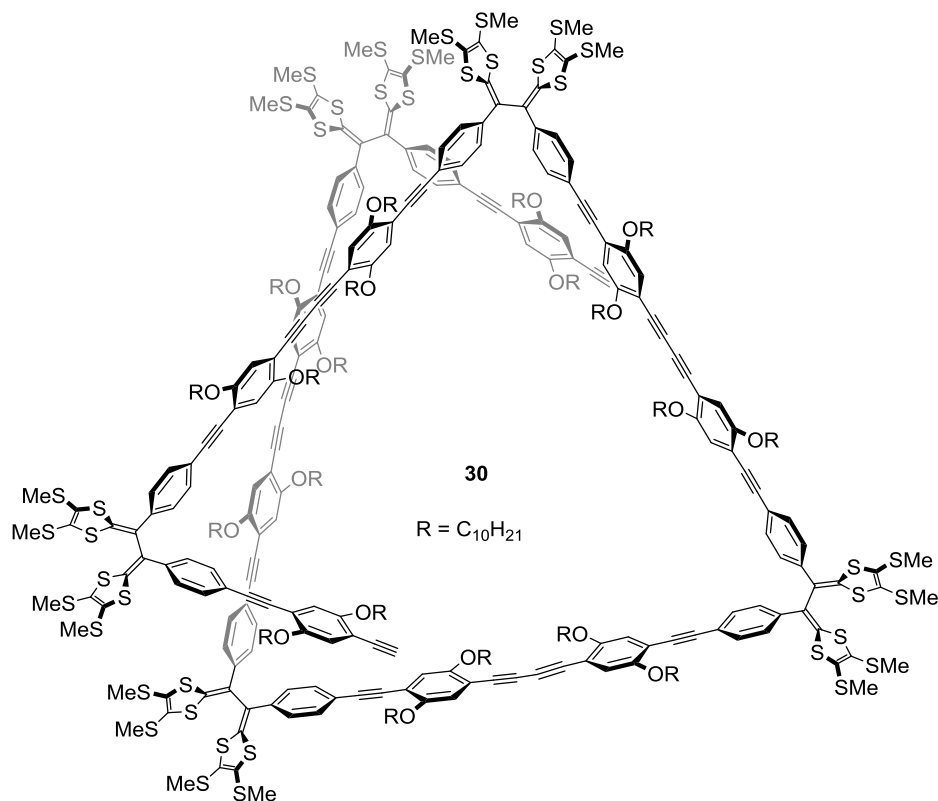


Figure 2.2: Molecular structure of a TTFV-based polymer **30** reported by the Zhao group previously.

In another recent work from our lab, a series of π -conjugated oligomers taking linear and Z-shaped architectures was constructed with DTF groups functionalized at terminal positions (Figure 2.3). The DTF-attached oligomers showed strong noncovalent

interactions with SWNTs resulting in effective dispersion of SWNTs. Of great interest is that these oligomers appear to be selective for small-diameter nanotubes.⁸

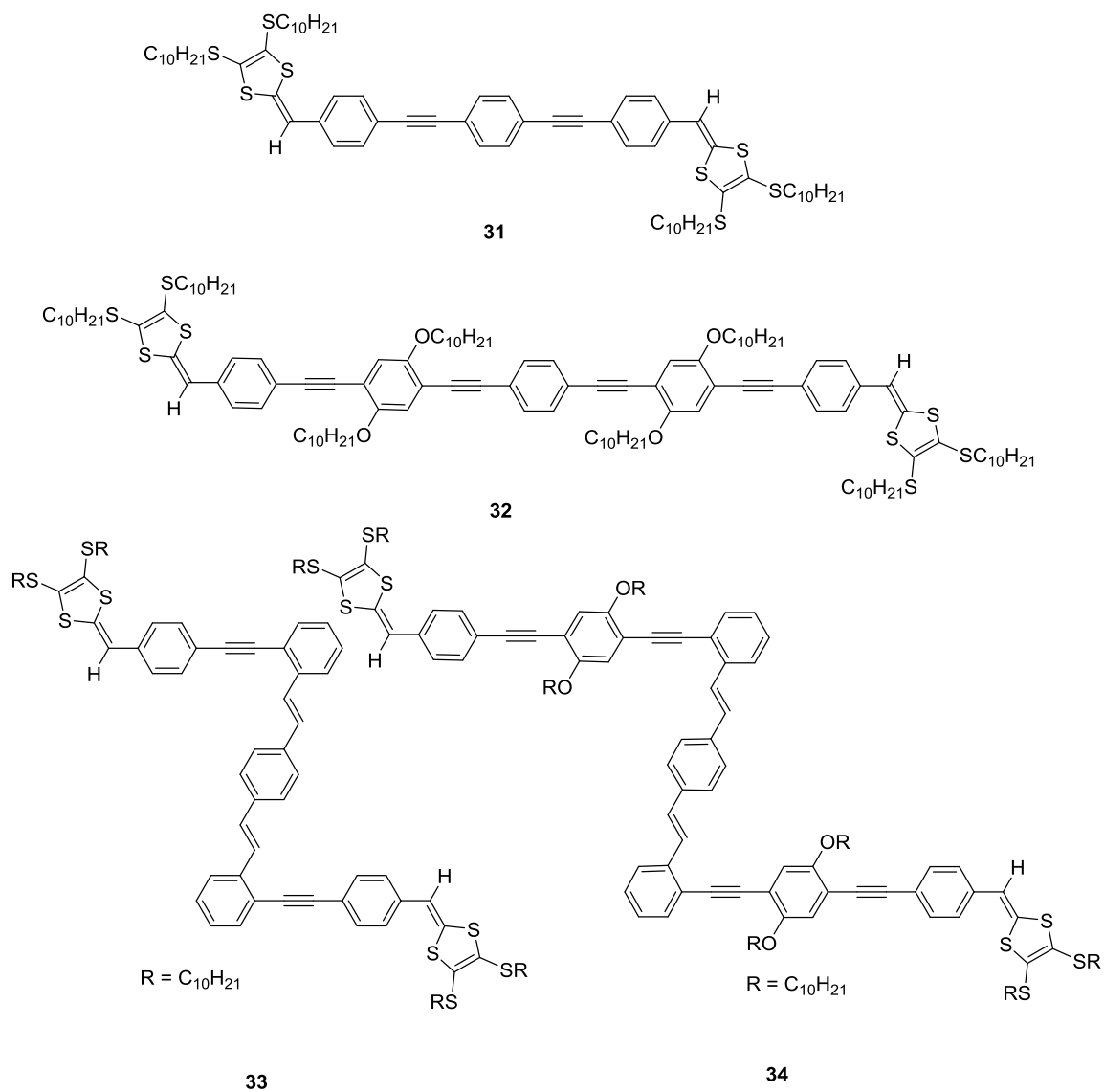


Figure 2.3: Molecular structures of DTF-attached oligomers **31-34**.

The results indicated that the dithiafulvenyl (DTF) groups could remarkably enhance the supramolecular interactions with SWNTs as a result of the strong electron donating properties of DTF.⁸ The excellent performance of DTF functionality in facilitating binding toward SWNTs thus promoted us to design and synthesize two phenylacetylene-based polymers **35** and **36** as shown in Figure 2.4. The following content describes the detailed synthesis of DTF-functionalized conjugated polymers.

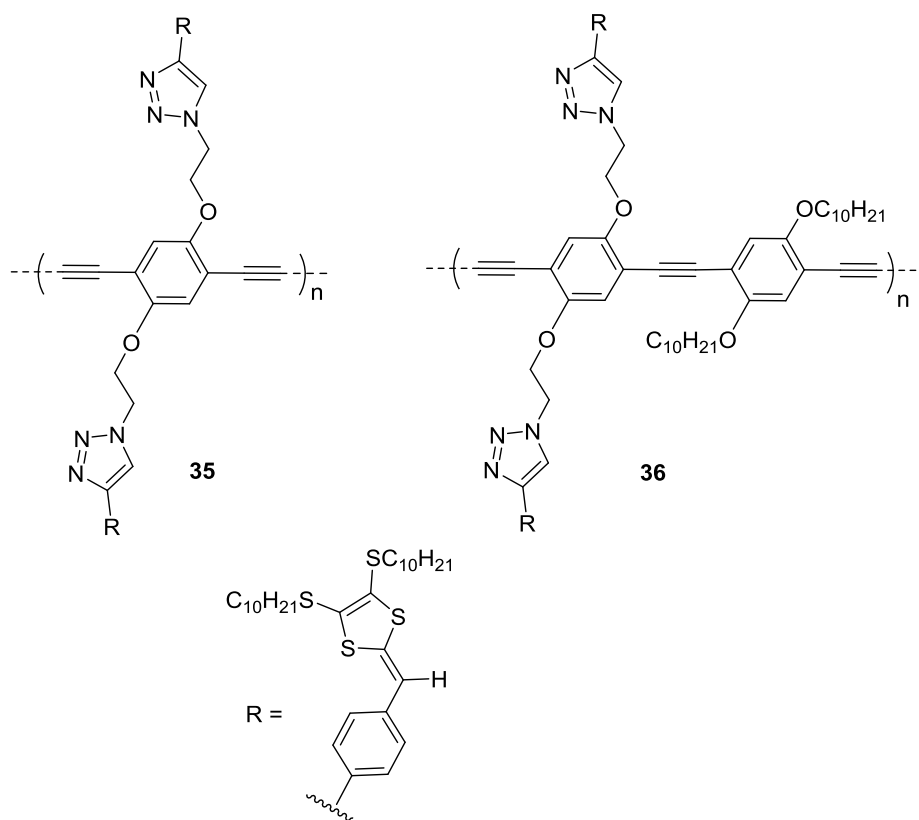
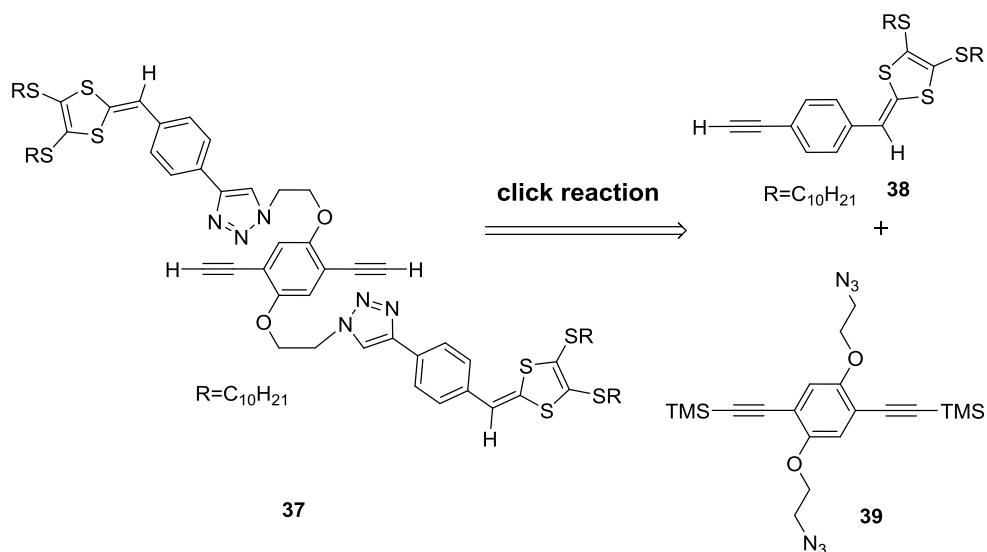


Figure 2.4: Molecular structures of target DTF-grafted conjugated polymers **35** and **36** in this chapter.

2.3 Results and discussion

Polymers **35** and **36** were achieved by polymerizing DTF-phenylacetylene building block **37** by cross coupling and homo-coupling reaction conditions. For the synthesis of DTF-phenylacetylene building block **37**, the two monomeric components such as dithiafulvene alkyne **38** and azido precursor **39** were prepared at first.

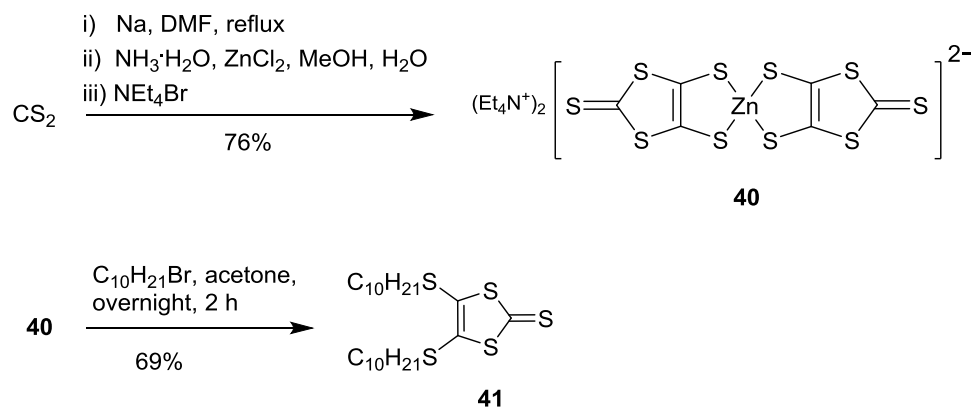
2.3.1 Synthesis of DTF-phenylacetylene building block **37**



Scheme 2.1: Click approach for DTF-phenylacetylene building block **37**.

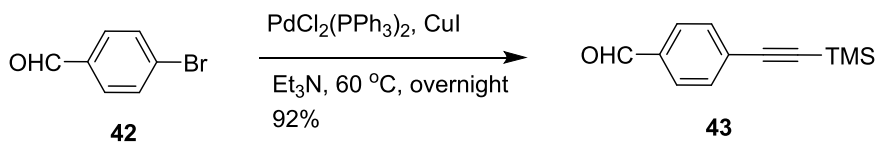
The synthesis for dithiafulvene alkyne **38** began with the preparation of *S*-decyl thione **41** by using a well established procedure by Zhao group. As shown in Scheme 2.2, the synthesis of *S*-decyl thione **41** started with a reaction between Na and CS₂ using dimethyl formamide (DMF) as solvent, and then, upon addition of ZnCl₂ and NH₃/H₂O,

the resulting dithiolate was chelated with Zn^{2+} and precipitated out as a stable red salt **40** in the presence of tetraethylammonium bromide. The overall yield of this sequence of reactions was 76%. Salt **40** was dissociated to give the free dithiolate in refluxing acetone, and the resulting intermediate was then alkylated with 1-decyl bromide to afford *S*-decyl thione **41** in 69% yield.



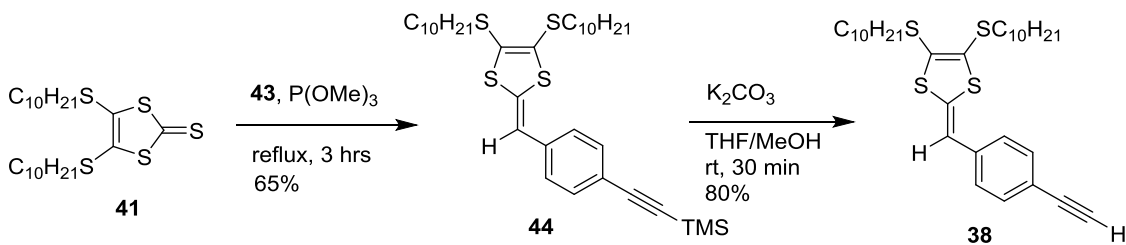
Scheme 2.2: Synthesis of *S*-decyl thione **41**.

Precursor **43** was easily prepared by a Sonogashira coupling reaction between 4-bromobenzaldehyde **42** and trimethylsilylacetylene (TMSA) using $\text{PdCl}_2(\text{PPh}_3)_2/\text{CuI}$ as the catalyst in trimethyl amine (Et_3N). The yield of aldehyde **43** was 92% (Scheme 2.3).



Scheme 2.3. Synthesis of aldehyde **43**.

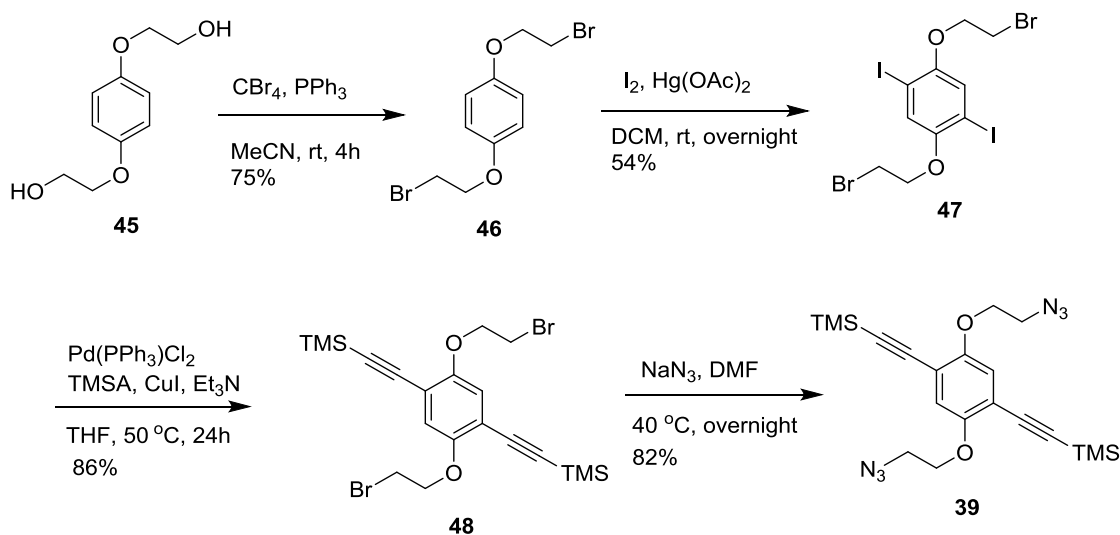
To achieve TMS protected dithiafulvene precursor **44**, a phosphite-mediated olefination strategy was applied as depicted in Scheme 2.4. In the presence of trimethyl phosphite, one molar equivalent of *S*-decyl thione **41** was reacted with one molar equivalent of aldehyde **43** to give compound **44**. Although the purification step is very tedious due to the presence of a large amount of trimethyl phosphite, TMS protected dithiafulvene alkyne **44** was successfully produced by this reaction in 65% yield. Among different conditions tried, the solvent-free condition was found to afford the highest yield. However, in this case, much more trimethyl phosphite was needed. The desilylation of compound **44** in the presence of K_2CO_3 and THF/MeOH at room temperature yielded the active precursor, dithiafulvene alkyne **38**.



Scheme 2.4: Synthetic route to dithiafulvene acetylene building block **38**.

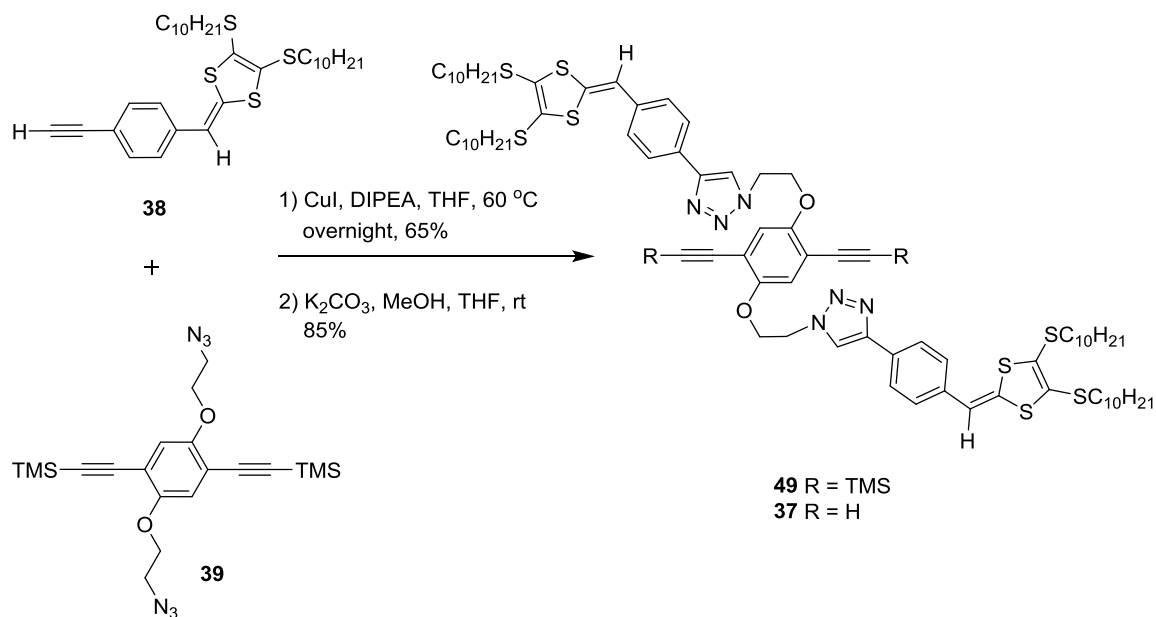
With the success in making dithiafulvene alkyne **38**, the synthesis was continued towards the preparation of the second important building block **39**. Commercially available 2,2'-(1,4-phenylenebis(oxy))diethanol **45** was subjected to an Appel reaction in the presence of CBr_4 and PPh_3 in MeCN at room temperature to afford compound **46**. Iodination of the product with $I_2/Hg(OAc)_2$ in methylene chloride yielded compound **47**.

(Scheme 2.5) which was subjected to Sonogashira reaction with TMSA to afford compound **48**. An azidation reaction was performed on compound **38** in the presence of sodium azide to afford an azido precursor **39** in 82% yield.



Scheme 2.5: Synthetic route to diazido-precursor **39**.

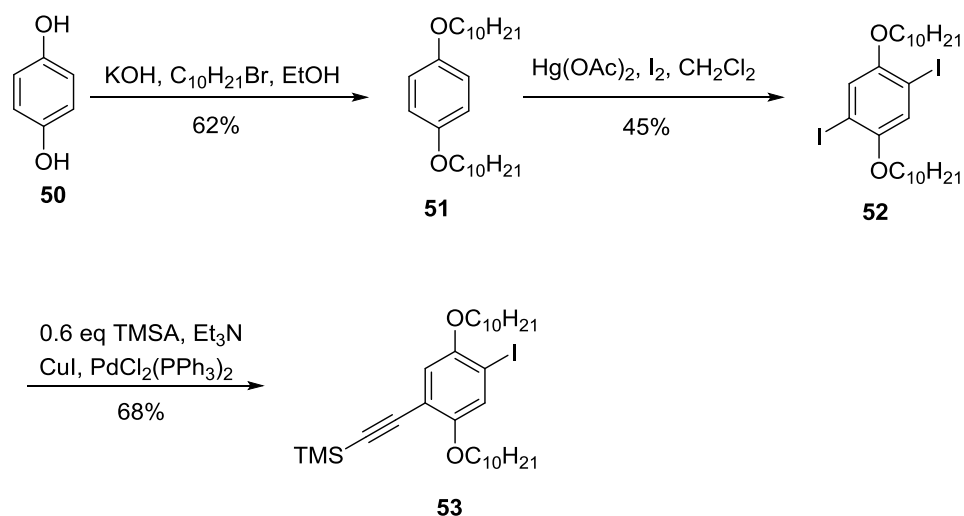
With the two active building blocks **38** and **39** in hand, the synthesis of the DTF-phenylacetylene building block **37** then became straightforward. A click reaction between precursors **38** and **39** in the presence of CuI catalyst afforded TMS protected DTF building block **49** in a moderate yield, which then was desilylated with K_2CO_3 to obtain the desired DTF-phenylacetylene building block **37** (Scheme 2.6).



Scheme 2.6: Synthetic route to DTF-phenyl acetylene monomer **37**.

2.3.2 Synthesis of endcapping reagent **53**

An endcapping reagent **53** was synthesized in order to exert controllability during the polymerization process. As demonstrated in Scheme 2.7, in the first step, commercially available 1,4-hydroquinone **50** was subjected to an alkylation reaction with 1-bromodecane in a basic ethanolic solution to afford compound **51**. Next, compound **51** was reacted with iodine chips under the catalysis of $\text{Hg}(\text{OAc})_2$ to produce diiodo compound **52** in a moderate yield of 45%. Finally, compound **52** underwent a Sonogashira reaction with 0.6 molar equivalent of TMSA in the presence of Et_3N and $\text{PdCl}_2(\text{PPh}_3)_2/\text{CuI}$ catalyst to afford aryl iodide **53** in 68% yield.

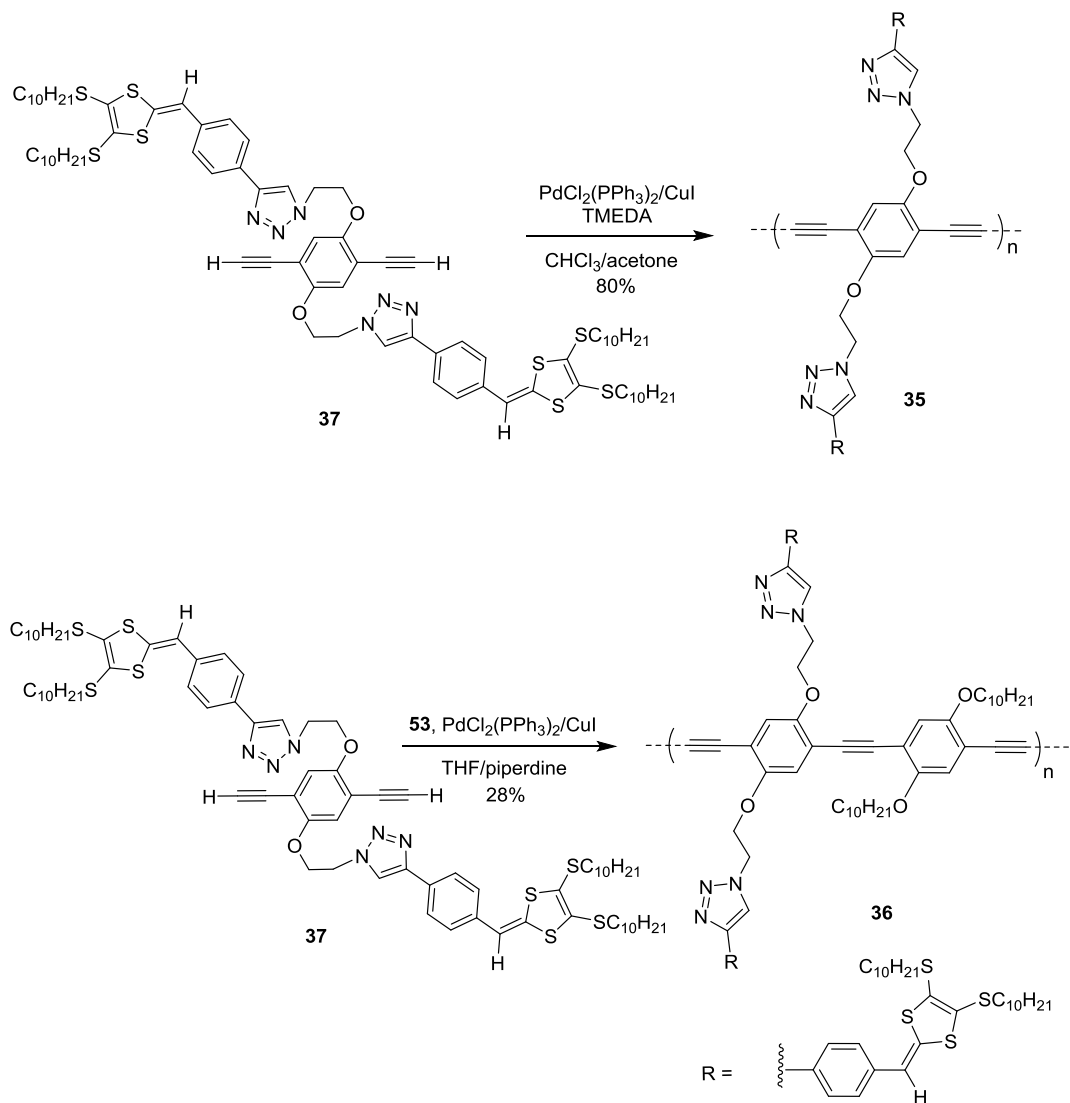


Scheme 2.7: Synthesis of iodoarene **53**.

2.3.3 Construction of DTF-functionalized homo-coupled polymer **35** and cross-coupled polymer **36**

As shown in Scheme 2.8, the DTF-phenylacetylene building block **37** was subjected to a Sonogashira coupling polymerization with diiodoarene **52** in the presence of Pd/Cu catalyst and piperidine as base to yield polymer **36**. In this polymerization reaction, a small amount of iodoarene **53** (0.1 molar equivalent) was added as endcapping agent in order to control the degree of polymerization as well as to attain satisfactory stability for polymer **36**. The cross-coupling polymerization, however, afforded polymer **36** in a rather modest yield of 28% in comparison to the synthesis of polymer **35**. The relatively low yield of **36** is likely due to the sulfur atoms in **37** which somewhat deactivate the Pd (II) catalyst. Alternatively, the monomer DTF-phenylacetylene building

block **37** was subjected to a Cu(I)-catalyzed homo-coupling polymerization to afford polymer **35** in a very good yield (80%).



Scheme 2.8: Synthesis of polymer **35** and **36**.

The two polymers are brown-coloured solids with good solubility in chlorinated and aromatic organic solvents, such as CHCl_3 , CH_2Cl_2 , chlorobenzene, and toluene. The molecular structures of two polymers were characterized by ^1H and ^{13}C NMR and spectroscopy.

2.3.4 GPC analysis

As shown in Figure 2.5, the average molecular weight and polydispersity of **35** were analyzed by gel permeation chromatography (GPC), which has a number-average molar mass (M_n) of 11532 g/mol relative to polystyrene standards and the polydispersity index (PDI) of 1.47.

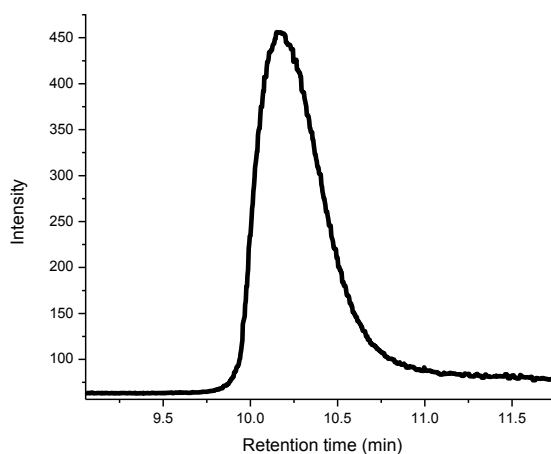


Figure 2.5: GPC chromatogram of polymer **35**. $M_n = 11523$ g/mol, $M_w = 16944$ g/mol, PDI = 1.47. Experimental conditions: columns: T6000M; standard: polystyrene; sample concentration: 1 mg polymer **35** in 3 mL THF.

For polymer **36**, however, from ^1H NMR analysis, the sample is found to contain polymers and low-molecular weight components, most likely some small oligomers. The compositional heterogeneity in the sample of polymer **36** was also reflected in GPC data (Figure 2.6). The polymer component in the sample is measured to have a M_n of 17995 g/mol and a PDI of 1.45.

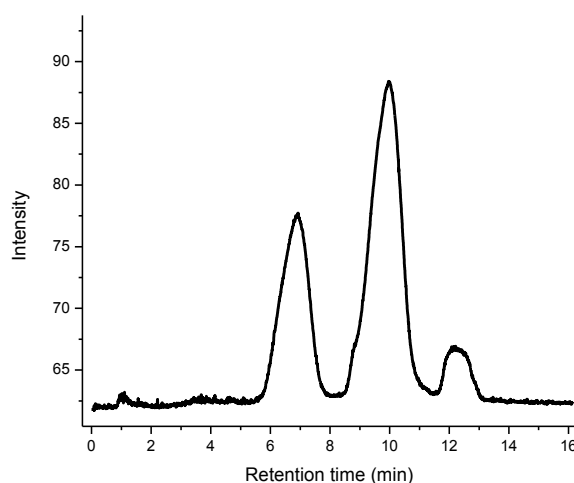


Figure 2.6: GPC chromatogram of polymer **36**. $R_t = 7.1$, $M_n = 17995$ g/mol, $M_w = 26510$ g/mol, PDI = 1.45. Experimental conditions: columns: T6000M; standard: polystyrene; sample concentration: 1 mg polymer **36** in 3 mL THF.

2.3.5 Electronic and electrochemical properties of polymers **35** and **36**

The electronic properties were investigated by UV-Vis absorption spectroscopy. The detailed data can be seen in Figure 2.7. The UV-Vis spectra of **35** and **36** both show

an intense absorption band at 380 nm, which is consistent with the maximum absorption band of precursor **37**, whereas the long wavelength region of the spectra reflects the higher degree of conjugation of the polymers. In addition, polymer **35** gives a prominent low-energy absorption peak at 450 nm, while polymer **36** only shows an absorption tail from 430 to 570 nm. The significantly different absorption properties of **35** and **36** in the long-wavelength region are attributable to their different degrees of polymerization as disclosed by the GPC analysis.

The electrochemical redox properties of both polymers and their DTF precursor were investigated by cyclic voltammetry (CV), and the detailed voltammograms are given in Figure 2.7. The CV profile of precursor **37** shows a quasi-reversible redox couple at $E_{pa} = +0.97$ V and $E_{pc} = +0.53$ V ascribed to the single-electron redox processes on DTF moieties. In contrast, the CV profiles of polymers **35** and **36** exhibit a completely irreversible pattern with only an oxidation peak detected at $E_{pa} = +0.88$ V for **35** and +0.89 V for **36**.

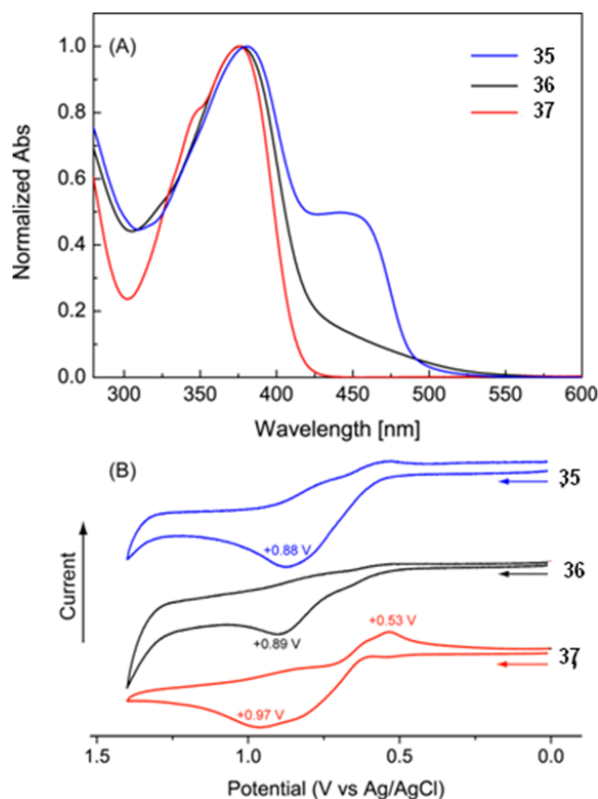


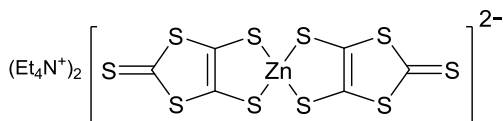
Figure 2.7: (A) UV-Vis absorption spectra of polymers **35** and **36** and DTF precursor **37** measured in CH_2Cl_2 at room temperature. (B) Cyclic voltammograms of **35**, **36**, and **37** measured in CH_2Cl_2 . Electrolyte: Bu_4NBF_4 (0.1 M); working: glassy carbon; counter: Pt wire; reference: Ag/AgCl; scan rate: 200 mV s^{-1} .

2.4 Experimental

Chemicals and reagents were purchased from commercial suppliers and used without further purification. All reactions were performed in standard dry glassware under an inert atmosphere of N_2 unless otherwise noted. Evaporation and concentration was done using an H_2O -aspirator at low pressure. Flash column chromatography was

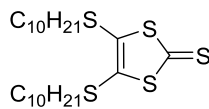
carried out with silica gel 60 (230-400 mesh) from VWR International. Thin-layer chromatography (TLC) was carried out with silica gel 60 F254 covered on plastic sheets and visualized by UV light. ^1H and ^{13}C NMR spectra were measured on a Bruker Avance 500 MHz spectrometer or a Tecmag APOLLO 300 MHz spectrometer. Chemical shifts are reported in ppm downfield from the signal of the internal reference SiMe_4 or relative to the signals of residual solvents (CHCl_3 : $\delta_{\text{H}} = 7.24$ ppm, $\delta_{\text{C}} = 77.2$ ppm; CH_2Cl_2 : $\delta_{\text{H}} = 5.32$ ppm, $\delta_{\text{C}} = 54.0$ ppm). Coupling constants (J) are given in Hz. UV-Vis-NR absorption spectra were recorded on a Cary 6000i spectrophotometer. Infrared spectra (IR) were recorded on a Bruker Tensor 27 spectrometer equipped with a ZnSe ATR module. MALDI-TOF MS were measured on an Applied Biosystems Voyager instrument using dithranol as the matrix. Polymer molecular weight and polydispersity index (PDI) were estimated from gel permeation chromatography (GPC) using a Waters 2695 Separations Module equipped with a Waters 2996 photodiode array detector, a Waters 2414 refractive-index detector, and two Jordi Labs Jordi Gel DVB columns. Polystyrene standards were used for calibration, and THF was used as the eluent at a flow rate of 1.0 mL/min. UV-Vis-NIR spectra were collected on a Cary 6000i spectrometer using a 10 mm quartz cuvette. Cyclic voltammetric (CV) and differential pulse voltammetric (DPV) experiments were carried out in a standard three-electrode setup controlled by a BASi Epsilon workstation.

Bis(tetraethylammonium) bis(1,3-dithiole-4,5dithiolate)zincate (40)



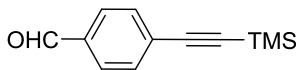
Na (8.23 g, 362 mmol) and CS₂ (45 mL, 749 mol) were mixed and then refluxed for 20 min under N₂ protection. Dried DMF (50 mL) was added dropwise over a period of 20 min. The mixture was refluxed for 2 h and then concentrated under vacuum at 30 °C. MeOH (60 mL) was added to the residue under cooling in an ice-water bath to quench unreacted Na. A solution of ZnCl₂ (12.8 g, 93.7 mmol) in 1:1 MeOH/NH₃/H₂O (100 mL) was then added carefully to the filtrate. To the resulting mixture, Et₄NBr (23.9 g, 113 mmol) in H₂O (80 mL) was then added. Then the mixture was left standing in the fumehood overnight. The resulting mixture was then subjected to suction filtration. The residue was sequentially washed with H₂O and Et₂O to yield **40** as a red-colored solid (25.7 g, 35.4 mmol, 76%). The salt was directly taken to the next step without further purification and characterization.

4,5-Bis(decylthio)-1,3-dithiol-2thione (41)



To a solution of **40** (10.3 g, 14.4 mmol) in acetone (100 mL) was added 1-decyl bromide (18.7 g, 83.5 mmol). The mixture was refluxed overnight and filtered. The residue was washed with acetone. The filtrate was cooled under ice bath conditions for 0.5 h. The precipitate was collected by suction filtration to afford **41** as a bright yellow solid (4.63 g, 9.69 mmol, 69%). $^1\text{H NMR}$ (500 MHz, CD_2Cl_2): δ 2.85 (t, $J = 7.2$ Hz, 4H), 1.69-1.63 (m, 4H), 1.42-1.27 (m, 28H), 0.88 (t, $J = 6.1$ Hz, 6H); The $^1\text{H NMR}$ data is consistent with those reported in the literature.⁹

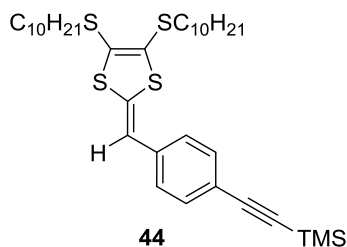
4-(Trimethylsilylethynyl)benzaldehyde (**43**)



43

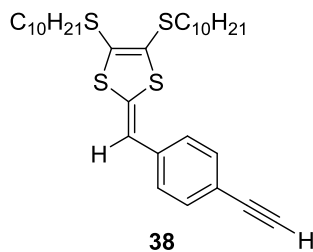
A mixture of 4-bromobenzaldehyde **42** (3.00 g, 16.2 mmol), TMSA (4.5 mL, 30 mmol), Et_3N (40 mL), CuI (180 mg, 0.985 mmol) and $\text{Pd}(\text{PPh}_3)_2\text{Cl}_2$ (225 mg, 0.320 mmol) were mixed and heated to 60 °C. The black mixture was stirred for overnight. After filtration, the filtrate was concentrated under vacuum. The residue was subjected to column chromatography (EtOAc/hexanes 1:9) to afford **43** (3.1 g, 14 mmol, 92%) as a light yellow solid $^1\text{H NMR}$ (500 MHz, CDCl_3): δ 10.00 (s, 1H), 7.82 (d, $J = 8.1$ Hz, 2H), 7.61 (d, $J = 8.1$ Hz, 2H), 0.25 (s, 9H). The $^1\text{H NMR}$ data is consistent with those reported in the literature.¹⁰

Silylated acetylenic DTF (**44**)



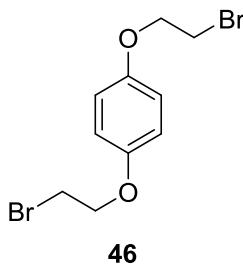
A solution of thione **41** (1.55 g, 3.23 mmol) and 4-(trimethylsilylethynyl)-benzaldehyde **43** (0.65 g, 3.25 mmol) in trimethylphosphite (15 mL) was stirred and heated to 130 °C for about 3 h under a N₂ atmosphere. After the reaction was complete as checked by TLC analysis, the excess trimethylphosphite was removed by vacuum distillation. The resulting crude product was purified by silica flash column chromatography (EtOAc/hexanes, 1:9) to yield pure compound **44** (1.47g, 2.09 mmol, 65%) as a reddish brown syrup. ¹H NMR (500 MHz, CD₂Cl₂): δ 7.42 (d, *J* = 8.4 Hz, 2H), 7.16 (d, *J* = 8.3 Hz, 2H), 6.45 (s, 1H), 2.83 (t, *J* = 7.3 Hz, 4H), 1.68-1.61 (m, 4H), 1.43-1.26 (m, 28H), 0.88 (t, *J* = 7.0 Hz, 6H), 0.24 (s, 9H); The ¹H NMR data is consistent with those reported in the literature.¹¹

Acetylenic DTF precursor (**38**)



To the solution of compound **44** (0.90 g, 1.42 mmol) in THF/MeOH (30 ml, 2:1 v/v) was added K_2CO_3 (0.58 g, 4.26 mmol). The reaction mixture was stirred for 30 min at rt. On completion, the solvent was removed under reduced pressure. The residue was dissolved in CH_2Cl_2 , washed with water, dried over MgSO_4 and concentrated under reduced pressure to obtain pure compound **38** (0.63 g, 1.12 mmol, 80%) as a brown solid. The compound was taken to the next step immediately.

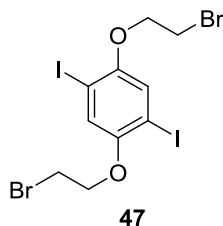
1,4-Bis(2-bromoethoxy)benzene (**46**)



Carbon tetrabromide (15.5 g, 46.8 mmol) was slowly added in small portions to a solution of 1,4-bis(2-bromoethoxy)benzene **45** (2.34g, 11.8 mmol) and triphenylphosphine (12.2 g, 46.4 mmol) in 100 mL of dry acetonitrile in 0 °C with stirring, followed by allowing the reaction mixture to warm up to room temperature. The resulting clear solution was stirred for another 4 h. Then 70 mL of cold water was added to the reaction, whereupon product **46** was precipitated out as a colorless solid. The product was collected by vacuum filtration and thoroughly washed with methanol/water (60:40 v/v), and then recrystallized from methanol. The obtained colorless flake-like crystals were dried under vacuum to afford pure **46** (2.9 g, 9.07 mmol, 75%). ^1H NMR

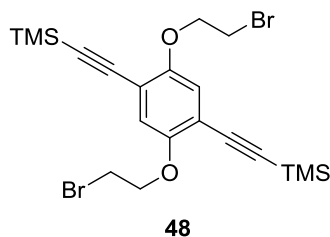
(500 MHz, CDCl₃): δ 6.86 (s, 2 H), 4.25 (t, $J = 6.30$ Hz, 4H), 3.61 (t, $J = 6.30$ Hz, 4H);
The ¹H NMR data is consistent with those reported in the literature.⁶

2,5-Diiodo-1,4-bis(2-bromoethoxy)benzene (47)



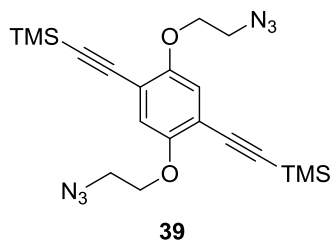
Compound **46** (3.0 g, 9.26 mmol), I₂ (9.165 g, 36.1 mmol), Hg(OAc)₂ (11.4 g, 35.6 mmol) and CH₂Cl₂ (150 ml) were mixed and the mixture was stirred overnight. Then it was filtered through MgSO₄, washed with Na₂S₂O₃, H₂O, dried over MgSO₄, and evaporated *in vacuo*. The residue was recrystallized from EtOH (70 mL) to afford **47** a colorless solid (2.9 g, 5.06 mmol, 54%). ¹H NMR (500 MHz, CDCl₃): $\delta = 7.22$ (s, 2 H), 4.27 (t, $J = 6.33$ Hz, 4H), 3.66 (t, $J = 6.29$ Hz, 4H). The ¹H NMR data is consistent with those reported in the literature.⁶

(2,5-Bis(3-bromopropyl)-1,4-phenylene)bis(ethyne-2,1-diyl)bis(trimethylsilane) (48)



A mixture of **47** (1.2 g, 2.08 mmol), Pd(PPh₃)₂Cl₂ (30 mg, 0.03 mmol), and CuI (39 mg, 0.21 mmol) were taken in 15 mL of dry THF/Et₃N (1:1). To this constantly stirred mixture a solution of TMSA (612 mg, 6.25 mmol) in THF (2 mL) was then added dropwise and stirred at room temperature for 24 h. The solvent was removed and the resulting solid mass was dissolved in CH₂Cl₂ and washed with H₂O. The organic layer was then dried over MgSO₄, filtered and finally column chromatographed (hexanes/ethyl acetate 6:1) to give compound **48** as an off-white solid (613 mg, 1.19 mmol, 86%). ¹H NMR (300 MHz, CDCl₃): δ = 6.93 (s, 2 H), 4.28 (t, *J* = 6.46 Hz, 4H), 3.63 (t, *J* = 6.49 Hz, 4H), 0.26 (s, 18H); The ¹H NMR data is consistent with those reported in the literature.⁶

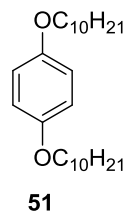
2,5-Bis(2-azidoethoxy)-1,4-phenylenebis(ethyne-2,1-diyl)bis(trimethylsilane) (39)



Compound **48** (800 mg, 1.81 mmol) was dissolved in DMF (10 mL) and NaN₃ (648 mg, 9.98 mmol) was added. The reaction mixture was stirred at 40 °C overnight. Cold water (5 mL) was added to the reaction mixture as well as dichloromethane (15 mL). The organic layer was washed with water and brine and dried over MgSO₄. The solvent was evaporated *in vacuo* to furnish **39** as colorless solid (720 mg, 1.59 mmol,

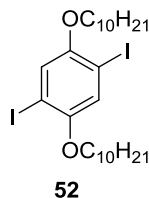
89%). ^1H NMR (300 MHz, CDCl_3): δ 6.94 (s, 2 H), 4.14 (t, $J = 4.88$ Hz, 4H), 3.60 (t, $J = 4.88$ Hz, 4H), 0.25 (s, 18H). The ^1H NMR data is consistent with those reported in the literature.⁶

1,4-Bis(decyloxy)benzene (**51**)



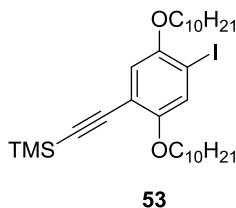
Hydroquinone **50** (2.01 g, 18.25 mmol), KOH (2.51 g, 45.6 mmol), EtOH (100 mL), and $\text{C}_{10}\text{H}_{21}\text{Br}$ (10.11 g, 45.6 mmol) were mixed. The resulting grey colored mixture was heated to 90 °C and refluxed for 60 h. It was then diluted with CH_2Cl_2 , washed with NH_4Cl , H_2O , and brine and dried over MgSO_4 . It was filtered through a short silica plug and washed with hexanes. The filtrate was concentrated *in vacuo*. The off-white solid was recrystallized from MeOH. The resulting colorless flakes were washed with cold MeOH to produce **51** as colorless flakes (4.40 g, 11.84 mmol, 62%). ^1H NMR (300 MHz, CDCl_3): δ 6.80 (s, 4H), 3.88 (t, $J = 6.59$ Hz, 4H), 1.78-1.68 (m, 4H), 1.44-1.37 (m, 28H), 0.86 (t, $J = 6.45$ Hz, 6H). The ^1H NMR data is consistent with those reported in the literature.¹²

1,4-Bis(decyloxy)-2,5-diiodobenzene (**52**)



Compound **51** (4.01 g, 10.3 mmol), I₂ (6.12 g, 25.72 mmol), Hg(OAc)₂ (8.21 g, 25.52 mmol), and CH₂Cl₂ (200 mL) were mixed and stirred for 24 h. Then it was filtered and washed with Na₂S₂O₃, water, brine, and dried over MgSO₄. The solvent was removed *in vacuo*. The crude product was recrystallized from EtOH to afford the product **52** as colorless flakes (2.98 g, 4.65 mmol, 45%). ¹H NMR (500 MHz, CDCl₃): δ 7.17 (s, 2H), 3.92 (t, *J* = 6.44 Hz, 4H), 1.82-1.77 (m, 4H), 1.52-1.46 (m, 4H), 1.36-1.32 (m, 24H), 0.88 (t, *J* = 6.79 Hz, 6H). The ¹H NMR data is consistent with those reported in the literature.¹²

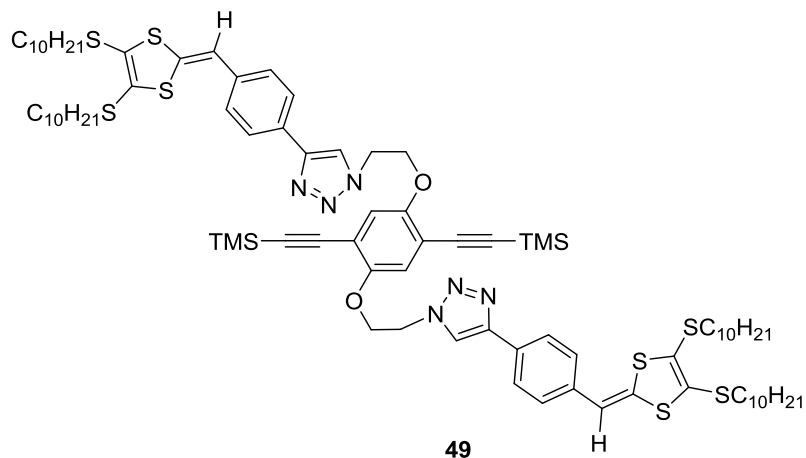
1,4-Bis(decyloxy)-2-iodo-5-(trimethylsilylethynyl)benzene (**53**)



A mixture of **52** (1.05 g, 1.63 mmol), Pd(PPh₃)₂Cl₂ (0.17 g, 0.23 mmol), and CuI (0.125 g, 0.66 mmol) were added in 60 mL of Et₃N. Then TMSA (0.67 mL, 4.6 mmol)

was added dropwise. The reaction mixture was then stirred at 60 °C for 24 h. The resulting mixture was filtered and the filtrate was washed with NH₄Cl, H₂O, and brine and dried over MgSO₄. The solvent was removed under vacuum. It was then subjected to column chromatography (hexanes/CH₂Cl₂, 9:1) to afford compound **53** (0.45 g, 0.92 mmol, 68%) as a colorless liquid. ¹H NMR (500 MHz, CDCl₃): δ = 7.25 (s, 1 H), 6.83 (s, 1H), 3.95-3.92 (m, 4H), 1.82-1.75 (m, 4H), 1.52-1.46 (m, 4H), 1.34-1.27 (m, 24H), 0.88 (t, *J* = 6.57, 6H), 0.25 (s, 9H). The ¹H NMR data is consistent with those reported in the literature.¹²

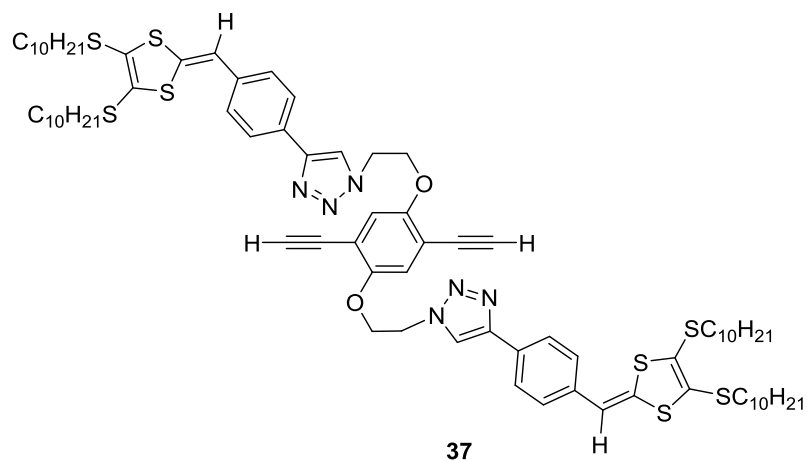
TMS protected DTF phenylacetylene building block (**49**)



To a solution of acetylenic phenyl-DTF **38** (1.28 g, 2.28 mmol) and diazido-phenylacetylene **39** (0.502 g, 1.14 mmol) in dry THF (100 mL) were added CuI (80.3 mg, 0.436 mmol) and DIPEA (1 mL). The reaction mixture was degassed by bubbling N₂ at rt for 5 min before it was heated to 60 °C overnight. On completion, the THF was removed

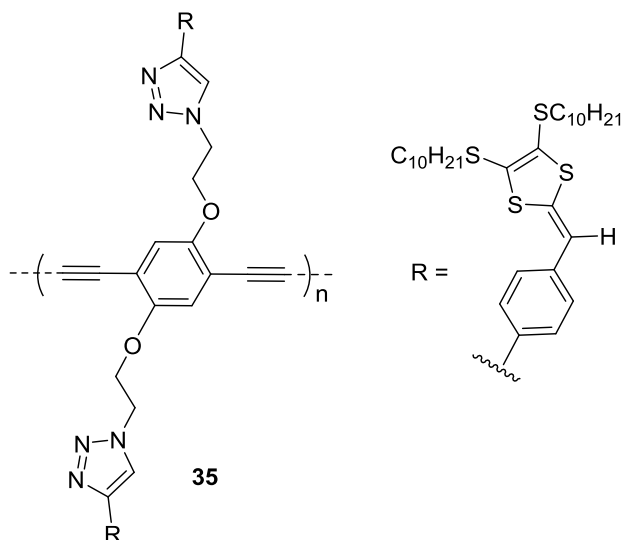
under reduced pressure. The residue which remained was dissolved in CH_2Cl_2 and filtered through a MgSO_4 pad. The filtrate was sequentially washed with brine and water. The organic layer was dried over MgSO_4 and concentrated under vacuum to give crude **49**, which was further purified by silica column chromatography (EtOAc/hexanes, 4:6) to yield pure compound **49** (1.04 g, 0.665 mmol, 65%) as a pale yellow solid. m.p. 120-123 °C; IR (neat): 2918, 2148, 1570, 1497, 1393, 1356, 1212, 1047, 977, 930, 852, 757 cm^{-1} ; ^1H NMR (500 MHz, CD_2Cl_2): δ 8.22 (s, 2H), 7.80 (d, $J = 8.4$ Hz, 4H), 7.26 (d, $J = 8.3$ Hz, 4H), 6.92 (s, 2H), 6.49 (s, 2H), 4.83 (t, $J = 4.5$ Hz, 4H), 4.36 (t, $J = 4.8$ Hz, 4H), 2.83 (t, $J = 7.3$ Hz, 8H), 1.70-1.59 (m, 8H), 1.41-1.27 (m, 56H), 0.90-0.84 (m, 12H), 0.24 (s, 18H); ^{13}C NMR (75 MHz, CDCl_3): δ 153.1, 136.2, 132.9, 127.9, 127.7, 127.2, 126.0, 121.1, 117.6, 114.2, 113.9, 101.7, 100.4, 77.2, 67.9, 49.8, 36.2, 31.9, 29.9, 29.7, 29.6, 29.5, 29.4, 29.21, 29.19, 28.62, 28.60, 22.7, 14.2; MS (MALDI-TOF, +eV) m/z calculated for $\text{C}_{84}\text{H}_{124}\text{N}_6\text{O}_2\text{S}_8\text{Si}_2$ was 1560.7090, and found was 1560.6237 $[\text{M}]^+$.

DTF phenylacetylene building block (**37**)



To the solution of compound **49** (0.50 g, 0.32 mmol) in THF/MeOH (40 ml, 2:1 v/v) was added K_2CO_3 (0.13 g, 0.96 mmol). The reaction mixture was stirred for 2 h at rt. On completion, the solvent was removed under reduced pressure. The residue was dissolved in CH_2Cl_2 , washed with water, dried over $MgSO_4$ and concentrated under reduced pressure to obtain pure compound **37** (0.43 g, 0.30 mmol, 97%) as a pale yellow solid. m.p. 109-112 °C; IR (neat): 3295, 2960, 2919, 2848, 2101, 1497, 1275, 1220, 1040, 1028, 973, 929, 894, 862, 830, 795, 714 cm^{-1} . 1H NMR (500 MHz, CD_2Cl_2): δ 8.21 (s, 2H), 7.80 (d, $J = 8.1$ Hz, 4H), 7.27 (d, $J = 8.3$ Hz, 4H), 6.96 (s, 2H), 6.49 (s, 2H), 4.82 (t, $J = 4.5$ Hz, 4H), 4.35 (t, $J = 4.6$ Hz, 4H), 3.48 (s, 2H) 2.84 (t, $J = 7.2$ Hz, 8H), 1.69-1.61 (m, 8H), 1.41-1.28 (m, 56H), 0.89-0.85 (m, 12H); ^{13}C NMR (75 MHz, CD_2Cl_2): δ 153.8, 147.6, 136.4, 133.3, 128.5, 128.2, 127.5, 125.9, 125.1, 121.9, 118.1, 114.0, 113.9, 83.9, 79.6, 68.3, 50.1, 36.5, 36.4, 32.3, 30.3, 30.1, 29.97, 29.94, 29.7, 29.5, 28.94, 28.91, 23.1, 14.3; HRMS (MALDI-TOF, +eV) m/z calculated for $C_{78}H_{108}N_6O_2S_8$ was 1416.6299, and found was 1417.6313 $[M + H]^+$.

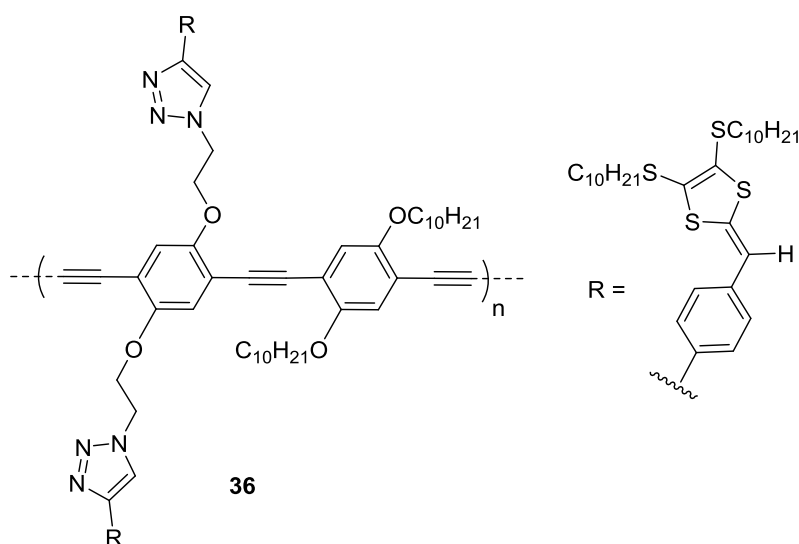
DTF functionalized homo-coupled polymer (**35**)



To a solution of compound **37** (110 mg, 0.070 mmol) in $\text{CHCl}_3/\text{acetone}$ (50 mL 1:1 v/v) were added CuI (7.30 mg, 0.038 mmol) and $\text{PdCl}_2(\text{PPh}_3)_2$ (10.8 mg, 0.015 mmol) and then TMEDA (0.5 mL). The reaction mixture was degassed by bubbling N_2 at rt for 5 min before it was heated to 60 °C for 2 h. Then the solvent was removed under reduced pressure. The residue which remained was dissolved in CH_2Cl_2 and sequentially washed with brine and water. The organic layer was dried over MgSO_4 and concentrated under vacuum to give a deep brown colored solid. This solid was re-dissolved in CH_2Cl_2 and slowly added to MeOH. The homo-coupled polymer **35** was precipitated as a brown solid, which was collected by filtration (88 mg, 0.056 mmol, 80%). IR (neat): 2921, 2850, 1614, 1563, 1496, 1458, 1362, 1171, 1066, 1014, 846, 801, 699 cm^{-1} ; ^1H NMR (500 MHz, CDCl_3): δ 8.18 (m, 2H), 7.87 (m, 4H), 7.05 (m, 4H), 6.79 (m, 2H), 6.22 (m, 2H), 4.69 (m, 4H), 4.17 (m, 4H), 2.83-2.67 (m, 8H), 1.56-1.23 (m, 64H), 0.86 (m, 12H);

^{13}C NMR (75 MHz, CD_2Cl_2): δ 153.9, 147.7, 136.4, 133.3, 128.5, 128.2, 127.5, 125.9, 121.9, 118.2, 114.0, 113.9, 87.3, 83.8, 79.6, 68.3, 50.1, 36.5, 36.4, 32.3, 30.3, 30.1, 29.97, 29.94, 29.7, 29.5, 28.93, 28.91, 23.1, 14.3. GPC: $M_n = 6233$ g/mol, $M_w = 10504$ g/mol, PDI = 1.7.

DTF functionalized cross-coupled polymer (36)



To the solution of compound **37** (0.22 g, 0.15 mmol) in dry THF/piperidine (50 ml 1:1 v/v) were added compound **52** (0.10 g, 0.15 mmol), CuI (14 mg, 0.071 mmol), $\text{PdCl}_2(\text{PPh}_3)_2$ (21 mg, 0.031 mmol) and compound **53** (9.5 mg, 0.015 mmol). The reaction mixture was degassed by bubbling N_2 at rt for 5 min and then allowed to stir at 60°C for 24 h. Then the solvent was evaporated under vacuum, obtained residual solid was dissolved in CH_2Cl_2 and sequentially washed with water and brine solution to give deep brown colored solid. This solid was redissolved in CH_2Cl_2 and MeOH was slowly

added to precipitate polymer **36** as brown color solid which was collected by filtration (56 mg, 0.038 mmol, 25%). IR (neat): 2901, 2750, 1594, 1563, 1466, 1428, 1302, 1091, 1066, 1011, 837, 801, 702 cm^{-1} . ^1H NMR (500 MHz, CD_2Cl_2): δ 7.84 (m, 6H), 7.25-7.10 (m, 6H), 6.48-6.26 (m, 6H), 4.71 (m, 4H), 4.36-4.08 (m, 4H), 2.84 (m, 12H), 1.74-1.26 (m, 96H), 0.86 (m, 18H); Meaningful ^{13}C NMR spectrum was not obtained due to limited solubility in organic solvents.

2.5. References

- (1) Britz, D. A.; Khlobystov, A. N. *Chem. Soc. Rev.* **2006**, *35*, 637-659.
- (2) Guldi, D. M.; Rahman, G. M. A.; Zerbetto, F.; Prato, M. *Acc. Chem. Res.* **2005**, *38*, 871-878.
- (3) Star, A.; Stoddart, J. F. *Macromolecules* **2002**, *35*, 7516-7520.
- (4) Hecht, D. S.; Ramirez, R. J. A.; Briman, M.; Artukovic, E.; Chichak, K. S.; Stoddart, J. F.; Gruner, G. *Nano Lett.* **2006**, *6*, 2031-2036.
- (5) Rice, N. A.; Soper, K.; Zhou, N.; Merschrod, E.; Zhao, Y. *Chem. Commun.* **2006**, 4937-4939.
- (6) Pourghaz, Y.; Dongare, P.; Thompson, D. W.; Zhao, Y. *Chem. Commun.* **2011**, *47*, 11014-11016.
- (7) Liang, S.; Chen, G.; Peddle, J.; Zhao, Y. *Chem. Commun.* **2012**, *48*, 3100-3102.

- (8) Mulla, K.; Zhao, Y. *J. Mater. Chem. C* **2013**, *1*, 5116-5127.
- (9) Moore, A. J.; Bryce, M. R. *Tetrahedron Lett.* **1992**, *33*, 1373-1376.
- (10) Yang, X.; Li, Z.; Zhi, J.; Ma, J.; Hu, A. *Langmuir* **2010**, *26*, 11244-11248.
- (11) Mulla, K.; Shaik, H.; Thompson, D. W.; Zhao, Y. *Org. Lett.* **2013**, *15*, 4532-4535.
- (12) Zhou, N. Ph.D. thesis, Memorial University, **2008**.

Chapter 3

Dithiafulvenyl-grafted phenylacetylene polymers as selective and reversible dispersants for single-walled carbon nanotubes

3.1 Introduction

As mentioned in previous chapters, the Zhao group recently disclosed that the presence of dithiafulvenyl (DTF) units in conjugated systems led to excellent supramolecular interactions with single walled carbon nanotubes mainly as a result of the strong electron donating properties of DTF.¹ The unique properties of the DTF functionality in enhancing the binding strength towards SWNTs thus led us to design and synthesize polymers **35** and **36** as described in Chapter 2. With polymers **35** and **36** in hand, dispersion of two commercially available SWNTs, HiPCO and CoMoCAT nanotubes SWNTs was then investigated. For the dispersion experiments, a straightforward ultrasonication protocol was used and the details are described as follows: pristine SWNTs were first added to the solutions of polymer **35** and **36**, and then the mixture was subjected to ultra-sonication for 30 min. After that, the resulting black suspension was filtered through a tightly packed cotton plug to remove insoluble

components and afford the stable solution of SWNT-polymer complexes. The work described in this chapter was mainly aimed at understanding the supramolecular interactions between the polymers and various types of single-walled carbon nanotubes. To fulfill this task, a number of spectroscopic and microscopic characterization techniques have been employed. In addition, it was envisioned that the polymers would show selective affinity for certain types of SWNTs in organic solutions. If such properties could be demonstrated, it would open a new avenue for effective isolation of structurally homogeneous SWNTs by straightforward polymer dispersion methods.

3.2 Characterization Techniques

To fully characterize the various properties of SWNTs-polymer supramolecular complexes, a large number of analytical techniques can be used. Among them electron microscopy, Raman spectroscopy, thermo gravimetric analysis (TGA), and optical absorption spectroscopy are the commonly used. The following section will highlight on the fundamentals and applications of some of these methods for the investigation of SWNT related nanosystems.

3.1.1 Absorption Spectroscopy

The relationship between excitation energies and nanotube diameter, chirality, and metallic or semiconductor character can be described by the Kataura plot.² Absorption spectra of SWNTs contain mainly three broad absorption regions, namely the S_{11} , S_{22} , and M_{11} bands, where the S_{11} and S_{22} bands are due to electronic transitions

taking place in semiconductor SWNT, and the M_{11} bands are due to the electronic transitions of metallic SWNTs. The electronic transitions in nanotubes can be explained by the one dimensionality of SWNTs. i.e., a simple one electron model of SWNTs.³ It indicates that the density of states (DOS) of nanotubes is characterized by singularities, called van Hove singularities (Figure 3.1). Each van Hove singularity belongs to a different quantum sub-band. In this model, (see Figure 3.1) dipole-allowed transitions occur between valence sub-bands to the corresponding conduction sub-bands. These transitions appear in a wide spectral window including the near infrared (NIR) and visible (Vis) regions. The first and second allowed transitions (S_{11} , S_{22}) for semiconducting SWNTs will appear in the Vis-NIR region, whereas for metallic SWNTs, the first allowed transition will appear within the Vis and near UV range (Figure 3.2)

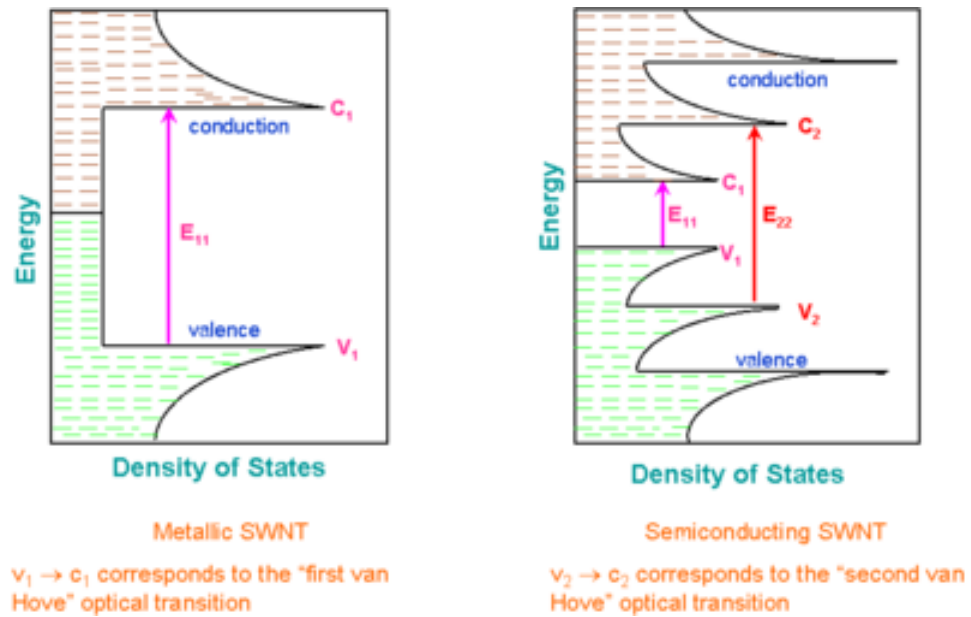


Figure 3.1: Schematic DOS diagrams for metallic and semiconducting single-walled carbon nanotubes based on a simple band theory model. Allowed optical transitions are illustrated as vertical arrows (copied from reference 3 with permission).

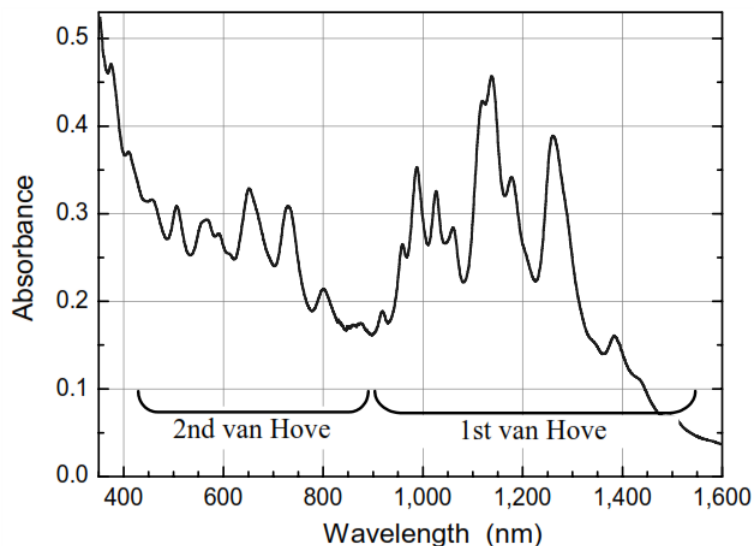


Figure 3.2: An exemplar electronic absorption spectrum of HiPCO single-walled carbon nanotubes (copied from reference 3 with permission).

3.1.2 Photoluminescence excitation (PLE) mapping studies

Photoluminescence mapping is another technique which has been intensively used for optical characterization of SWNTs. A PL map is a two dimensional map which is obtained by plotting PL emission intensities as a function of excitation and emission energies. Figure 3.3 was adopted from Adronov research group as part of collaboration which shows a typical PL map of SWNTs dispersed in D_2O with sodium dodecylbenzene sulfonate (SDBS). Each high intense peak observed in a PL map is due to the excitation transition energy of the second sub-band E_{22} and the corresponding emission energy of the first sub-band E_{11} of a specific SWNT structure defined by particular chiral indices. As the energies of E_{11} and E_{22} are dependent on the structure of SWNT, a PLE map can

provide information about the specific chiral indexes (n , m) of SWNTs measured. Currently, PL mapping studies are considered to be one of the most effective approaches to disclose the structure distribution in a bulk SWNTs sample.

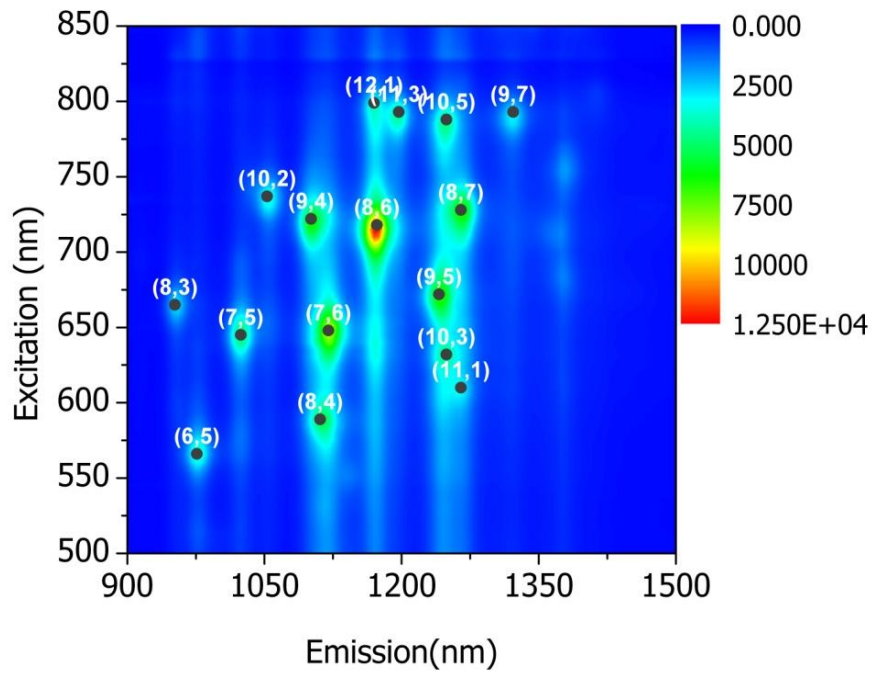


Figure 3.3: PLE map of HiPCO SWNTs dispersed with SDBS in water.

3.1.3. Scanning Electron Microscopy (SEM)

Scanning electron microscopy (SEM) is a surface probing technique in which a high voltage accelerated electron beam scans the surface of the sample to give a high resolution image at the nanometer scale level. This technique allows visualization of the overall SWNT dispersion within the polymer matrix as well as the identification of individual or bundled SWNTs at high resolution. A qualitative evaluation of nanotubes can be possible as amorphous carbon, graphite and metal nanoparticles are distinguishable from SWNTs according to the SEM images. When the SEM equipment combines closely related techniques such as energy dispersive X-ray (EDX) microanalysis, it can provide a quantitative estimate of the metal contents in microscopic surface regions of SWNT samples.

3.1.4 Atomic force microscopy (AFM)

In the AFM technique, a three dimensional topographical image of a carbon nanotube is attained due to the interaction forces between the AFM cantilever tip and the nanotube sample. An AFM cantilever is a sharp tip, where the radius of curvature is in the nanometer range. As the tip is brought into the proximity of the sample surface to be investigated, the tip-sample surface interactions generated induce a deflection in the cantilever orientation. The deflection is measured by a transmitting laser beam on the working cantilever and the reflected laser beam is measured using position sensitive photodiodes.

A deflection in the cantilever is possible not only by the direct contact of tip and sample surface but also by long range interactions such as van der Waals, electric and magnetic forces. Due to these possible interactions, an AFM can be operated in different modes such as contact mode, non contact mode or tapping mode depending on the required type of nanotube characterization. AFM imaging provides information about the morphological characteristics of the nanotubes, homogeneity, dispersability and the purity of the investigated sample.

3.1.5 Thermogravimetric analysis (TGA)

TGA can quantitatively determine the weight loss of a sample as a function of increasing temperature. It is particularly useful as a technique to study the SWNTs covalently or non-covalently functionalized with other molecular/macromolecular moieties. In a TGA experiment, the sample is gradually heated to high temperatures, up to as high as 1000 °C. Combustion of different types of carbon starts as the temperature reaches about 300 °C. Below these temperatures, weight losses are due to the evaporation of adsorbed humidity and pyrolytic evolution of surface functional groups. Combustion of the nanotubes and the carbonaceous impurities takes place at temperatures between 300 and 600 °C, and several band components are usually observed in the TGA derivative (dTG). If dTG bands could be assigned to different types of carbon, the evaluation of SWNT purity would be possible from the band integral areas. It is commonly accepted that combustion temperatures for different types of carbon present in SWNT samples

should be inversely proportional to their structural order or graphitization level. Accordingly, amorphous carbon is expected to react at lower temperatures than nanotubes, and graphite particles should react at temperatures somewhat higher than nanotubes. However, SWNT samples are complex mixtures of nanotubes and other types of carbon, and the experimental dTG band assignments are usually ambiguous.⁴

3.1.6. Raman Spectroscopy

Raman spectroscopy is another useful technique to characterize the structure of SWNTs. Raman features of nanotubes are strongly dependent on the specific characteristics of various nanotubes such as diameter, chirality, conducting or semiconducting nature, and functionalization degree.⁵

The prominent bands in the Raman spectrum of SWNTs (Figure 3.5) are:

Tangential modes or G band: In a Raman spectrum of SWNTs, the region between 1500-1600 cm^{-1} is called tangential mode or G-band. The tangential region is comprised of two superimposed high intensity peaks labeled as G^+ and G^- . The G^+ band is due to the vibrations of carbon atoms on the SWNT walls in the direction along the tube axis, whereas the G^- band is generated by the vibrations along the circumferential direction as shown in Figure 3.4. The shape of G^- band is different for metallic and semiconducting SWNTs.

The radial breathing modes (RBM): The region around 100-400 cm^{-1} is the RBM mode. This band arises from the in phase vibrations of carbon atoms in radial direction of nanotube, as if the nanotube is breathing. Their frequencies are inversely proportional to the diameters of SWNTs. The frequency- diameter relationship is useful to characterize the diameters of SWNTs as it provides information regarding the diameter distribution of a SWNT sample.

The D band: around 1300 cm^{-1} is associated with disordered carbon forms or defects in SWNTs.

The G' band: around 2600 cm^{-1} , is the second order harmonic of the D band. The G band intensity, or the G/D intensity ratio, is useful for the purity assessment of SWNT samples. If SWNT samples are homogeneous, the relative purity of several samples could be directly compared from the G band intensity measured under identical experimental conditions. However, the heterogeneity of SWNT samples often limits the purity evaluation by this technique.

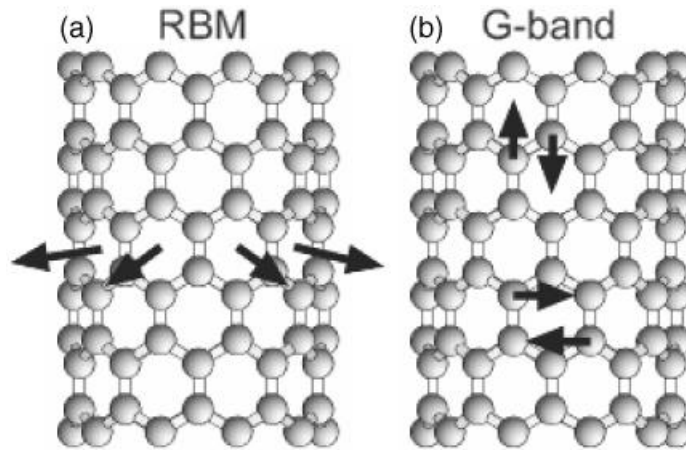


Figure 3.4: (a) Vibration of carbon atoms in radial direction. (b) Vibrations along the nanotube axis, and along the circumference direction (Copied from reference 5 with permission).

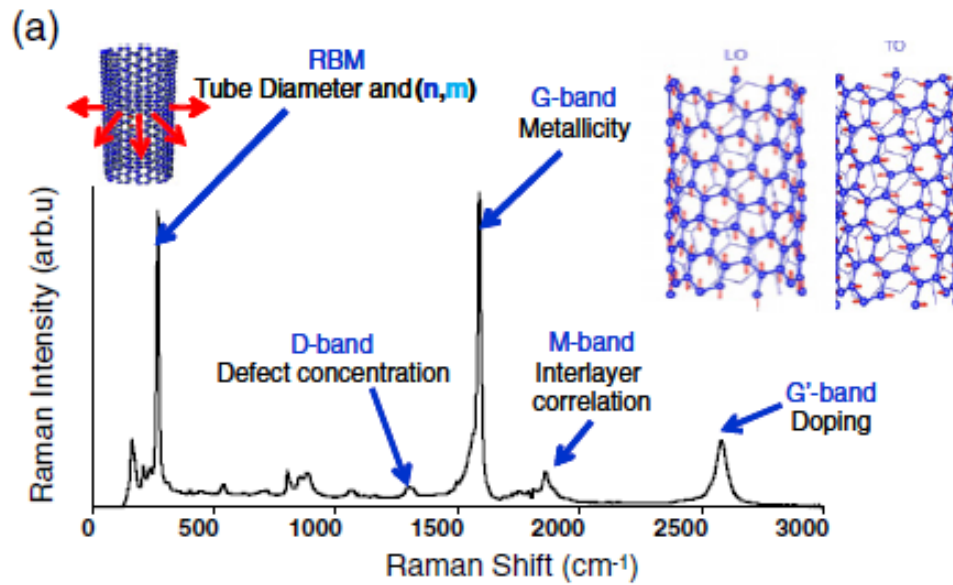


Figure 3.5: A representative Raman spectrum of SWNTs (copied from reference 5 with permission).

3.2 SWNTs–polymer dispersion studies

Usually, the effective dispersion of SWNTs in a given solvent requires dispersing agents (dispersants) with sufficient binding forces toward SWNTs so as to break down their heavily entangled bundles. As shown in Figure 3.6, two design strategies, namely π -stacking⁶⁻⁸ and helical wrapping^{9,10-13} have been so far popularly employed in the development of SWNT dispersants based on a large variety of molecular and macromolecular systems.

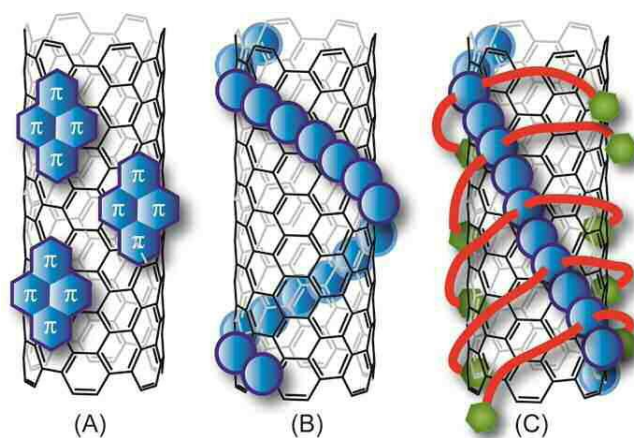


Figure 3.6: Schematic illustrations of three design strategies for SWNT dispersion: (A) π -stacking, (B) helical wrapping, and (C) centipede wrapping.

Whereas linear-shaped π -conjugated polymers such as poly(phenylene ethynylene)s (PPEs) and poly(phenylene butadiynylene)s (PPBs) were previously deemed to be unable to wrap around SWNTs due to their structural rigidity,¹⁴ a recent molecular dynamic (MD) study by Savens and co-workers has demonstrated that PPEs

could adhere to the surface of SWNTs by adopting a robust helical superstructure.¹⁵ It has also been found that the side chains of linear π -conjugated polymers play a critical role in dictating both the effectiveness and selectivity for SWNT interactions.¹⁶ Inspired by these findings, a new centipede wrapping strategy has been conceived for SWNT dispersion by using our DTF-grafted polymers as depicted in Figure 3.6. The DTF functionality, which has an electron rich aromatic end group in the side chains of a linear conjugated polymer, are expected to give strong π -stacking on the sidewall of SWNTs, resulting in a second wrapping motif orthogonal to the helical wrapping direction of the polymer backbone. The proposed centipede like wrapping strategy of polymers and SWNTs was supported by molecular modeling studies using the molecular mechanics (MM) method. Figure 3.7 shows the minimum energy conformation of the trimer of **35** in interaction with a (6, 6) SWNT. The modeling results show that the trimer adopts a folding conformation as expected via intimate π - π contact with the nanotube sidewall. The phenylacetylene backbone of the trimer adheres to the SWNT at an angle of 19° with respect to the longitudinal axis of the tube, while the DTF-appended side chains embrace the tube circumferentially at an angle of 90° .

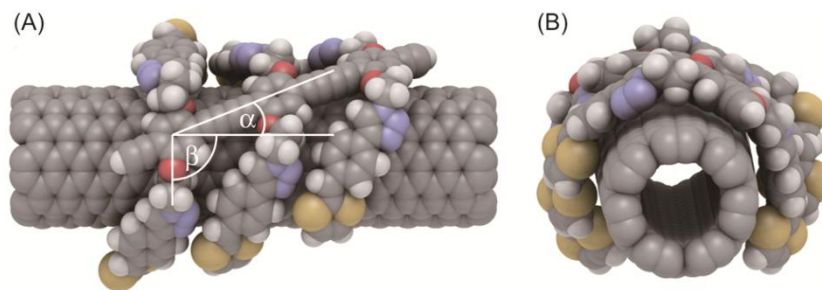


Figure 3.7: Geometry of the trimer of **35** wrapped around a (6, 6) nanotube optimized by the MMFF force field (Note that the $\text{SC}_{10}\text{H}_{21}$ groups were replaced by hydrogens to save computational cost). (A) Side view, (B) front view. Wrapping angles: $\alpha = 19^\circ$, $\beta = 90^\circ$.

Dispersion experiments were carried out in various organic solvents using polymers **35** and **36** as dispersants. Both polymers were found capable of effectively dispersing SWNTs in organic solvents, including CHCl_3 , CH_2Cl_2 , chlorobenzene, toluene, and THF. The polymer-nanotube supramolecular composites obtained were then examined by various analytical techniques and discussed in following sections.

3.2.1. Characterization of DTF-polymer/SWNTs complexes

3.2.1.1. UV-Vis-NIR results

Figures 3.8 to 3.11 show the UV-Vis-NIR absorption spectra of a HiPCO nanotube composite with polymer **35** (1.5 mg/mL) in chloroform, chlorobenzene, dichloromethane, and toluene (Figure 3.8 A) respectively. Spectra show distinctive absorption bands which are characteristic of the van Hove electronic transitions. The peaks appearing in the range of 500-600 nm are the due to first van Hove electronic

transitions of metallic tubes (M_{11}), the second van Hove electronic transitions of semiconducting (S_{22}) tubes are in the range of 550-900 nm, while the peaks from 900-1600 nm are due to semiconducting tubes (S_{11}) with smaller diameter.

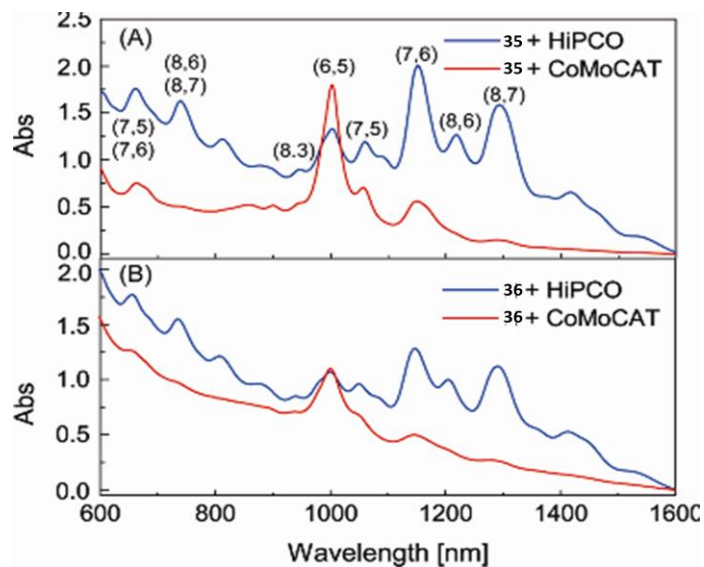


Figure 3.8: UV-Vis-NIR spectrum of HiPCO and CoMoCAT SWNTs dispersed with polymers **35** (A) and **36** (B) in toluene.

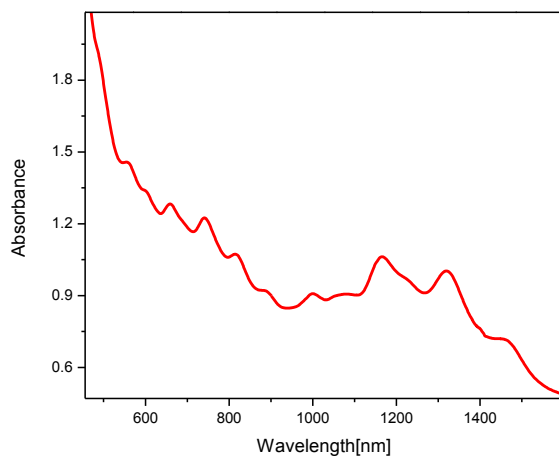


Figure 3.9: UV-Vis-NIR spectrum of HiPCO SWNTs dispersed with polymer **35** in CHCl_3 .

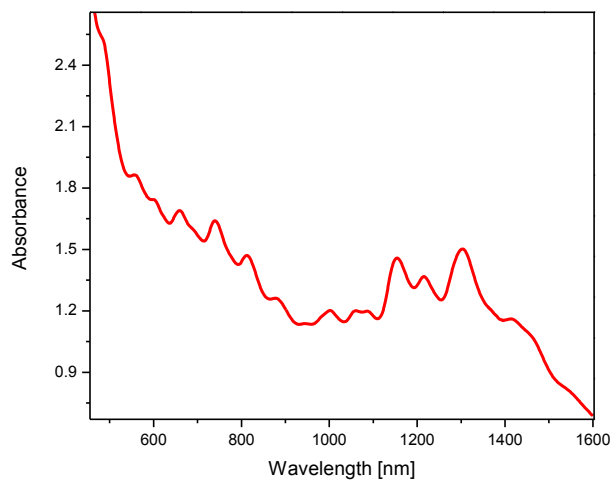


Figure 3.10: UV-Vis-NIR spectrum of HiPCO SWNTs dispersed with polymer **35** in chlorobenzene.

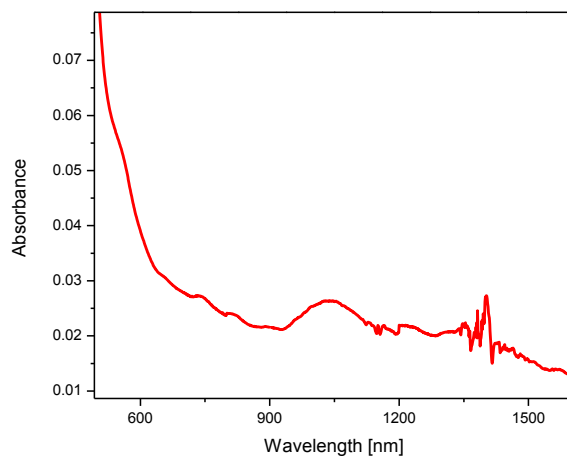


Figure 3.11: UV-Vis-NIR spectrum of HiPCO SWNTs dispersed with polymer **35** in CH_2Cl_2 .

Figure 3.12 shows the UV-Vis-NIR spectrum of CoMoCAT SWNT/**35** solution in chlorobenzene, chloroform, dichloromethane, and toluene (Figure 3.8 A). A prominent peak in the spectrum at 999 nm is observed, which is assigned to SWNTs with chiral index of (6, 5) and the other less intense peaks at 578 and 670 nm are assigned to (7, 5) and (7, 6) SWNTs respectively.

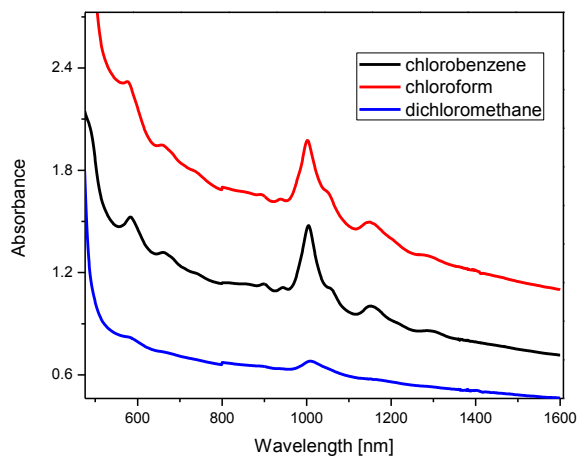


Figure 3.12: UV-Vis-NIR spectrum of CoMoCAT SWNTs dispersed with polymer **35** in chlorobenzene, CHCl_3 , and CH_2Cl_2 .

Figure 3.8 B, and 3.13 to 3.17 shows the Vis-NIR absorption spectra of HiPCO and CoMoCAT nanotube composites with polymer **36** (1.5 mg/mL) in different solvents. The well-resolved peaks in the Vis-NIR region are due to the interband electronic transitions between the van Hove singularities in the valence and conduction bands of SWNTs.¹⁷ Assignments of these peaks to specific chiral indexes are made based on literature data¹⁸⁻²⁰ which is supported by photoluminescence excitation mapping studies.

The results indicate that the SWNTs were well dispersed and debundled in the solution of polymer **35** and **36**. It is observed that polymer **35** imparts a much better solubility to SWNTs in comparison to polymer **36**, as a result of its higher polymerization degree and more DTF-functionalities per repeat unit. The nanotubes dispersed by polymer **35** in solution are of much better quality than those dispersed by polymer **36**.

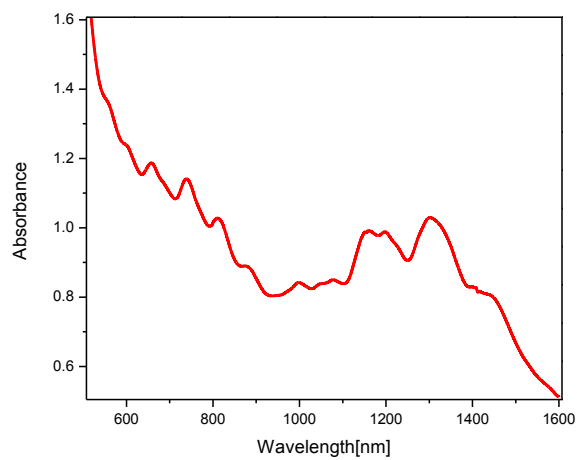


Figure 3.13: UV-Vis-NIR spectrum of HiPCO SWNTs dispersed with polymer **36** in CHCl_3 .

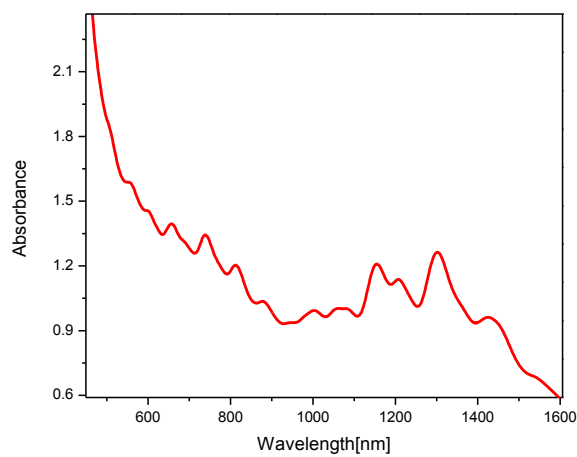


Figure 3.14: UV-Vis-NIR spectrum of HiPCO SWNTs dispersed with polymer **36** in chlorobenzene.

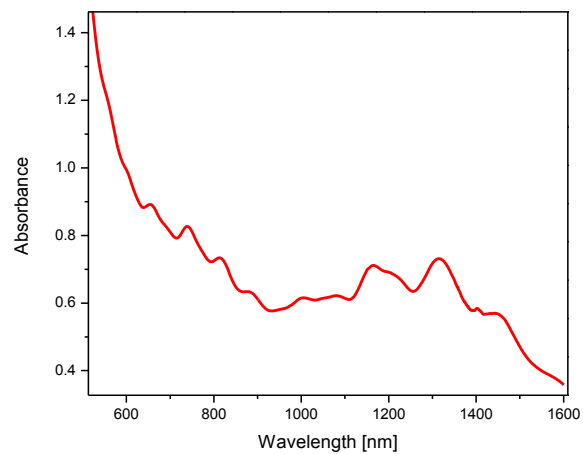


Figure 3.15: UV-Vis-NIR spectrum of HiPCO SWNTs dispersed with polymer **36** in CH_2Cl_2 .

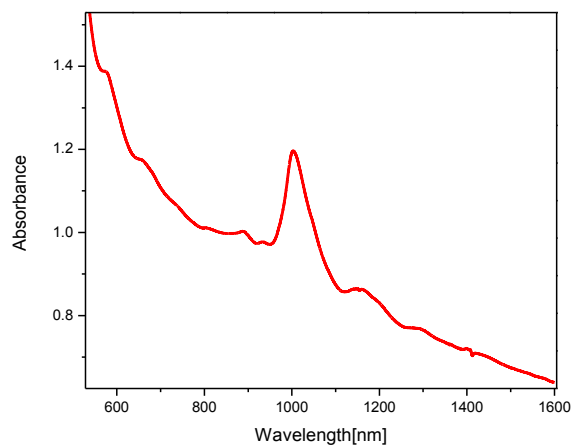


Figure 3.16: UV-Vis-NIR spectrum of CoMoCAT SWNTs dispersed with polymer **36** in CHCl_3 .

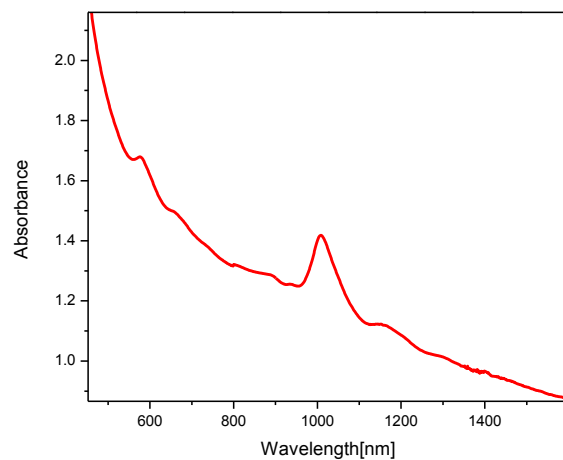


Figure 3.17: UV-Vis-NIR spectrum of CoMoCAT SWNTs dispersed with polymer **36** in CH_2Cl_2 .

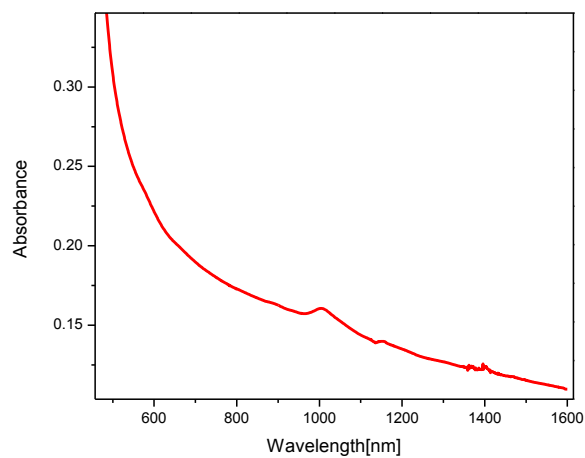


Figure 3.18: UV-Vis-NIR spectrum of CoMoCAT SWNTs dispersed with polymer **36** in chlorobenzene.

3.2.1.2. Photoluminescence excitation mapping studies

As part of collaboration, the Adronov's research group acquired the PLE maps on dispersed solutions of polymers **35** and **36**, and the data is presented in this section. The selectivity of polymer **35** toward SWNT dispersion was further characterized by the PLE maps in comparison with sodium dodecyl benzenesulfonate (SDBS) as most of the SWNTs with different chiral indexes can be assigned by using photoluminescence mapping studies (Figure 3.20).

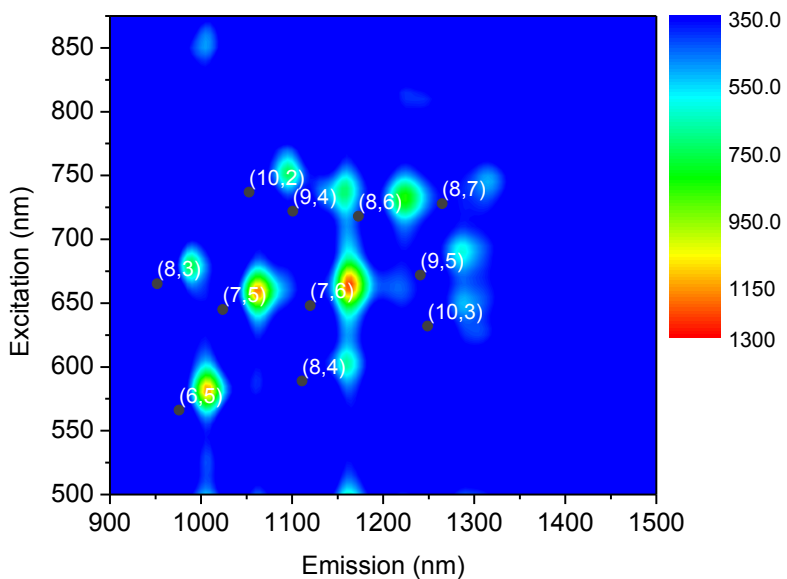


Figure 3.19: PLE maps of HiPCO dispersed in CH_2Cl_2 polymer **36**.

As shown in Figure 3.21, the dispersion of CoMoCAT tubes, (6, 5) and (7,5) are favored along with some (8,3) tubes co-existing in the suspension. However, for HiPCO nanotubes, as shown in Figure 3.20, the dispersion selectivity is strongest for tubes with (6,5), (7,5), and (7,6) chiral indexes, while a number of nanotubes with other chirality are also present in the suspension, including (8,3), (8,4), (8,6), (8,7), (9,4), (9,5), (10,2) and (10,3). Overall, polymer **35** appears to exhibit a high selectivity for (6,5), (7,5) and (7,6) tubes which are of relative small diameter (0.75 to 0.90 nm) in nature. Such kind of selectivity is in line with the theoretically predicted “centipede wrapping” mode, wherein the electron-rich DTF end groups act as a major driving force for effective SWNT binding.

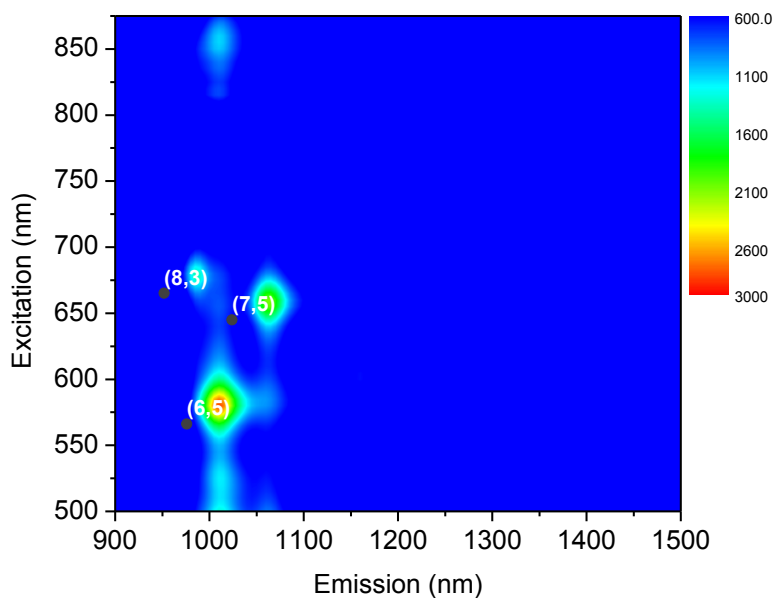


Figure 3.20: PLE maps of CoMoCAT dispersed in CH_2Cl_2 with polymer **35**.

3.2.1.3. AFM Studies

The morphology of SWNTs with DTF- polymers has been investigated by using atomic force microscopy (AFM). The samples for AFM measurement were prepared by spin-coating of dilute solution of HiPCO SWNT-DTF polymers suspensions on a freshly cleaved mica surface. The excess DTF-polymers were rinsed off with chloroform followed by drying with a flow of nitrogen gas. Figure 3.21 shows the AFM image of the supramolecular assemblies of HiPCO SWCNTs and DTF-polymer **35**, and Figure 3.22 depicts an AFM image of SWNT-polymer **36**. One can see that the features of an individual strand of SWNT can be clearly observed in both images.

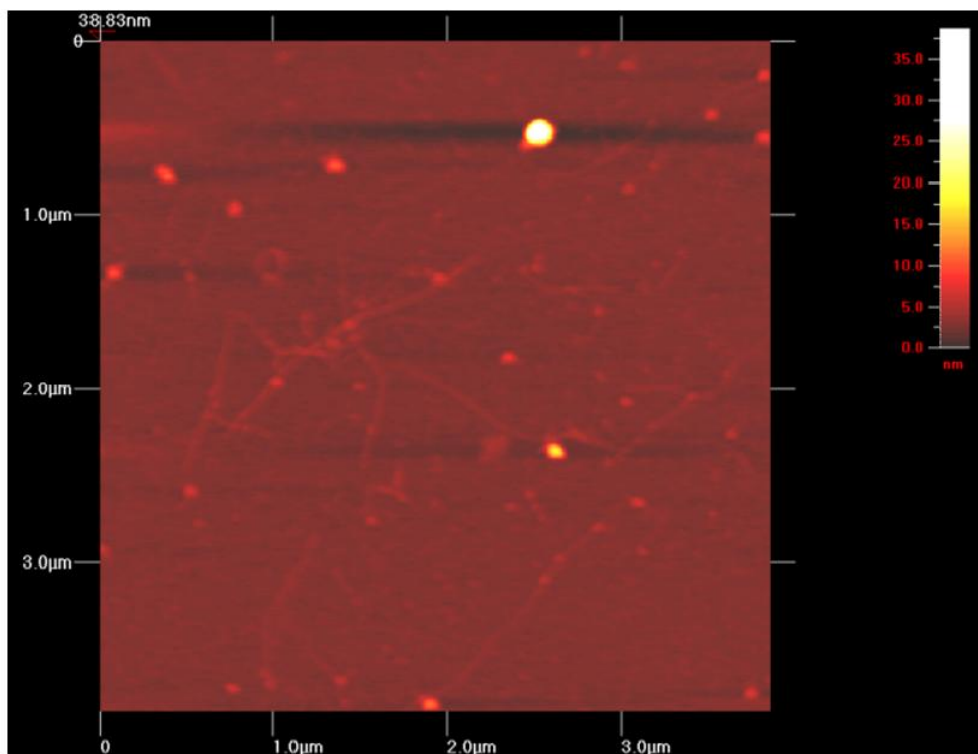


Figure 3.21: AFM image of the suspension of polymer **35** and HiPCO SWNTs drop-cast on a freshly cleaved mica substrate (tapping mode)

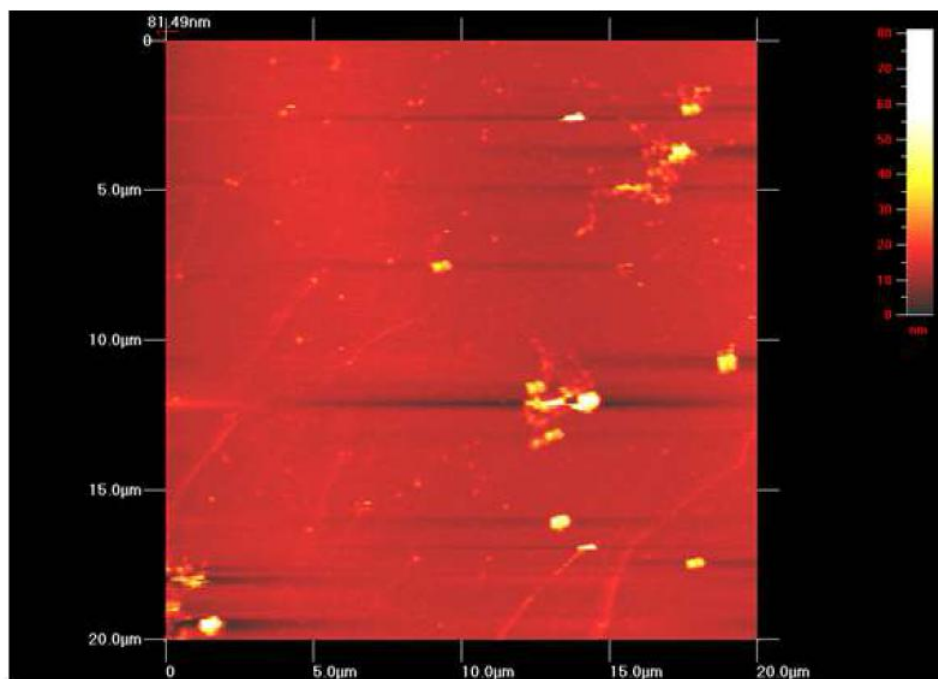


Figure 3.22: AFM image of the suspension of polymer **36** and HiPCO SWNTs drop-cast on a freshly cleaved mica substrate (tapping mode).

AFM imaging of the assemblies of CoMoCAT SWNTs with both polymers **35** and **36**, however, did not reveal any discrete nanotube features despite numerous trials under various conditions, and making individual SWNT strands unobservable by AFM

3.2.1.4. SEM studies

The SEM image (Figure 3.23) of SWNTs from a polymer dispersed solution shows a clear homogenous dispersion of nanotubes in polymer **36**/SWNT composites within the laser spot area of 1 μm . The polymer **35** and SWNTs composite image is shown in Figure 3.24. Dispersed nanotube strands are noticeable along with aggregated nanotube bundles. The presence of aggregated nanotube bundles is likely due to the fact that the dispersion process was not sufficient enough to completely debundled SWNTs into individual strands.

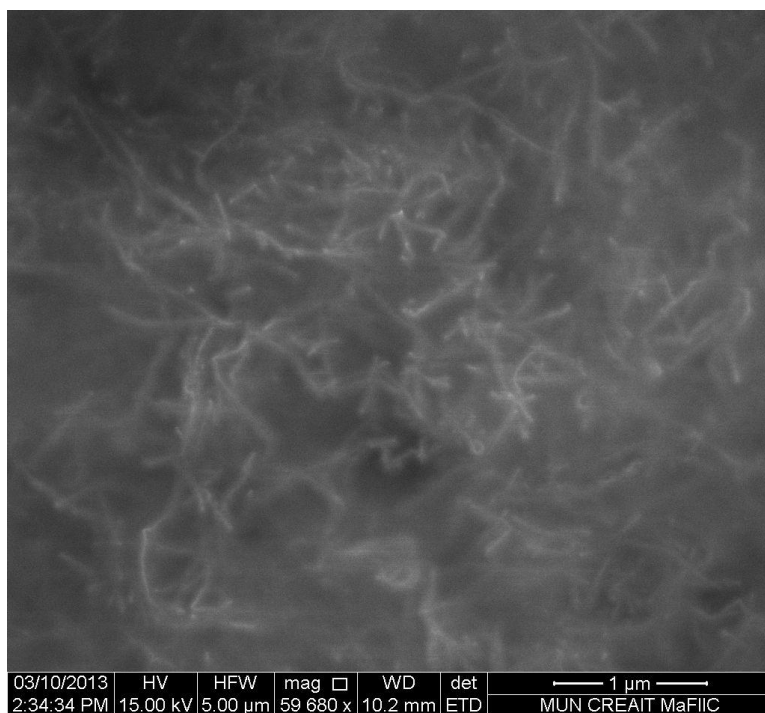


Figure 3.23: SEM image of the complex of polymer **36** and HiPCO SWNTs after solvent evaporation.

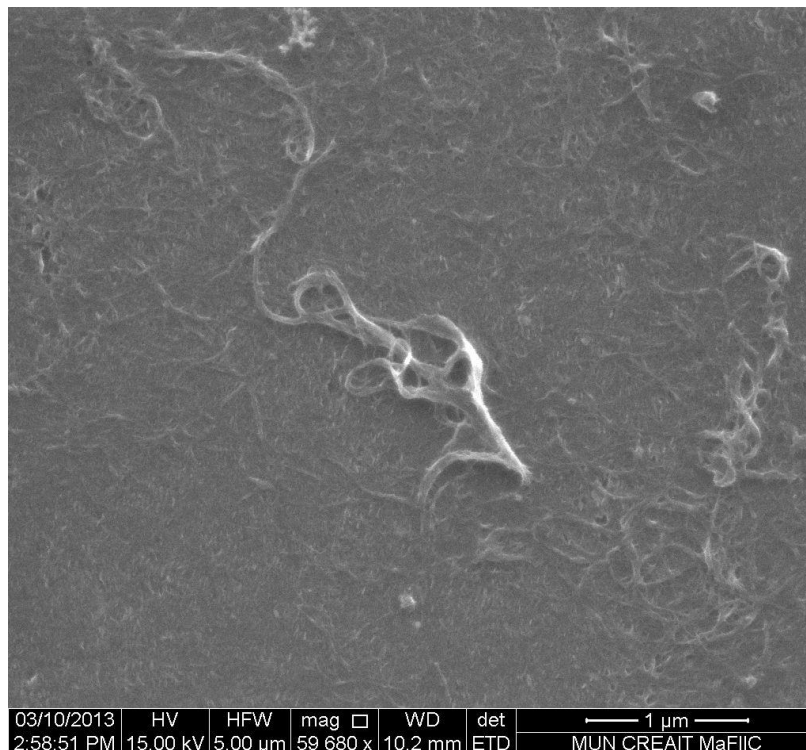


Figure 3.24: SEM image of the complex of polymer **35** and HiPCO SWNTs after solvent evaporation.

3.2.1.5. Raman Spectroscopic Studies

Raman spectroscopy was used for the further characterization of SWNTs-DTF polymer complexes. Raman measurements were carried out at 785 nm. The radial breathing mode profiles at this excitation wavelength can be useful for evaluation of the

extent of aggregation occurring in a sample.²¹ The RBM profiles of the raw HiPCO-SWNTs and polymer **35**-SWNT complexes are shown in Figure 3.25. The pristine HiPCO SWNTs have five major RBM bands at Raman frequencies of 270-210 cm^{-1} , which is consistent with reported values of HiPCO nanotubes.^{21,22} The Raman spectrum of HiPCO SWNTs complexed with polymer **35** exhibits all the characteristic signals of SWNTs. A significant change in its RBM profile is observed when compared to the RBM signals of the raw SWNTs. All of the peaks of the polymer **35**-SWNT complexes show a characteristic red shift of 3-6 cm^{-1} relative to the equivalent peaks in the spectrum of the raw HiPCO. The signal at 270 cm^{-1} is much more dominant in the spectra of pristine bundled SWNTs; in the polymer functionalized samples, a decrease in intensity of this signal is observed. This result indicates that the nanotubes are individually dispersed by polymers in solution. The region between 1200 to 2000 cm^{-1} exhibits the characteristic G and D bands of SWNTs, which are convoluted with some broad Raman peaks attributable to polymer **35**. It is worth noting that the G' band typical of pristine SWNTs disappears in the spectrum of HiPCO/polymer **35**, which is indicative of strong electronic interaction²³ between polymer **35** and SWNTs. Figure 3.27 shows is the Raman spectrum of both raw CoMoCAT and Polymer **35** complexed with CoMoCAT SWNTs, the latter showing all the characteristic signals of SWNTs but with significant changes having been observed in its RBM profile, the G¹ and D bands, in comparison to pristine CoMoCAT SWNTs.

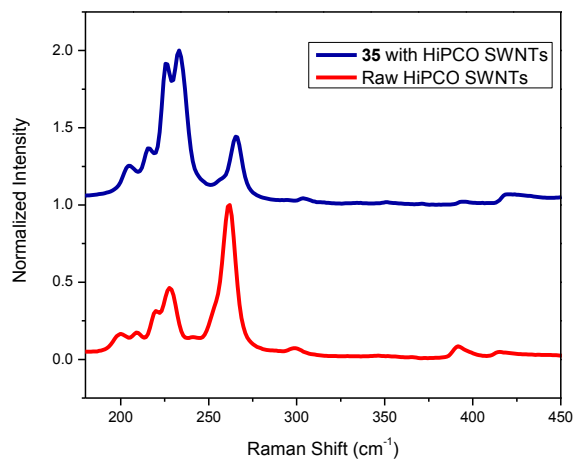


Figure 3.25: Raman spectra of polymer **35** complexed with HiPCO-SWNTs (RBM mode) vs Raw HiPCO SWNTs.

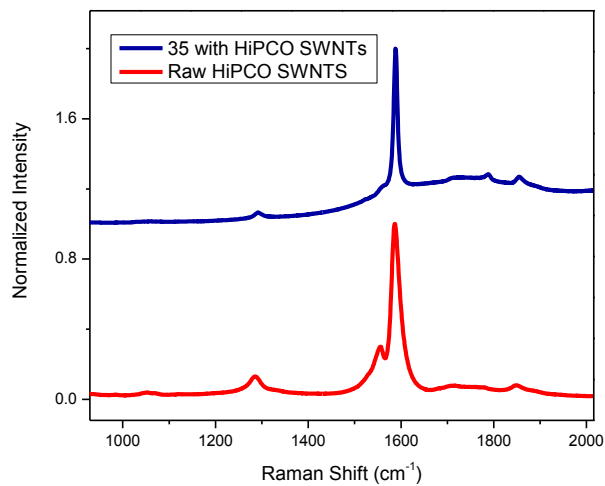


Figure 3.26: Raman spectra of polymer **35** complexed with HiPCO-SWNTs (tangential mode) vs Raw HiPCO SWNTs.

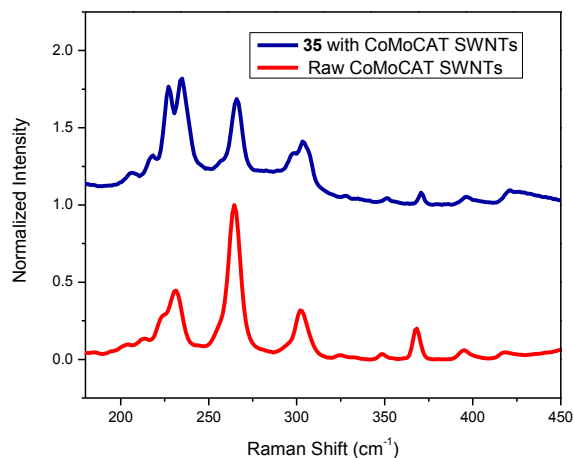


Figure 3.27: Raman spectra of polymer **35** complexed with CoMoCAT-SWNTs (RBM mode) vs Raw CoMoCAT SWNTs.

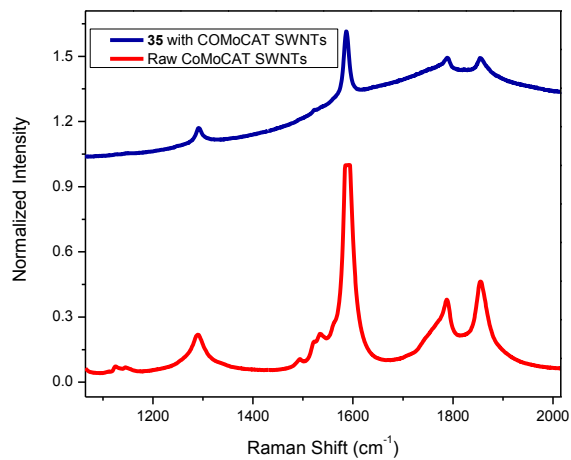


Figure 3.28: Raman spectra of polymer **35** complexed with CoMoCAT-SWNTs (tangential mode) vs Raw CoMoCAT SWNTs.

3.2.1.6 TGA results

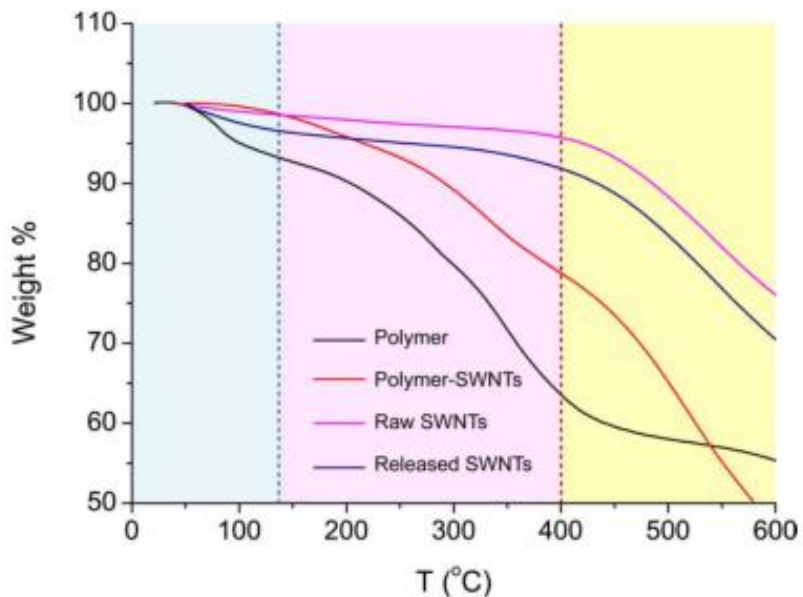


Figure 3.29: TGA profiles of polymer **35**, polymer **35**/CoMoCAT nanotube complexes, raw CoMoCAT nanotubes, and released CoMoCAT nanotubes. Scan rate: 10 °C/min.

Polymer **35**/SWNT complexes were prepared by sonication of excess CoMoCAT nanotubes with a CHCl_3 solution of **35** for 40 min. The resulting black suspension was filtered through a tightly packed cotton plug, and the filtrate was evaporated under vacuum to afford the polymer/SWNT complexes. Released SWNTs were obtained by addition of an equal volume of hexanes to the suspension of Polymer **35**/SWNTs in chloroform. The resulting mixture was subjected to centrifugation to separate the released SWNTs and the polymer solution. Next, three cycles of CHCl_3 washing and

centrifugation separation were performed to further remove the polymer component. Finally, the SWNTs were collected by vacuum filtration and dried in an oven at 80 °C.

From Figure 3.29, a noticeable amount of weight loss can be seen in the TGA curves of polymer **35** and released SWNTs in the range from room temperature to 137 °C. The weight loss is attributable to desolvation and/or desorption of moisture. From 137 °C to 400 °C, polymer **35** shows a significant degree of weight loss as a result of decomposition reactions. Raw CoMoCAT nanotubes, on the other hand, do not show any significant weight loss below 400 °C. Given the TGA behavior observed, it is reasonable to estimate the polymer content associated with released SWNTs by examining the weight loss occurring in the temperature range of 137-400 °C. Table 3.1 lists the detailed data.

Table 3.1: TGA data of polymer **35**, polymer **35**/SWNT complexes, raw SWNTs, and released SWNTs measured at 137 °C and 400 °C.

Entry	Wt % (137 °C)	Wt % (400 °C)	Δ Wt %	Wt % Polymer*
Polymer 35	93.3%	63.5%	29.8%	
Raw SWNTs	98.6%	95.7%	2.9%	
Polymer 35 /SWNTs	98.6%	78.7%	19.9%	77%
Released SWNTs	96.6%	91.8%	4.8%	7.6%

Assuming the weight percent of polymer 35 is $x\%$ and the weight percent of SWNTs is $y\%$ in a polymer/SWNTs complex, then the relationship between the measured Δ Wt% values can be described by the following equations:

$$\Delta \text{Wt \% (polymer/SWNTs)} = \Delta \text{Wt \% (polymer)} \times x\% + \Delta \text{Wt \% (SWNTs)} \times y\%$$

$$x\% + y\% = 100\%$$

Combining the above two equations, the weight percent (y %) of polymer components in the polymer/SWNT complex is calculated to be 77%. For the released SWNTs, the weight percent of polymer **35** is only 7.6%.

3.3 Releasing of SWNTs from polymer-SWNT complexes

In previous studies from our lab, DTFs (dithiafulvenes) were found to exhibit two very interesting properties. First, DTF is a highly redox active group that can readily release a single electron to form an aromaticity-stabilized ditholium cation,¹ second, the supramolecular interactions of DTF-functionalized π -oligomers with SWNTs show solvent-dependent behavior. The two properties can be utilized to exert control over reversible dispersion and release of SWNTs by external stimuli such as redox reactions and/or solvent control.¹² Indeed, controlled dissociation/release of pristine SWNTs from their suspension in solution has become a topic of growing interest over the past years,²⁴⁻²⁶ driven by the critical demand for additive-free SWNTs in the fabrication of advanced electronic and optoelectronic devices.

SWNTs dispersed with polymer **35** and **36** in chlorinated or aromatic organic solvents formed very stable homogenous suspensions. There was no precipitation of SWNTs observed even after a long-term storage. Addition of aliphatic hydrocarbon solvents to these suspensions, however, was found to quickly induce precipitation of SWNTs out of the polymer solution. This observation is in line with the results of DTF-end capped π -oligomers in our previous study, indicating a facile means to release

pristine SWNTs from their polymer suspensions using solvent control. To further explore this behaviour of solvent-controlled SWNT release, experiments on hexanes-induced SWNT release were undertaken. Figure 3.30 A and B depicts a reversible process of dispersing and releasing HiPCO SWNTs under solvent control, which could be turned into a very useful technique applicable in material preparation and device fabrication where “additive-free” SWNTs¹⁷ are desired after solution-phase processing (*e.g.*, dispersion) in order to maximize electronic and/or optoelectronic performances.

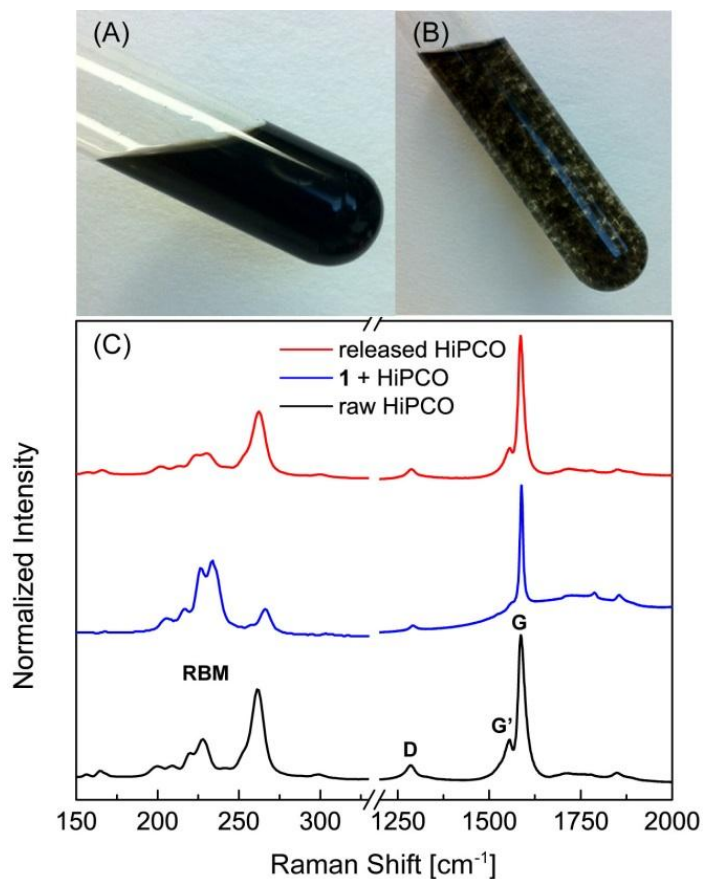


Figure 3.30: (A) Photographic image of HiPCO SWNTs dispersed in a CHCl_3 solution of polymer **35** (1.5 mg/mL). (B) Photographic image showing HiPCO SWNTs precipitated out of the solution of polymer **35** after addition of an equal volume of hexanes. (C) Raman spectra ($\lambda_{\text{ex}} = 785 \text{ nm}$) of raw HiPCO SWNTs, HiPCO SWNTs dispersed with polymer **35**, and HiPCO SWNTs released from polymer **35** after addition of hexanes to the solution.

To further evaluate the efficiency of the solvent-controlled release of SWNTs, comparative Raman spectroscopic analyses were performed. As shown in Figure 3.29 C, the Raman spectrum of HiPCO SWNTs released from the polymer solution after addition of hexanes does not exhibit any sign of broad polymer Raman bands. Instead, it shows a spectral pattern closely resembling that of the raw pristine HiPCO sample. The comparative Raman study confirms that the DTF-grafted polymers are able to effectively release SWNTs out the polymer dispersant, which in turn presents a significant advantage over others ways of releasing SWNTs (*e.g.*, redox, pH, light^{23,27-29}) in terms of cleanness, ease of operation, and cost-effectiveness. Thermal gravimetric analysis (TGA) shows that only a small amount of polymer dispersant (*ca.* 7.7 wt%) still remains in the released SWNTs; nevertheless, given the redox activity of the DTF groups in the polymer side chains, it is expected that complete removal of polymer dispersant can be readily achieved using the redox or acidity-controlled methods as previously developed in our lab for a class of tetrathiafulvalene-based polymers.¹²

3.4 Conclusion

A new and highly effective “centipede polymer wrapping” strategy for dispersion of SWNTs in various organic solvents using DTF-grafted linear π -conjugated polymers as dispersants was developed. Furthermore, the dispersion appeared to be selective for small semiconducting (6,5), (5,6), and (7,6) tubes, and “dispersant-free” SWNTs could be readily released from the SWNT/polymer suspensions under easy solvent control.

3.5 Experimental

Chemicals and reagents were purchased from commercial suppliers and used without further purification. HiPCO SWNTs were purchased from Carbon Nanotechnologies Inc. CoMoCAT SWNTs were purchased from Southwest NanoTechnologies Inc. UV-Vis-NR absorption spectra were recorded on a Cary 6000i spectrophotometer. Atomic force microscopy (AFM) images were taken with a Q-Scope AFM operated in tapping mode. Scanning electron microscopy (SEM) images were taken with a Hitachi S570 SEM operated at 15 kV. Raman spectra were performed with a Renishaw InVia Laser Raman spectrometer, equipped with a 300 mW Renishaw laser (785 nm, grating 1200 lines/mm). Photoluminescence excitation (PLE) mapping was carried out using the Jobin-Yvon SPEX Fluorolog 3.22 equipped with a 450 W Xe lamp, and fitted with a liquid-nitrogen cooled InGaAs photodiode H and c detector. Slit widths were set to a 10 nm band-pass for both excitation and emission, and samples were illuminated in a quartz cell using 5 nm wavelength steps. UV-Vis-NIR spectra were collected on Cary 5000 spectrometers using a 10 mm quartz cuvette.

3.6 References

- (1) Mulla, K.; Zhao, Y. *J. Mater. Chem. C* **2013**, *1*, 5116-5127.
- (2) Kataura, H.; Kumazawa, Y.; Maniwa, Y.; Umezu, I.; Suzuki, S.; Ohtsuka, Y.; Achiba, Y. *Synthetic Metals* **1999**, *103*, 2555-2558.

- (3) Dresselhaus, M. S. *Science of Fullerenes and Carbon Nanotubes*, Academic Press, San Diego, **1996**.
- (4) Itkis, M. E.; Perea, D. E.; Niyogi, S.; Rickard, S. M.; Hamon, M. A.; Hu, H.; Zhao, B.; Haddon, R. C. *Nano Lett.* **2003**, *3*, 309-314.
- (5) Souza Filho, A. G. *Nanotechnology* **2003**, *14*, 2043-2061.
- (6) Zhao, Y.-L.; Stoddart, J. F. *Acc. Chem. Res.* **2009**, *42*, 1161-1171.
- (7) Backes, C.; Hauke, F.; Hirsch, A. *Adv. Mater.* **2011**, *23*, 2588-2601.
- (8) Chen, R. J.; Zhang, Y.; Wang, D.; Dai, H. *J. Am. Chem. Soc.* **2001**, *123*, 3838-3839.
- (9) Kang, Y. K.; Lee, O.-S.; Deria, P.; Kim, S. H.; Park, T.-H.; Bonnell, D. A.; Saven, J. G.; Therien, M. J. *Nano Lett.* **2009**, *9*, 1414-1418.
- (10) Deria, P.; Von Bargen, C. D.; Olivier, J.-H.; Kumbhar, A. S.; Saven, J. G.; Therien, M. J. *J. Am. Chem. Soc.* **2013**, *135*, 16220-16234.
- (11) Zheng, M.; Jagota, A.; Strano, M. S.; Santos, A. P.; Barone, P.; Chou, S. G.; Diner, B. A.; Dresselhaus, M. S.; Mclean, R. S.; Onoa, G. B.; Samsonidze, G. G.; Semke, E. D.; Usrey, M.; Walls, D. J. *Science* **2003**, *302*, 1545-1548.
- (12) Liang, S.; Chen, G.; Peddle, J.; Zhao, Y. *Chem. Commun.* **2012**, *48*, 3100-3102.

- (13) Liang, S.; Zhao, Y.; Adronov, A. *J. Am. Chem. Soc.* **2013**, *136*, 970-977.
- (14) Rice, N. A.; Soper, K.; Zhou, N.; Merschrod, E.; Zhao, Y. *Chem. Commun.* **2006**, 4937-4939.
- (15) Von Bargen, C. D.; MacDermaid, C. M.; Lee, O.-S.; Deria, P.; Therien, M. J.; Saven, J. G. *J. Phy. Chem. B* **2013**, *117*, 12953-12965.
- (16) Yuan, W.; Li, W.; Mu, Y.; Chan-Park, M. B. *ACS Appl. Mater. Interfaces* **2011**, *3*, 1702-1712.
- (17) O'Connell, M. J.; Bachilo, S. M.; Huffman, C. B.; Moore, V. C.; Strano, M. S.; Haroz, E. H.; Rialon, K. L.; Boul, P. J.; Noon, W. H.; Kittrell, C.; Ma, J.; Hauge, R. H.; Weisman, R. B.; Smalley, R. E. *Science* **2002**, *297*, 593-596.
- (18) Bachilo, S. M.; Strano, M. S.; Kittrell, C.; Hauge, R. H.; Smalley, R. E.; Weisman, R. B. *Science* **2002**, *298*, 2361-2366.
- (19) Lian, Y.; Maeda, Y.; Wakahara, T.; Akasaka, T.; Kazaoui, S.; Minami, N.; Choi, N.; Tokumoto, H. *J. Phy. Chem. B* **2003**, *107*, 12082-12087.
- (20) Hagen, A.; Hertel, T. *Nano Lett.* **2003**, *3*, 383-388.
- (21) Heller, D. A.; Barone, P. W.; Swanson, J. P.; Mayrhofer, R. M.; Strano, M. S. *J. phy. Chem. B* **2004**, *108*, 6905-6909.

- (22) Backes, C.; Schmidt, C. D.; Hauke, F.; Böttcher, C.; Hirsch, A. *J. Am. Chem. Soc.* **2009**, *131*, 2172-2184.
- (23) Shin, H.-J.; Kim, S. M.; Yoon, S.-M.; Benayad, A.; Kim, K. K.; Kim, S. J.; Park, H. K.; Choi, J.-Y.; Lee, Y. H. *J. Am. Chem. Soc.* **2008**, *130*, 2062-2066.
- (24) Englert, B. C.; Bakbak, S.; Bunz, U. H. F. *Macromolecules* **2005**, *38*, 5868-5877.
- (25) Binder, W. H.; Sachsenhofer, R. *Macromol. Rapid. Commun.* **2007**, *28*, 15-54.
- (26) Durmaz, H.; Sanyal, A.; Hizal, G.; Tunca, U. *Polym. Chem.* **2012**, *3*, 825-835.
- (27) Liu, W.-B.; Pei, S.; Du, J.; Liu, B.; Gao, L.; Su, Y.; Liu, C.; Cheng, H.-M. *Adv. Funct. Mater.* **2011**, *21*, 2330-2337.
- (28) Remy, E.; Hérold, C.; Valsaque, F.; Marêché, J.-F.; Fontana, S.; Desforges, A.; Cahen, S.; Ghanbaja, J.; Gleize, J.; Vigolo, B. *J. Phy. Chem. C* **2013**, *117*, 19245-19252.
- (29) Varghese, N.; Ghosh, A.; Voggu, R.; Ghosh, S.; Rao, C. N. R. *J. Phy. Chem. C* **2009**, *113*, 16855-16859.

Chapter 4

Attempted Synthesis of a TTFV-Cyclic Tetramer

4.1 Introduction

The interest in design and synthesis of novel macrocyclic molecules has been growing considerably because of the significant roles they play in the development of modern supramolecular chemistry. Representative examples of macrocyclic structures include crown ethers,¹ cyclodextrins,² cucurbiturils,³ and their structurally similar scaffolds⁴ have been abundantly documented in the literature, while many of which are regarded as promising supramolecular hosts for numerous guest species. In this project, a new class of macrocyclic molecules consisting tetrathiafulvalene vinyllogue (TTFV) building blocks is designed, with the aim of exploring their unique structural and electrochemical features. Being a redox active unit, the TTFV moiety can change its confirmation upon oxidation,⁵ and the V-shaped geometry of TTFV in the neutral state is a beneficial feature for macrocyclization reactions. Macrocyclic structures derived from TTFV building blocks are expected to exhibit new properties that can be useful in the design and preparation of sensors,^{6,7} molecular switches or as organic electronic materials and devices.^{8,9}

Previously, the Zhao group has successfully synthesized, through a homocoupling reaction sequences, a triangular shaped TTFV-phenylacetylene macrocycle (Figure 4.1) which is a cyclic trimer of TTFV-phenylacetylene.⁵ However, the crude product of this macrocyclization reaction was also found to contain small amounts of larger macrocycles (e.g., tetramer and pentamer), which were detected by MALDI-TOF MS analysis. The skeletal expansion of the trimer macrocycle can be achieved by stepwise synthesis, which is the primary goal of this project. Such a higher macrocycle (Figure 4.2) is expected to show expanded inner cavity, which will be suitable to host some interesting carbon nanomaterials such as [60]fullerene or its derivatives. Given the excellent electron-donating properties of the TTFV unit and the electron-accepting properties of [60]fullerene, the macrocycle is envisioned to have favored binding with [60]fullerene by strong charge transfer interactions in addition to π -stacking.

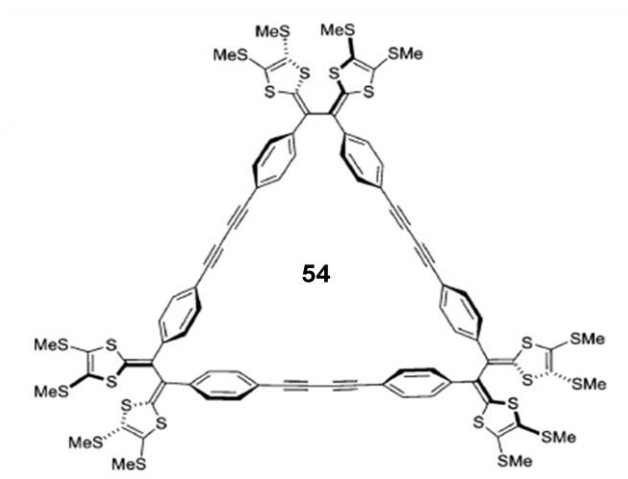


Figure 4.1: Structure of TTFV-phenylacetylene trimer macrocycle **54**.

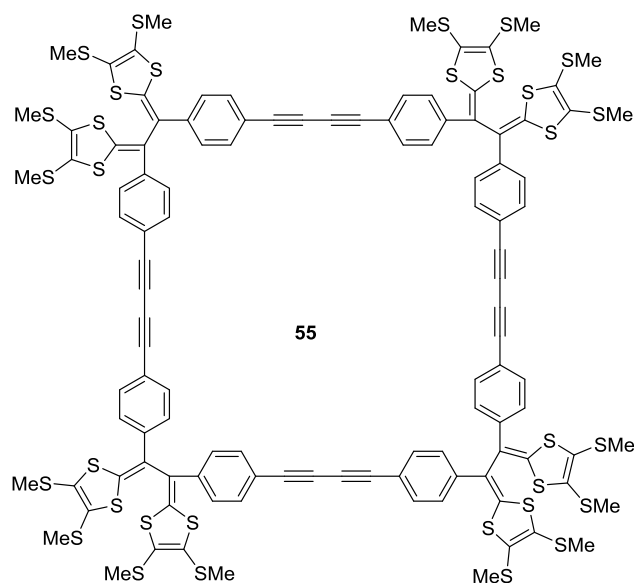
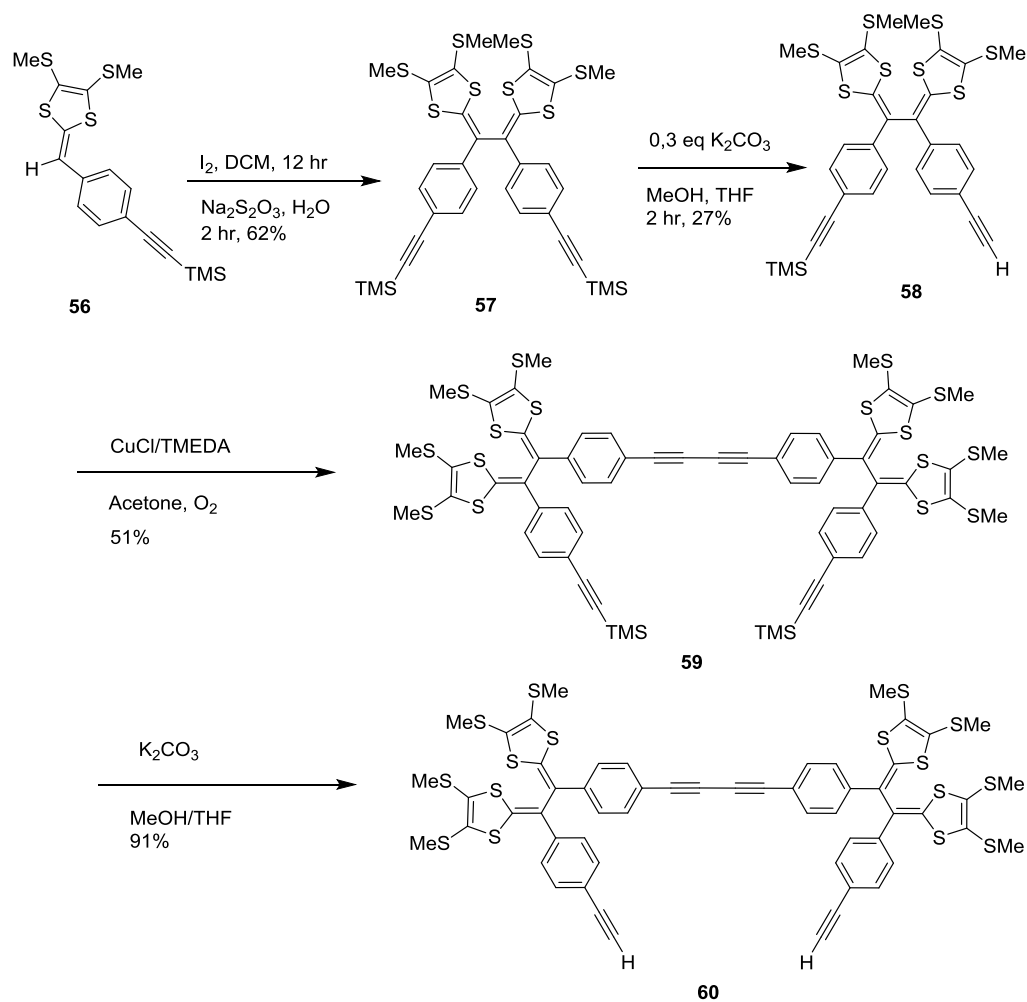


Figure 4.2: Structure of the target TTFV-phenylacetylene tetramer macrocycle **55**.

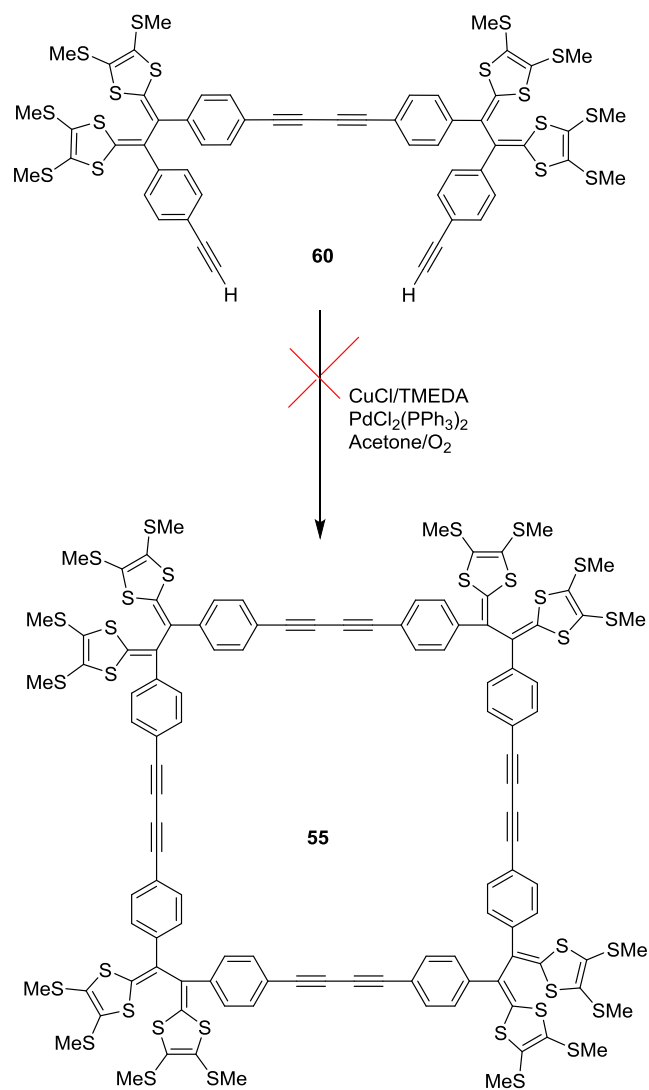
The synthetic attempt to macrocycle **55** was made through the route shown in Scheme 4.1. First, the TMS protected DTF precursor **56** was subjected to oxidative coupling reaction in the presence of molecular iodine followed by reduction with sodium thiosulphite, resulting in a dimerized TTFV building block **57**. The controlled mono-desilylation reaction was carried out on TTFV building block with 0.3 equiv of K_2CO_3 to give acetylenic TTFV building block **58**. Further, the homocoupling reaction on TTFV building block, using the synthetic procedure previously reported by the Zhao group,⁵ afforded bis-TTFV dimer **59**.



Scheme 4.1: Synthetic route for acetylenic bis-TTFV dimer **59**.

Dimer **59** was subjected to desilylation using excess K_2CO_3 to yield an acetylenic bis-TTFV building block **60**. An intermolecular cyclization was carried out on **60** using the method reported by a former group member Dr. Guang to synthesise triangular shaped TTFV macrocycle.⁵ In details, the reaction was carried out under the catalysis of $CuI/TMEDA$ and $PdCl_2(PPh_3)_2$ in acetone in the presence of oxygen. However, the

resulting crude product from the reaction was completely insoluble in any solvent, which prevented its characterizations. It was reasoned that the ring strain of the desired macrocycle could possibly hinder the cyclization. If such were the case, the reaction might have favoured the formation of acyclic higher oligomers and polymers. Although this reasoning may account for the unsuccessful results of the macrocyclization reaction, the possibility of the macrocycle 55 being insoluble cannot be ruled out. To further address this issue, a strategy of replacing the less soluble methyl groups on sulfur atoms with more soluble *n*-decyl chains should be investigated in the future work, and the macrocyclization is better to be conducted under ultra-dilute conditions so as to reduce the formation of disfavoured acyclic products.



Scheme 4.2: Attempted synthesis of the TTFV-phenylacetylene tetramer macrocycle **55** through homocoupling macrocyclization reaction.

4.2 Conclusion

Although the target TTFV-phenylacetylene macrocycle has not been successfully prepared, the synthetic route developed in this project does provide access to the key intermediate to the macrocycle. It is worth mentioning that a controlled mono-desilylation of TMS protected phenylacetylene-TTFV **57** was achieved. So far, the optimized yield of this reaction is kind of moderate (27%); however, it is still possible to make further improvement. The advantage of having access to a precursor like **58** is that it enables step-wise construction of various monodisperse oligomers. The main synthetic obstacle in this project is the low solubility of relevant oligomer products, due to the presence of less soluble methyl groups on dithiol rings. This prevents meaningful characterizations on these products, which in turn hinders clear identification of the reaction pathways involved in the macrocyclization. For this reason, methyl groups should be replaced by more soluble *n*-decyl group in future investigations. Another difficulty encountered in the formation of designed macrocycle could be the sharply increased ring strain. This problem may be overcome through some templating synthetic strategies, by using more active catalysts and more pre-organized precursors for the macrocyclization.

Based on the above rationalizations, this project certainly needs more time and efforts to develop. On the other hand, the key intermediates obtained so far can foster new research directions on other novel TTFV-phenylacetylene based oligomeric and

polymeric systems. It is also envisioned that Cu-catalyzed azide-alkyne coupling (i.e., click chemistry) can be implemented to functionalize the TTFV-phenylacetylene building block to various substrates, and the potential in developing new functional nanomaterials is without doubt very interesting and promising.

4.3 References

- (1) Gokel, G. W.; Leevy, W. M.; Weber, M. E. *Chem. Rev.* **2004**, *104*, 2723-2750.
- (2) Harada, A.; Hashidzume, A.; Yamaguchi, H.; Takashima, Y. *Chem. Rev.* **2009**, *109*, 5974-6023.
- (3) Bhasikuttan, A. C.; Pal, H.; Mohanty, J. *Chem. Commun.* **2011**, *47*, 9959-9971.
- (4) Wang, M.-X. *Acc. Chem. Res.* **2011**, *45*, 182-195.
- (5) Chen, G.; Mahmud, I.; Dawe, L. N.; Zhao, Y. *Org. Lett.* **2010**, *12*, 704-707.
- (6) Mulla, K.; Shaik, H.; Thompson, D. W.; Zhao, Y. *Org. Lett.* **2013**, *15*, 4532-4535.
- (7) Guerro, M.; Pham, N. H.; Massue, J.; Bellec, N.; Lorcy, D. *Tetrahedron* **2008**, *64*, 5285-5290.
- (8) Bendikov, M.; Wudl, F.; Perepichka, D. F. *Chem. Rev.* **2004**, *104*, 4891-4946.
- (9) Canevet, D.; Salle, M.; Zhang, G.; Zhang, D.; Zhu, D. *Chem. Commun.* **2009**, 2245-2269.

Chapter 5

Conclusions and Future Work

This thesis work has been mainly focused on the rational design, synthesis DTF-functionalised phenylacetylene conjugated polymers and their application as selective and reversible dispersants for single-walled carbon nanotubes (SWNTs). For effective dispersion of SWNTs, two phenylacetylene based polymers **35** and **36**, which carry electron-rich phenyl-DTF side groups, were designed and synthesized successfully. In the polymer synthesis, Cu-catalyzed alkyne-azide coupling (click reaction) was used as the key step to achieve efficient side chain functionalization, and Cu(I)-catalyzed homocoupling and Sonogashira cross coupling reactions were employed to construct the conjugated polymer backbones. The presence of phenyl-DTF units on polymer backbones is a key factor allowing the polymers to strongly bind to the sidewall of SWNT via π -stacking, resulting in wrapping mode resembling “centipede”.

The supramolecular interactions of DTF-functionalized π -conjugated polymers with SWNTs show solvent-dependent behavior. This property was utilized to exert control over reversible dispersion and release of SWNTs by addition of aliphatic hydrocarbon solvents to the SWNT /polymer suspension in chlorinated or aromatic solvents. Indeed, a reversible process of dispersing and releasing SWNTs under solvent control, which could be turned into a very useful technique applicable in material

preparation and device fabrication where “additive-free” SWNTs are desired after solution-phase processing in order to maximize electronic and/or optoelectronic performances. Furthermore, the supramolecular interactions between DTF-polymers towards SWNTs exhibit a high selectivity for (6,5), (7,5) and (7,6) tubes which are of relative small diameter (*ca.* 0.75 to 0.90 nm) in nature. Such kind of selectivity is line with the theoretically predicted “centipede wrapping” mode, wherein the electron-rich DTF end groups act as a major driving force for effective SWNT binding. It is envisaged that continued efforts to finely tune the structure and functionality of this type of polymers would serve a springboard towards successful delivery of some useful SWNT processing techniques to tackle the challenge issues of cost-effective and large-scale preparation of SWNTs in a homogeneous manner.

An attempt has been made for the synthesis of TTFV-based cyclic tetramer; however, the synthesis has not yet been accomplished because of the following reasons. Firstly, the macrocyclization reaction produced insoluble substances. As a result, further analysis could not be undertaken to determine their structures. The low solubility issue can be overcome by introducing more soluble *n*-decyl chains on the sulfur atoms instead of methyl groups. Secondly, the ring strain in the target macrocycle may hinder the formation of cyclic tetramer and thus divert to the reaction to form less strained acyclic oligomer or polymers. However, the presence of a single free terminal alkynyl group in precursor **60** point to a new research direction, as it allows selective skeletal extension by iterative synthetic strategies. Different fluorogenic and large aromatic units such as

anthracene and pyrene can therefore be introduced by using alkyne-enabled chemistry such as coupling reactions and click reactions. It is expected that proper structural design with suitable functional moieties, TTFV-based macrocycles can serve as supramolecular hosts for [60] fullerene and related carbon nanostructures. The complexes may find new applications in organic photovoltaic devices and photoredox catalysis.